Max-Planck-Institut für Metallforschung
Stuttgart

Characterization of the CO Sensitivity of Electrode Materials by Solid Electrolyte Galvanic Cells

Vladimir Plashnitsa

Dissertation
an der
Universität Stuttgart

Bericht Nr. 156
Juli 2004

Characterization of the CO sensitivity of electrode materials by solid electrolyte galvanic cells

Von der Fakultät Chemie der Universität Stuttgart
zur Erlangung der Würde eines Doktors der
Naturwissenschaften (Dr.rer.nat.) genehmigte Abhandlung

Vorgelegt von

Vladimir Plashnitsa

Aus Kirow, Russland

Hauptberichter:	Prof. Dr. F. Aldinger
Mitberichter:	Prof. Dr. E. Roduner
Tag der mündlichen Prüfung:	21 Juli, 2004

Institut für Nichtmetallische Anorganische Materialien der Universität Stuttgart
Max-Planck-Institut für Metallforschung, Stuttgart
Pulvermetallurgisches Laboratorium

2004

Dedicated to my wife, Larisa, and my parents with love

There are more things in heaven and earth, Horatio,
Than are dreamt of in your philosophy.

(Mr. William Shakespeare,
"Hamlet")

Acknowledgements

This doctoral thesis was done from October 2000 to June 2004 in Max-Planck-Institute für Metallforschung, Stuttgart, supported by a scholarship of the Max-Planck-Geselschaft.

I would like to thank my advisor Prof. Dr. F. Aldinger for encouraging me to investigate the topic of this work which I found very interesting. During the three years in MPI I not only learned the methods for scientific research, but also was trained to become an independent scientist, which may be of more value. Without the encouragement and continual support from Prof. Dr. F. Aldinger, my achievement would not be possible.

I want to thank Dr. H. Näfe, who was my group leader, for initiation and subject of this work, the excellent scientific support, lively discussions and assistance during the whole period. Working with him is a very good experience. Most importantly, I learned much from his serious attitude toward scientific work and making scientific reports.

I want to thank Prof. Dr. E. Roduner who accepted to become the 'Mitberichter' for my final examination. I want also to thank Prof. Dr. E. J. Mittemeijer who, together with my advisor and Prof. Dr. E. Roduner, gave me final examination.

My special very many thanks are given to Mrs. Gisela Feldhofer, the good soul of the "Functional Ceramics Working Group", for her technical support of the experimental work and also for her encouragement during the difficult times.

Furthemore, there were many people who trained me and helped me. My thanks are given to all colleagues in Powder Metallurgical Laboratory (PML) and engineers of the service groups of the MPI for Metal Research and the MPI for Solid State Research. In particular, to Mrs. S. Paulsen and Mrs. J. Weber-Bock for administrative work; to Mr. H. Labitzke and Mr. G. Kaiser for all their advices with regard to SEM and chemical analyses; to Mr. I. Kozmon, Mr. M. Zeindelmeier, Mr. H. Eckstein for technical assistance; to Ms. M. Thomas for XRD analyses. The very important computer services are provided by Mr. E. Bruckner. Therefore, I would like to take this opportunity to express my sincere thanks to them.

I would like to thank my friends and colleagues from "Functional Ceramics Working Gorup": Bogdan Khorkounov, Krenar Shqau, Ruhul Amin, Gautam Devendraprakash and Steffi Golhofer.

There were many other people who made my working and living easier and full of fun. There are many same kinds of things, which I cannot list all but indeed, make me fell very happy and very lucky to work in such a group. Here, I would like to thank all of my colleagues who have ever helped me. My family is a source of support in many forms. My parents always sent E-mails to me with motherly care. Without a doubt, the biggest support was from my lovely wife: Larisa. I thank you so much.

List of symbols and abbreviations

μ_j	…	Chemical potential of component *j*
$\tilde{\mu}_j$	…	Electrochemical potential of component *j*
$\tilde{\mu}_j^0$	…	Standard electrochemical potential of component *j*
σ	…	Total conductivity
p_j	…	Partial pressure of compound *j*
X_2	...	Gas molecule
X_X^x	...	Gas atom at the lattice position
$V_X^{\cdot\cdot}$	...	Gas ion vacancy
$O^{\delta-}$	…	Adsorbed ionic oxygen
O^{2-}	…	Oxygen ion in zirconia anion sublattice
O_O	…	Oxygen atom at the lattice position
O_i''	…	Interstitial oxygen
$V_O^{\cdot\cdot}$	…	Oxygen ion vacancy
G	…	Free adsorption site on the electrode surface
e^-	…	Electron
h	...	Electron hole
a_j	…	Activity of compound *j*
c_j	…	Concentration of component *j*
N_j	…	Amount of component *j*
U	…	Cell voltage
U^0	…	Standard cell voltage
R_i	…	Resistance
I	…	Cell current
E^0	…	Electrode potential
E_m	…	Mixed electrode potential
t_{ion}		Transference number of the mobile ion
C	…	Capacitance
R	…	Universal gas constant
T	…	Absolute temperature
n	...	Number of electrons involved in electrochemical reaction
F	…	Faraday’s constant

D	...	Diffusion coefficient
q_j	...	Charge of component *j*
V	...	Enclosed volume
$\Delta_f G_j^0$	…	Standard Gibbs free enthalpy of formation of compound *j*
ΔH	...	Reaction enthalpy
s	…	Active site on the catalyst surface
τ	…	Time
θ_j	…	Fraction of three-phase-boundary sites occupied by component *j*
K, K^0	…	Adsorption constants
Q	…	Heat of adsorption
Ψ^0	…	Flux of gas molecules at 1 atm
ν	…	Frequency of gas molecule vibration
n_s	…	Number of the three-phase-boundary sites
Z′, Z′′	…	Real and imaginary parts of impedance
ΔU	…	CO sensitivity
E_a	…	Activation energy

SEP	…	Solid electrolyte potentiometry
NNEP	…	Non-Nernstian electrode potential
tpb	…	Three-phase boundary
M_j	...	Conductors
YSZ	…	Y_2O_3-stabilized ZrO_2, oxygen ion-conducting solid electrolyte
NASICON	…	$Na_3Zr_2Si_2PO_{12}$, sodium ion-conducting solid electrolyte
NBA	…	Na-(β+β′′)-Al_2O_3, sodium ion-conducting solid electrolyte
Nafion®	...	Perfluorosulfonic acid in (H^+) form
RE	…	Reference electrode
SE	…	Sensing electrode
cat	…	catalyst
IS	…	Impedance spectroscopy
SEM	…	Scanning electron microscopy
EDX	…	Energy dispersive X-ray analysis

Content

Page

1 Summary

The voltage of a galvanic cell using stabilized zirconia as a solid electrolyte can exhibit deviations from the equilibrium value given by the Nernst equation, if oxygen together with traces of an oxidizable gas like CO is exposed to one of the electrodes of the cell. This is called the non-Nernstian voltage behaviour. The basic principle of operation is not yet finally cleared since the experimental results are in accordance with two theoretical approaches present. Aiming at a better understanding of the background of this phenomenon the mechanism of functioning of solid electrolyte galvanic cells with various sensing electrode materials ($Pt_{1-x}Au_x$ alloys) in oxygen containing atmospheres with different CO concentrations at moderate temperatures has been studied by means of electrochemical methods.

The characterization of the CO sensitivity and understanding the behaviour of the $Pt_{1-x}Au_x$ sensing electrodes was done by means of the one-electrolyte galvanic cell

$$Pt \mid Pt_{1-x}Au_x,Ar,CO(p_{CO}=5\text{-}1\cdot10^2\ Pa),O_2(p_{O_2}=1\cdot10^3\ Pa) \mid YSZ \mid O_2(p_{O_2}=1\cdot10^5\text{-}1\cdot10^{-33}\ Pa),Pt \qquad (I)$$

and by new approaches based on the bi-electrolyte measuring principle which can be written as

$$Pt|Au,O_2,CO,Na_2CO_3(Au)\text{-catalyst} \mid Na\text{-}(ß+ß'')\text{-}Al_2O_3 \mid YSZ \mid O_2,\ CO,\ Pt_{1-x}Au_x\ (x=0,\ 0.2)|Pt\ , \qquad (II)$$

$$Pt \mid Au,O_2,CO,Na_2CO_3(Au)\text{-catalyst} \mid Na\text{-}(ß+ß'')\text{-}Al_2O_3(Au) \mid YSZ \mid O_2,CO,Pt_{1-x}Au_x \mid Pt\ , \qquad (III)$$

$$Pt \mid Au,O_2,CO,Na_2CO_3(Au)\text{-catalyst} \mid Na\text{-}(ß+ß'')\text{-}Al_2O_3 \mid YSZ \mid O_2,Pt \mid Pt\ , \qquad (IV)$$

$$Pt \mid Au,O_2,CO,Na_2CO_3(Au)\text{-catalyst} \mid Na\text{-}(ß+ß'')\text{-}Al_2O_3(Au) \mid YSZ \mid O_2,Pt \mid Pt\ , \qquad (V)$$

where yttria-stabilized zirconia (YSZ) and $Na\text{-}(ß+ß'')\text{-}Al_2O_3$ (NBA) represent oxygen and sodium ion-conducting solid electrolytes, respectively. In the cell (I) YSZ was employed in the form of an one-end-closed tube. The cells (II) and (III) represent a planar geometry, whereas the cells (IV) and (V) have two gas compartments. The cells (II) and (IV) can be regards as a combination of sodium and oxygen concentration cells and the overall voltage (U) of these bi-electrolyte cells is the sum of the voltages generated due to chemical potential differences that are established between the interfaces of both of these concentration cells. Due to the short-circuited NBA pellet the voltage of the cells (III) and (V) as well as for the cell (I) can be calculated by the Nernst equation. For the conversion of CO to CO_2 in the bi-electrolyte cell arrangement the sodium carbonate counter electrode is partially covered by the catalyst ("Hopkalit HTK15") layer.

The different $Pt_{1-x}Au_x$ sensing electrode materials (x=0, 0.2, 0.5, 0.8, and 1) have been prepared by simultaneous co-precipitation from their corresponding metal compounds ($PtCl_6^{2-}$ and $AuCl_4^{2-}$). The $Pt_{1-x}Au_x$ alloys were characterized by X-ray powder diffraction (XRD) and scanning electron microscopy (SEM) analyses showing bimetallic, finely divided solids in accordance with nominal chemical compositions.

The CO sensitivity, defined as the difference between the experimental voltage at finite CO concentrations and that under zero CO content, was characterized by the cell voltage measurements within the temperature range of 400-700 °C as a function of the CO concentration in the measuring gas (0-40 000 ppm), the composition of the $Pt_{1-x}Au_x$ sensing electrodes as well as the reference electrode potential (under O_2 and H_2/H_2O) while the oxygen partial pressure in the measuring gas is kept constant. The resistance of the electrode process on the sensing electrodes has been studied by means of impedance spectroscopy under the same experimental conditions.

The dependence of voltage of the cell (I) with $Pt_{0.2}Au_{0.8}$ and pure Au sensing electrodes repeats practically that for the Pt electrode, which is close to the theoretical curve. On the other hand, the voltage response of the cell (I) with $Pt_{0.8}Au_{0.2}$ and $Pt_{0.5}Au_{0.5}$ sensing electrodes differs greatly from that expected theoretically. This tendency is preserved at all the investigated temperatures.

The CO sensitivity for the same sensing electrodes varies slightly using different reference electrode potentials. At 400 °C, in the case of a high reference electrode potential, the CO sensitivity increases sharply with increasing CO concentration, whereas it has significantly smaller response with the alternative electrode. With raising temperature the CO sensitivity of the $Pt_{1-x}Au_x$ sensing electrodes decreases using the high reference electrode potential and becomes comparable to that determined at the lower one. The $Pt_{1-x}Au_x$ ($x \neq 0$ and 1) sensing electrodes show much higher CO sensitivity than the pure metals, whose values are always close to zero. Among the $Pt_{1-x}Au_x$ sensing electrodes, the $Pt_{0.8}Au_{0.2}$ material exhibits the maximum sensitive properties in presence of CO in gas phase independent of the experimental conditions. In view of the maximum CO sensitivity the most preferable temperature range for using the $Pt_{1-x}Au_x$ sensing electrodes in the cell (I) is 400-500 °C.

The values of CO sensitivity for the $Pt_{1-x}Au_x$ sensing electrodes are not reproducible after the first and the second runs of the experiment and they are increasing/decreasing depending on the experimental conditions. However, the CO sensitivity is well reproducible after the second, third, and also at further investigations. The CO sensitivity for the $Pt_{1-x}Au_x$ sensing electrodes is much higher under high reference electrode potential than those under the low one at the first run of experiment. After repetition of experiments this difference is not so considerable but it is still exist. Moreover, the CO sensitivity obtained under high reference electrode potential is always higher than that under the low one. It is possible to conclude that it is necessary to be very careful at the estimation of the experimentally obtained CO sensitivity. The experimental conditions (at least, temperature, time, and pretreatment of electrode materials), as well as reference electrode potential, could play an important role for the determination of the voltage response and characterization of the CO sensitivity for the $Pt_{1-x}Au_x$ sensing electrodes by the cell (I) in presence of CO in the gas.

According to the impedance spectroscopy investigations, the resistance of the electrode process on the $Pt_{1-x}Au_x$ ($x \neq 0, 1$) electrodes increases substantially with respect to CO concentration, whereas the magnitude of that for the pure metals (Pt and Au) does not depend on the presence of CO at all the investigated temperatures, independent of the nature of the reference electrode potential. The temperature dependence of the electrode resistance for the $Pt_{1-x}Au_x$ electrodes shows linear behavior at all CO concentrations. Under high reference electrode potential the presence of carbon monoxide in the gas phase has a definite influence on the electrode resistance and the activation energies increase mainly at finite CO concentration. The same dependence, under low reference electrode potential, shows that the activation energies are close to each other at finite CO concentration and without CO. It is possible to assume that the presence of CO in the gas phase can influence directly the electrochemical processes proceeding on the $Pt_{1-x}Au_x$ sensing electrodes.

All the investigated bi-electrolyte cell configurations with the $Pt_{1-x}Au_x$ sensing electrodes show stable, reversible, and reproducible response on changing CO concentration in the gas phase, revealing very good sensing properties.

The planar bi-electrolyte cells (II) and (III) exhibit a very clear linear dependence of the voltage as on the CO concentration as on temperature. Moreover, the slope of the experimentally obtained lines depends on which working electrode material was used. The $Pt_{0.8}Au_{0.2}$ electrode used in the cell (II) shows a better voltage response (sensing properties) compared to the Pt one in the whole investigated temperature range. However, since the influence of CO on the working electrode processes is not known, the theoretical voltages for the planar cells (II) and (III) cannot be calculated. This can be avoided using the two-compartment configurations (IV) and (V).

The voltages of the two-compartment cell (IV) are very low in comparison with the theory, and such low values are achieved after extremely long time. Such a behaviour can be explained by the long time to achieve the thermodynamic ß/ß´´-equilibrium into non-short-circuited NBA solid electrolyte. In contrast, the results for the bi-electrolyte cell (V) with the short-circuited one seem to be most promising. The steady-state voltages are achieved relatively quickly and they have values that are very close to the theoretical ones. Cell (V) shows a very well defined voltage dependence in the whole determined CO concentration range and in the temperature interval of 400-700 °C. One important point for the theoretical and practical investigations is that since the experimental dependences repeat completely the theory, there is no necessity to make a calibration curve.

Summing up all the obtained results it could be preliminarily concluded that real progress is achieved in the development of the bi-electrolyte principle and such bi-electrolyte cell configurations (planar and two-compartment) could be used for the characterization and determination of CO in the gas phase in a wide range of carbon monoxide concentrations.

2 Zusammenfassung

Die Spannungen galvanischer Zellen mit Y_2O_3-stabilisiertem ZrO_2 als Festelektrolyt zeigten oft Abweichungen von der Nernst-Spannung. Dieses wird oft dann beobachtet, wenn Sauerstoff mit geringen Konzentrationen (oxidierbare Gase wie z.B. CO) als Gasatmosphäre an einer Elektrode wirkt. Dieser Effekt wird in der Literatur als Nicht-Nernst'sche Spannung bezeichnet. Dieser Effekt ist bisher noch nicht vollständig geklärt. Diese Tatsache könnte dadurch erklärt werden, dass alle experimentellen Ergebnisse an solchen galvanischen Zellen durch zwei verschiedene theoretische Vorstellungen (Nicht-Nernst'sche Elektroden Potenziale und CO Adsorption an O_2-Plätzen) interpretiert werden kann. Um die grundlegenden Prinzipien dieses Phänomens besser zu verstehen, wurde in der vorliegenden Arbeit der Mechanismus galvanischer Zellen mit verschiedenen Festlelektrolyten und unterschiedlichen Elektrodenmaterialien ($Pt_{1-x}Au_x$-Legierungen) untersucht. Diese Untersuchungen erfolgten mit Hilfe elektrochemischer Messmethoden bei mittleren Temperaturen (400-700 °C) in sauerstoffhaltigen Gasatmosphären mit unterschiedlichen CO-Konzentrationen (0-40 000 ppm).

Die CO-Empfindlichkeit und die Eigenschaften der $Pt_{1-x}Au_x$-Sensor-Elektroden wurden in der Ein-Elektrolyt-Zelle des Types (I)

$$Pt \,|\, Pt_{1-x}Au_x,Ar,CO(p_{CO}=5\text{-}1\cdot10^{2}\ Pa),O_2(p_{O_2}=1\cdot10^{3}\ Pa) \,|\, YSZ \,|\, O_2(p_{O_2}=1\cdot10^{5}\text{-}1\cdot10^{-33}\ Pa),Pt \qquad (I)$$

und mit Hilfe speziell entwickelter Bi-Elektrolyt-Zellen der Typen (II)-(V)

$$Pt|Au,O_2,CO,Na_2CO_3(Au)\text{-catalyst} \mid Na\text{-}(ß+ß'')\text{-}Al_2O_3 \mid YSZ \mid O_2,\ CO,\ Pt_{1-x}Au_x\ (x=0,\ 0.2)|Pt\ , \qquad (II)$$

$$Pt \mid Au,O_2,CO,Na_2CO_3(Au)\text{-catalyst} \mid Na\text{-}(ß+ß'')\text{-}Al_2O_3(Au) \mid YSZ \mid O_2,CO,Pt_{1-x}Au_x \mid Pt\ , \qquad (III)$$

$$Pt \mid Au,O_2,CO,Na_2CO_3(Au)\text{-catalyst} \mid Na\text{-}(ß+ß'')\text{-}Al_2O_3 \mid YSZ \mid O_2,Pt \mid Pt\ , \qquad (IV)$$

$$Pt \mid Au,O_2,CO,Na_2CO_3(Au)\text{-catalyst} \mid Na\text{-}(ß+ß'')\text{-}Al_2O_3(Au) \mid YSZ \mid O_2,Pt \mid Pt\ , \qquad (V)$$

charakterisiert. Hier wirkt YSZ als Sauerstoffionenleiter und Na-(ß+ß´´)-Al_2O_3 (NBA) durch seine Eigenschaften als Natriumionenleiter.

In der Zellanordnung des Typs (I) wurde ein YSZ-Elektrolyt in Form eines einseitig geschlossenen Rohres verwendet. Die Zelltypen (II) und (III) haben hingegen einen planaren Aufbau. Die Messzellen (II) und (III) bestanden nur aus einem Gasraum. Die Zellen der Typen (IV) und (V) bestanden hingegen aus zwei Gasräumen. Die Messzellen (II) und (IV) können als eine Kombination einer Sauerstoffkonzentrationszelle und einer Natriumkonzentrationszelle verstanden werden. Die Zellspannung (U) dieser Zellen (II) und (IV) ist die Summe der Sauerstoffkonzentrationsmesszelle und der Natriumkonzentrationsmesszelle. In den Zellen (III) und (V) wurde ein kurzgeschlossener NBA-Festelektrolyt benutzt, so dass die galvanischen Spannungen dieser Zellen als Nernst-Spannung betrachtet werden kann. Die galvanische Spannung der Zelle (I) kann ebenfalls mit Hilfe der Nernst-Gleichung berechnet werden. Um das thermodynamische

Gleichgewicht der Oxidation von CO zu CO_2 in den Bi-Elektrolyt-Zellen möglichst schneller zu erreichen, wurde die Oberfläche der Na_2CO_3-Referenzelektrode mit einer dünnen Schicht eines kommerziellen Katalysators "Hopkalit HTK15" bedeckt.

Die verschiedenen $Pt_{1-x}Au_x$-Elektrodenmaterialien (x=0, 0.2, 0.5, 0.8 und 1) wurden mittels Abscheidungsverfahren aus den Lösungen der Salze der entsprechenden Metalle ($PtCl_6^{2-}$ und $AuCl_4^{2-}$) hergestellt. Die so hergestellten Elektrodenmaterialien wurden mit Hilfe der Röntgenphasenanalyse und der Rasterelektronenmikroskopie charakterisiert. Die Ergebnisse der Charakterisierung zeigen, dass die Elektrodenmaterialien eine homogene Struktur aufweisen.

Die CO-Empfindlichkeit wurde als Unterschied zwischen der experimentell ermittelten Zellspannung bei einer bestimmten CO-Konzentration im Messelektroden-Gas und der Zellspannung ohne CO ermittelt. Die Messungen der CO-Empfindlichkeit erfolgten in einem Temperaturbereich von 400-700 °C und im Bereich von CO-Konzentrationen im Messgas von 0-40 000 ppm in Abhängigkeit von der Zusammensetzung des Elektrodenmaterials und dem Potenzial an der Referenzelektrode. Der Sauerstoffpartialdruck im Messgas wurde ebenfalls konstant gehalten. Der Widerstand der Elektrodenreaktion an den Messelektroden wurde bei den oben erwähnten Messbedingungen mit der Impedanzspektroskopie gemessen.

Die Zellspannungen der Zellen $Pt_{0.2}Au_{0.8}$-Elektrode und der Au-Elektrode weisen eine ähnliche Temperaturabhängigkeit auf, wie im Fall der Pt-Elektrode, wobei die Zellspannung der Pt-Elektrode den theoretischen Verlauf der Temperaturabhängigkeit zeigt. Die Temperaturabhängigkeiten der Zellspannungen für die Zellen mit den Elektroden aus $Pt_{0.8}Au_{0.2}$ und $Pt_{0.5}Au_{0.5}$ unterscheiden sich aber in starkem Maße vom theoretischen Charakter. Diese Tendenz ist im gesamten untersuchten Temperaturbereich zu beobachten.

Die CO-Empfindlichkeit der gleichen Messelektroden in den Zellen (I) verändert sich nur wenig bei Änderung des Potenzials der Referenzelektrode. Bei 400 °C steigt die CO-Empfindlichkeit dieser Elektroden unter der Benutzung eines hohen Potenzials der Referenzelektrode (O_2) durch die Erhöhung der CO-Konzentration drastisch an. Zugleich wurde keine Abhängigkeit der CO-Empfindlichkeit bei der Verwendung anderer Referenzelektroden bemerkt (H_2/H_2O). Mit dem Anstieg der Temperatur nimmt die CO-Empfindlichkeit der $Pt_{1-x}Au_x$-Elektroden ab, wenn ein hohes Potenzial an der Referenzelektrode verwendet wird. Dadurch wird die Höhe der CO-Empfindlichkeit vergleichbar mit der Größe, die unter den Bedingungen eines niedrigeren Potenzials der Referenzelektrode ermittelt wird. $Pt_{1-x}Au_x$-Elektroden ($x \neq 0$ und 1) zeigen eine viel höhere Empfindlichkeit gegenüber CO als unlegierte Pt- und Au-Elektroden, deren CO-Empfindlichkeit sehr gering ist. Unter den untersuchten $Pt_{1-x}Au_x$-Elektroden weist die $Pt_{0.8}Au_{0.2}$-Elektrode den maximalen Wert der CO-Empfindlichkeit auf, unabhängig von den experimentellen

Bedingungen. Um die maximale Messempfindlichkeit dieser Elektroden für CO in den Zellen (I) zu erreichen, ist der Temperaturbereich von 400-500 °C zu bevorzugen.
Die Werte der CO-Empfindlichkeit sind nach der ersten und zweiten Messung nicht reproduzierbar. Nach weiteren Wiederholungen der Messungen wird die CO-Empfindlichkeit jedoch gut reproduzierbar. Beim ersten Messverlauf ist die CO-Empfindlichkeit bei einem hohen Potenzial an der Referenzelektrode wesentlich höher. Bei weiteren Wiederholungen ist der Unterschied zwischen den Werten, die bei einem hohen und einem niedrigeren Potenzialwert der Referenzelektrode ermittelt wurden, relativ unbedeutsam. Bei einem hohen Potenzial der Referenzelektrode ist die CO-Empfindlichkeit aber immer höher, als die bei einem niedrigeren Wert des Referenzelektroden-Potenzials. Das könnte bedeuten, dass solche experimentellen Mess-bedingungen, wie die Temperatur und das Potenzial der Referenzelektrode, sowie die Vorgeschichte der Elektrodenmaterialien eine wichtige Rolle für die Spannungsmessungen bei der Ermittlung der CO-Empfindlichkeit von $Pt_{1-x}Au_x$-Sensorelektroden in den Zellen (I) spielen könnten.

Die impedanzspektroskopischen Messungen zeigten, dass der Widerstand der Elektrodenreaktion an $Pt_{1-x}Au_x$-Elektroden ansteigt mit Erhöhung der CO-Konzentration. Für die unlegierten Elektroden aus Pt und Au zeigt der Elektrodenwiderstand dagegen keine Abhängigkeit von der CO-Konzentration. Letzteres gilt für den gesamten untersuchten Messtemperaturenbereich und für alle untersuchten Potenziale der Referenzelektroden. Die Temperaturabhängigkeiten des Elektroden-widerstandes für die $Pt_{1-x}Au_x$-Elektroden zeigen einen linearen Verlauf. Die Größe der Aktivierungsenergie des Widerstandes des Elektrodenprozesses der $Pt_{1-x}Au_x$-Elektroden, unter Benutzung von Sauerstoff als Referenzgas, wird ebenfalls durch die Anwesenheit von CO beeinflusst. Die Werte der Aktivierungsenergie steigen mit der Erhöhung der CO-Konzentration an. Unter Verwendung von H_2/H_2O-Mischungen als Referenzgase sind die Werte der Aktivierungenergien des Elektrodenprozesses mit und ohne CO vergleichbar. Daraus ist zu schlussfolgern, dass die Anwesenheit von CO in der Gasphase einen Einfluss auf die Elektrodenprozesse der $Pt_{1-x}Au_x$-Elektroden hat.

Alle untersuchten Bi-Elektrolyt galvanischen Zellen wiesen stabile und reproduzierbare Zellspannungssignale auf und zeigten gute Sensor-Eigenschaften.
Die Abhängigkeiten der Zellspannungen in den Zellen (II) und (III) von der Temperatur und von der CO-Konzentration zeigen ebenfalls einen linearen Verlauf. Jedoch wird der Anstieg dieser Abhängigkeiten in stärkerem Maße von der Zusammensetzung des Elektrodenmaterials bestimmt, als das für die unlegierte Elektroden (Zellen (IV) und (V)) der Fall ist. Auch hier zeigt die $Pt_{0.8}Au_{0.2}$-Elektrode jeweils die besten Sensoreigenschaften (CO-Empfindlichkeit) bei allen

untersuchten Temperaturen. Die theoretischen Spannungen der Zellen (II) und (III) können nicht exakt berechnet werden, da sich nach wie vor die an der $Pt_{1-x}Au_x$-Elektroden ablaufenden Prozesse einer quantitativen Beschreibung entziehen. Demgegenüber können die Zellspannungen für die Zellen (IV) und (V) berechnet werden, da in diesen Zellen eine Zellanordnung mit zwei getrennten Gasräumen verwendet wurde.

Die experimentell ermittelten Spannungen für die Zelle (IV) sind zu niedrig im Vergleich zu den theoretischen Werten. Um das thermodynamische Phasen-Gleichgewicht zwischen ß/ß´´ mit nicht kurzgeschlossenem NBA-Festelektrolyten zu erreichen, sind sehr lange Zeiten notwendig. Im Gegensatz dazu sind bei der Bi-Elektrolyt-Zelle (V) mit einem kurzgeschlossenen NBA-Elektrolyten stabile Spannungswerte wesentlich schneller erreichbar. Die Spannungswerte dieser Zellen stimmen sehr gut mit der Theorie überein und sind deutlich abhängig von der CO-Konzentration im Temperaturbereich von 400 °C bis 600 °C. Dies gilt für alle untersuchten CO-Konzentrationen. Aus diesen Gründen besteht keine Notwendigkeit, für diese Zelle eine Kalibrationskurve zu erstellen.

Die Ergebnisse der vorliegenden Arbeit zeigen, dass mit dem neu entwickelten Prinzip der Bi-Elektrolyt-Zellanordnung mit einer planaren Geometrie und mit zwei separaten Gasräumen die Analyse der CO-Konzentration in einem breiten Konzentrationsmessbereich erfolgreich durchgeführt werden kann.

3 Introduction

The rising environmental awareness of the public and the corresponding rise in environmental legislation has led to a growing demand for sensors to control and monitor processes with environmental impact. One issue of high environmental impact is the area of combustion processes which cover large centralized power plants, mid-sized decentralized heat and power generation and the mass-market applications for internal combustion engines and house firings. Solid-state electrochemical cells involving oxygen-ion-conducting electrolytes have been investigated extensively in the last 30 years. Such devices are being widely used as oxygen sensor, particularly for the monitoring and control of combustion processes.

Sensors for combustion control have to face severe working conditions. Main applications are the control of the air/fuel ratio in automobiles with three-way catalysts and the control of burners and combustion engines by the measurement of the remaining oxygen content in the flue gas.

Sensors for other gas components would be of high interest to improve the existing methods for the control and surveillance of the combustion process. Their potential advantages in in-line applicability, quick response time, low maintenance needs and lower price level outweigh the – in general existing – disadvantages of lower selectivity when compared with other measuring technologies.

Solid electrolyte potentiometry (SEP) is one of the techniques that can be used to extract *in situ* information about adsorbed species on catalyst surfaces at practically important pressure and temperature conditions.

Until today only a small number of materials could be identified that are useful for the development of long-term stable, in-line chemical sensors with zirconia being the best known and proven sensor material. For the detection low concentration of oxidizable gases as CO sensors based on zirconia solid electrolyte have been investigated. Carbon monoxide is one of important reducing gases to be detected in petroleum and automobile industries, combustion furnaces and also in the first stages of fire. In order to better understanding the mechanism of functioning of existing solutions zirconia-based solid electrolyte galvanic cells with $Pt_{1-x}Au_x$ working electrodes are studied in presence of CO in the gas phase.

3.1 Motivation

A zirconia solid electrolyte sensor shows a highly sensitive and long-time stable response to the presence of products of combustion processes and is therefore suited for use in combustion quality control systems. However, long-term stable performance in flue gases and high sensitivity towards

the products of incomplete combustion processes of such sensor devices still are problems to be solved.

It is well known that zirconia sensors show a non-Nernstian electrode potential (NNEP) in the presence of oxidizable gases as CO and the NNEP effect can be used for sensor applications. The basic principle of operation is not yet clarified completely as the experimental results can be interpreted by two theoretical hypotheses. The first assumption is the generation of a mixed potential at the three-phase-boundary (tpb) due to electrochemical reduction of oxygen and oxidation of carbon monoxide. The second hypothesis proceeds from the adsorption of CO molecules at the electrode due to which the number of oxygen adsorption sites is reduced and thus the oxygen activity at the electrode is decreased. The experimental data are frequently non-reversible and non-reproducible.

A fundamental understanding of the CO sensing mechanisms to make a better solution is crucial for the development of reliable sensors, which can operate in industrial environments over extended periods and cycles.

3.2 Aims and tasks of the investigation

The aim of the study is the investigation of the mechanism of functioning of potentiometric galvanic cells based on yttria-stabilized zirconia as a solid electrolyte and metal electrodes (Pt, $Pt_{1-x}Au_x$ alloys) in oxygen containing atmospheres with different CO concentrations (0-40 000 ppm) in the temperature interval of 400-700 °C.

Within the frame of this investigation it is necessary to establish the influence of working parameters such as concentration of CO, operating temperature, composition of sensing electrode, and reference electrode potential on the CO sensitivity of the metal electrodes by means of electrochemical methods of investigation.

Different configurations of solid electrolyte galvanic cells with various sensing electrode materials have been performed for the development of an optimal pair of electrode/electrolyte which is chemically stable in the flue gas environment, shows a high sensitivity to CO, exhibits reproducible behaviour at several cycles of measurements, and is suitable for the use in combustion process control or sensor devices.

4 Literature survey

4.1. Introduction and historical remarks about sensors

The industrial field has always been dependent on measuring instruments for the registration of physical parameters. For this reason, the technology of sensors is not new. Wilhelm von Siemens, for example, built one of the first sensors in 1860. He made use of the temperature dependence of a resistor made of copper wire for temperature measurements. Due to rapid development in semiconductor technology in a decade or so, the design of measuring instruments and systems changed to such an extent that it is now possible to realize as many functions and components by electronic means as possible.

Initially, when the development started in the field of sensor technology around 1960s, there was a fundamental problem, namely, the lack of sensors capable of converting the generally available non-electrical parameters into electronic compatible signals. These sensors and the appropriate electronics should not only be precise, reliable and capable of integration, but also have to be accepted with regard to their overall dimension and price.

Sensor technology is now greatly promoted in the international market. The difficulty is that the activities have to encompass many details in order to cover the vast range of applications in industrial measurement technology and research instrumentation.

4.2 Definition and classification of sensors

In general words, a sensor is defined as “a device which provides a usable output response to a specified measurand” [1]. An output may be an electrical quantity and a measurand is a physical quantity, property or condition which is measured.

The various ways in which sensors can be defined are as follows

1) The IEC (International Electrochemical Committee) draft (65/84) [2] defines a sensor as being “the primary element of a measuring chain which converts the input variable into a signal suitable for measurement”.
2) Wolber and Wise [3] defined a sensor as a “single-parameter measuring instrument which transduces a physical parameter into a corresponding electrical signal with significant fidelity”.
3) Middelhoek and Noorlag [4] defined a sensor as an “input transducer of an information processing system”.

Certain requirements are set for sensors [5]. These may be basic (concerning all types of sensors), and specific (concerning a definite type of sensors only). The basic requirements, met in different ways, according to the operation principle and the construction of the sensor, are:

- High sensitivity;
- Linearity;
- High accuracy;
- Absence of hysteresis;
- Reproducibility;
- High response rate;
- Selectivity;
- Interchangeability;
- Broad range of measurement;
- Broad range of operating temperatures;
- Stability to disturbances (noise immunity);
- Possibility of easy correction (simple calibration);
- High reliability;
- Long period of operation (durability);
- Resistance to ageing;
- Resistance to the ambient influences (heat, vibration, acids, alkalis, gas, water, dust);
- Safety (the sensor should do no harm);
- Low price;
- Small dimensions, small weight and high strength.

The different criteria on which sensors have been classified are as follows [6]:

- Physical ar chemical effect/transduction principle;
- Measurand (primary input variable);
- Technology and material;
- Application;
- Cost;
- Accuracy.

The classification of sensors according to their principle of operation is shown in Table 4.1 [5]. They can be divided into physical and chemical ones. Physical sensors employ physical effects, such as piezoelectric, magnetostrictional, ionization, thermoelectric, photoelectric, magnetoelectric, etc. Chemical sensors include sensors based on chemical adsorption, electrochemical reaction, etc. In both cases the smallest changes in the quantity being measured are converted into an electrical signal.

Sensors	
Physical sensors	Chemical sensors
Optical sensors	Gas sensors
Pressure sensors	Humidity sensors
Temperature sensors	Ionic sensors
Magnetic Sensors	Biochemical sensors
Acoustic Sensors	
Sensors for radioactive radiation	

Table 4.1 Classification of sensors according to the principle of operation [5]

4.3 Gas sensors

Availability of a reliable and a self-calibrating sensor capable of detecting and continuosly monitoring gases under consideration during service and industrial operation over a long period of time making a major impact. In recent years, many efforts have been focused on the development of sensor technologies to detect the content of gases in various conditions, such as chemoluminescence, ion selective electrode, biochemical sensor, optical sensor and solid electrolyte sensor (electrochemical sensors).

Sample turbidity, color and the presence of metal ions affect chemoluminiscence methods. They require a long response time and additional reagents. Ion selective electrodes have been commercially available since 1974. They have the advantage of simple design, rapid response, possible interfacing with automatic and computerized systems and can be applied in case of turbidity, and coloured samples. However, they can only be used in aqueous solution. Biochemical gas sensors using a gas-permeable membrane with immobilized bacteria can detect gases in the ppm (parts per million) range. The selectivity of the microbial sensor is also satisfactory. However, biochemical sensors can not be applied to gas detection in industrial gases at elevated temperatures.

Optical gas sensors have recently attracted growing attention. The advantages of optical sensors, which rely on electrical signals, are higher resistivity to electromagnetic noise, less danger of fire ignition, compatibility with optical fibres and the potential of multi-gas detection using differences in the intensity, wavelength, phase and polarization of the output light signals [7].

Solid electrolyte (electrochemical) sensor is one of the most promising gas sensors for commercial application because of its high selectivity, ease of operation, fast response and simple construction. Moreover, detection of gases using solid state chemistry is a relatively new field, which has generated a great deal of interest from academic and industrial application viewpoints. Particularly,

electrochemical devices have received a major share of attention in the development of galvanic sensors.

4.3.1 Solid state electrochemical gas sensors

In recent years, much progress has been made in the direction of development and application of solid state electrochemical sensors. The work, to a large extent, is related to the understanding of the electrode reaction at the side exposed to the test gas. It has become increasingly important to detect various oxidizable gases for technological reasons and global protection. The electrochemical gas sensors are generally categorized into several modes of operation: potentiometric, amperometric, coulometric, pump-gauge and semiconducting [8].

The amperometric sensors became interesting alternatives in providing better sensitivity with a simpler device configuration that eliminates the use of a reference electrode. A schematic diagram of the limiting-current sensor is shown in Fig. 4.1 [9]. The device is used to pump gas X_2 from the cathode to the anode, the processes occurring at the electrodes being

$$X_2 + 2V_X^{\cdot\cdot} + 4e \xleftrightarrow{\text{cathode / anode}} 2X_X^x . \qquad (4.1)$$

This equation assumes that X is divalent for simplicity but Eq. (4.1) may readily be transformed for alternative valency of the active species.

A porous barrier is fixed in front of the cathode to restrict transport of X_2 to the electrode. If a sufficient voltage is applied between the anode and the cathode then the partial pressure of X_2 at the cathode is reduced to a value close to zero. This is the limiting condition and the current flowing, I_{lim}, is controlled by the rate of diffusion of X_2 through the porous barrier according to Fick's first law

$$I_{lim} = nFD\left(\frac{Q}{L}\right)c_{X_2} . \qquad (4.2)$$

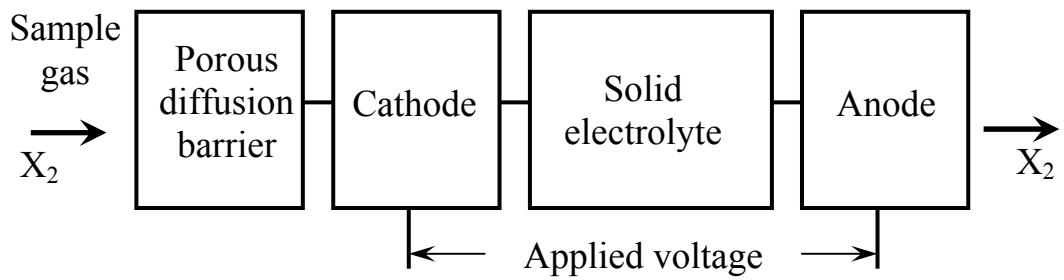

Fig. 4.1: Schematic diagram of the limiting-current sensor [9]

n is the number of electrons transferred per molecule of X_2 and D is the diffusion coefficient; Q is the sum of the cross sections of the pores of effective length L, c_{X_2} is the concentration of X_2 in the sample gas, and F is Faraday's constant. Equation (4.2) shows that the limiting current is proportial to the gas concentration. It means that the sensors measure limiting current that are related linearly to oxygen concentration [9].

In coulometry a given volume of gas is quantitatively converted by electrolysis and the partial pressure determined from the charge passed. The device comprises an electrochemical pump and a leak into an enclosed volume. Initially a constant current is applied to the pump to remove gas rapidly from the cavity much faster than its leakage rate through the aperture [10].

When almost all the gas is removed the voltage on the pump rises sharply. The current is then discontinued and a period follows during which gas leaks into the enclosed volume from the surrounding gas. This period is long enough so that the inner and outer gases closely approach equilibrium. The pump current is then re-applied and the cycle repeated. The oxygen partial pressure in the sample gas can be calculated by invoking Faraday's law as follows

$$p_1 = \frac{RTq}{4FV_1} \tag{4.3}$$

where q is the charge passed, V_1 is the enclosed volume, R and T represent the universal gas constant, absolute temperature of the active region of the electrolyte, respectively. If the current applied is constant (I) then p_1 is given by

$$p_1 = \frac{RTI\tau_1}{4FV_1}. \tag{4.4}$$

The measured value τ_1 is directly proportioned to the partial pressure, p_1.

Pump-gauge devices employ appropriate ionic conductors in both the pumping (Eq. (4.1)) and sensing modes (Eq. (4.6)). The device consists of an enclosed volume and two ionically conducting materials each in contact with both the internal and external gases. There may also be a pore or porous material connecting the inter and outer regions [8]. These arrangements allow the measurement of external gas partial pressure via a number of operating modes such as coulometric [11], amperometric without fixed reference [12], amperometric with fixed reference [9] and potentiometic with monitored internal reference [13].

It is well known that a semiconducting oxide can change its electrical resistance when its surface comes into contact with a gas. Such a material is thus a potential gas sensor. In an n-type semiconductor, the concentration of conducting electrons can be decreased by an oxidizing reaction or increased by a reducing reaction. In a p-type semiconductor with holes as major charge carriers, the reverse changes in hole concentration are observed. These phenomena are the result of the change in concentration of the adsorbed gas and/or the gas vacancies on the surface of the

semiconductor by the adsorption of the gases. Important semiconducting oxide ceramic materials are titania (TiO_2), SnO_2, ZnO, perovskite-type oxides (e.g., $BaTiO_3$) etc [6].

Among the mentioned above semiconductors, another route for selectivity involves the use of both p- and n-type semiconductors in various architectures, including p-n transition sensors, heterocontacts and composites. Several semiconducting metal oxides, such as Ta_2O_3 and $BaTiO_3$ exhibit transitions between n- and p-type behavior that are dependent on temperature, oxygen partial pressure and impurity concentrations. The transition between n- and p-type regimes has been observed upon exposure to gases. Additionally, keeping the temperature constant and increasing the CO concentration also resulted in transition from n- to p-type behavior [14].

The potentiometric solid electrolyte gas sensor can be depicted as follows [15]

$$X_2(p_2), M_2 \mid SE \mid M_1, X_2\ (p_1) \tag{4.5}$$

where M_1 and M_2 are electronic conductors and act as cell electrodes to which electrical connections may be made; the solid electrolyte (SE) should be physically impervious to the gas X_2 which is at partial pressures p_1 and p_2; the electrolyte usually has a mobile ion which is a charged species of the gaseous atom.

The voltage (U) of cell (4.5) assuming reversibility is given by

$$U = \frac{RT}{nF}\int_{p_2}^{p_1} t_{ion}\, d\ln p\,. \tag{4.6}$$

t_{ion} is the transport number of the mobile ion. The electrolytes generally chosen have a very low electronic transfer number under the conditions of operation, so that t_{ion} is close to unity [15].

Oxygen potentiometric sensors based on stabilized zirconia have been one of the most successful application of solid electrolytes. In 1961, Weissbert and Ruka [16] reported the first solid electrolyte oxygen sensor using zirconia solid electrolyte. A typical example is the “zirconia oxygen sensor”, an elementary arrangement of which is represented by

$$p_{O_2}\,(\text{known}), Pt \mid YSZ \mid Pt,\ p_{O_2}\,(\text{unknown}) \tag{4.7}$$

where YSZ is yttria-stabilized zirconia. These sensors have been widely used for industrial processing under controlled atmosphere or for the control of oxygen in molten salts. Partially and fully stabilized zirconia composition have been applied. Beside Y_2O_3, CaO and MgO are widely used for the stabilization of zirconia in commercially oxygen sensors since 1970.

Potentiometric sensors are performed when two gas compartments are separated by a solid electrolyte with platinum electrodes attached to both sides (see Eq. (4.7)). The potentiometric mode of operation employs the Nernst equation

$$U = \frac{RT}{4F}\ln\left[\frac{p_{O_2}(\text{known})}{p_{O_2}(\text{unknown})}\right], \tag{4.8}$$

in which the measured cell voltage (U) represents the logarithm of the ratio of the oxygen partial pressures in the environment (p_{O_2}(unknown)) and a known reference (p_{O_2}(known)) such as air.

The pace of advance in potentiometric gas sensing devices is related to the progress in the field of solid state ionics. A number of solid electrolytes (anion- and cation-conducting) and mixed conductors (ionic and electronic) are made available for advanced solid-state gas sensors. Inherent simplicity and obtaining a direct electrical readout made them more attractive over the conventional volumetric methods. Success with solid state oxygen detector based on stabilized zirconia in the ppm concentration range has simulated much interest among scientists and engineers to construct other types of electrochemical gas detectors for the measurement of ambient and industrial pollutants. Such devices are called "mixed-potential sensors". Oxygen (usually, air) is present as one component of a nonequilibrium gas mixture containing products of incomplete combustion. Other important components include CO, NO_x, and a variety of hydrocarbons [17]. As different types of electrochemical solid state mixed-potential gas sensors for some kinds of oxidizable gases, various combinations of solid electrolytes and electrodes have been tested, as listed in Table 4.2 [18].

Gas	Sensor structure[a] Air, (cat), RE|electrolyte|SE, (cat), target gas	Sensing property		Year	Ref.
		Operating temp. [°C]	Gas conc.		
CO	Air,Pt|YSZ|Pt(Pd),CO(+air)	500-700	0-1.5 %	1978	[19]
	CO(+air),(Pt-Al_2O_3),Pt|YSZ|Pt,CO(+air)	260-350	0-100 ppm	1980	[20]
	CO(+air), (Pt-Al_2O_3),Pt|YSZ|Pt,(SnO_2+KCl),CO(+air)	360	100-3000 ppm	1980	[21]
	CO(+air),WO_3(+Pt)|$Sb_2O_5 \cdot 4H_2O$|SnO_2(+Pt),CO(+air)	Room temp.	0-1000 ppm	1985	[22]
	Air,Pt|YSZ|Pt,(CuO-ZnO/Al_2O_3),CO(+air)	450	0-10 000 ppm	1990	[23]
	CO(+air),Au|ß-alumina|Pt,CO(+air)	500	75-600 ppm	1993	[24]
	Air,Pt|YSZ|Pt,CO(+air)	500	32-800 ppm	1995	[25]
	CO(+air),$LaMnO_3$|YSZ|$LaMnO_3$,(Pt-Al_2O_3),CO(+air)	350-450	0-7000 ppm	1997	[26]
	CO(+air),Pt,SnO_2|YSZ|CdO,Pt,CO(+air)	600	20-4000 ppm	1997	[27]
NO_x	O_2,ref.electrode|YSZ|sensing electrode,NO(+air)	500	0-500 ppm	1991	[28]
	Air,Pt|NASICON|Cr_2O_3,Au,NO_x(+air)	250	5-200 ppm	1996	[29]
	Air,Pt|YSZ|$CdMn_2O_4$,Pt,NO_x(+air)	500-600	5-4000 ppm	1996	[30]
	Air,Pt|YSZ|$CdCr_2O_4$,Pt,NO_x(+air)	500-600	20-600 ppm	1997	[31]
	Air,Pt|YSZ|WO_3,Pt,NO_x(+air)	500-700	4-800 ppm	1998	[32]
C_xH_y	Air,Pt|YSZ|SnO_2,Au,C_xH_y(+air)	380	0-1000 ppm	1991	[33]
	Air,Pt|$CaZr_{0.9}In_{0.1}O_3$|Au,C_xH_y(+air)	700	0-1 %	1994	[34]
	Air,Pt|YSZ|Au,C_xH_y(+air)	600	0-500 ppm	1998	[35]

[a]RE: reference electrode, SE: sensing electrode, cat:catalyst.

Table 4.2: Typical examples of electrochemical solid state gas sensors [18]

Fleming [36] first introduced the exhaust mixed-potential gas sensor consisting of an yttria-stabilized zirconia (YSZ) tube with porous platinum electrodes formed on both its inner and outer surfaces for the determination of air-fuel (A/F) ratio in the exhaust gas stream. One end of the tube is closed so that it can be inserted into exhaust stream which heats the tube; a schematic illustration of the sensor is shown in Fig. 4.2. Sensor voltage curves calculated by Nernst equation are shown in Fig. 4.3, but actual sensor behaviour deviates from the ideal one.

4.4 Different possibilities of sensing the CO

4.4.1 Sensors based on oxygen ion-conducting solid electrolytes

Electrochemical gas sensors depend on the ionic transport property of the solid electrolyte as described by Kiukkola and Wagner [37, 38]. Since Weissbart and Ruka [16, 39] reported their solid-state oxygen sensor using yttria-stabilized zirconia (YSZ) solid electrolyte, many different cell designs and operating modes have been proposed [9, 40-53]. Among the various solid electrolytes, YSZ was the most commonly used in these designs [20, 21, 36, 54-65].

According to literature, most investigations of the CO sensitivity are based on two types of construction of the galvanic cells: two-compartment and one-compartment (or planar) cell configurations.

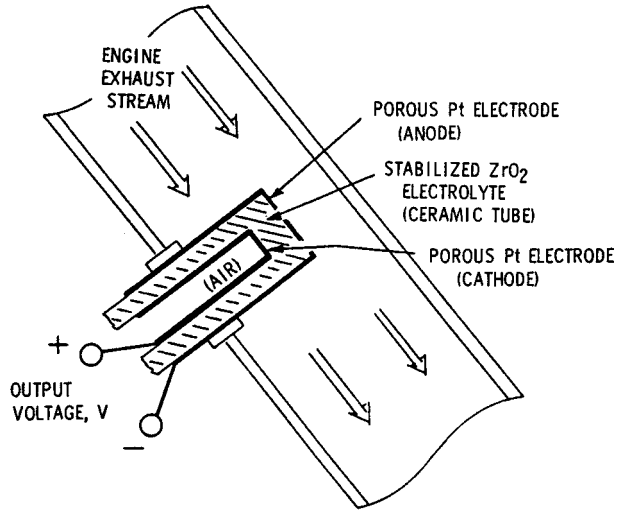

Fig. 4.2: Schematic illustration of zirconia exhaust sensor (cross view) [36]

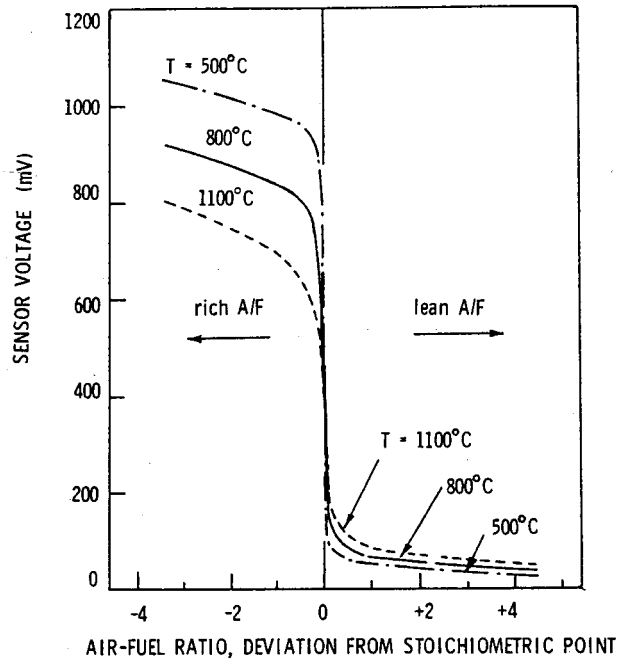

Fig. 4.3: Ideal sensor voltage curves [36]

4.4.1.1 Two-compartment sensor configuration

The general principle of this galvanic cell configuration is that the gas stream is divided by two parts with different oxygen partial pressures. Thus, one of the electrodes is working and another is the reference one. Constructions can be as two tubes with solid electrolyte in between [20, 35, 36, 58-61, 66-69], or one-end-closed tube and surrounding atmosphere [27, 56, 57, 66, 70-73], etc.

Besides the sensors based on YSZ, which were discussed above, several other oxygen ion-conducting solid electrolytes are described in the literature used in those sensors.

Pt|$Ce_{0.8}Gd_{0.2}O_{1.9}$|Au sensors were found to have a lower but more stable response than YSZ-based sensors in the presence of reducing gases. This difference in response characteristics has been attributed to the better oxygen reduction kinetics of metal electrodes on ceria-based electrolytes [74]. All Pt|$Ce_{0.8}Gd_{0.2}O_{1.9}$|Au sensors exhibited a mixed potential in the presence of reducing gases at both 600 and 550 °C. The individual mixed-potentials at the Pt and Au electrodes with respect to an air-reference are plotted in Fig. 4.4 (a) and (b) to CO in O_2 (1 %) of sensors at 600 and 550 °C, respectively [75]. It is seen that the Pt electrode at equilibrium at these temperatures and the sensor response is primarily due to the mixed potential at the Au electrode. The potential of the Au electrode was as high as –91 mV for 500 ppm of CO at 550 °C, which corresponds to a mixed potential of 61 mV [75].

Considering stability of Pt and Au electrodes, it should be noted that while the Pt electrode is stable at both temperatures, the Au electrode changes with time and reaches a steady state only at 550 °C. The decrease in the mixed potential of the Au electrode with time was accompanied by the recrystallization of the Au. These results suggest that the sensor response is dependent on the morphology of the electrode. Moreover, the response from the Au electrode stabilized at 550 °C, probably due to the stabilization of the gold morphology at this lower temperature [75].

Thus, the Pt|$Ce_{0.8}Gd_{0.2}O_{1.9}$|Au sensor showed a stable mixed-potential response to various reducing gases at 550 °C. The mixed potential on an electrode was dependent on both the total amount of electrochemical oxidation of the reducing gas and the overpotential for oxygen reduction on that electrode. The Au electrode always exhibited a greater overpotential than Pt electrode for the oxygen reduction reaction, resulting in larger mixed potentials [75].

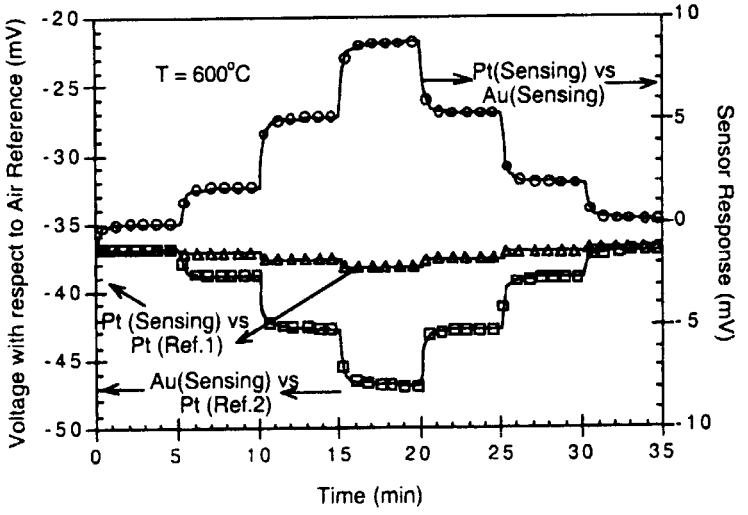

(a)

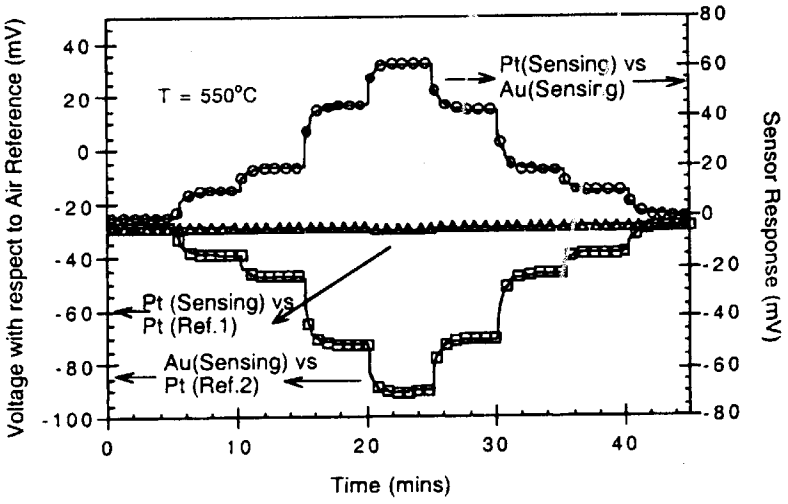

(b)

Fig. 4.4: Response of a Pt|$Ce_{0.8}Gd_{0.2}O_{1.9}$|Au sensor to CO in O_2 (p_{O_2} =1·10^3 Pa). (a) T=600 °C: 0, 100, 300, 500, 300, 100, 0 ppm CO. (b) T=550 °C; 0, 50, 100, 300, 500, 300, 100, 50, 0 ppm CO [75]

4.4.1.2 Planar sensors

This type of construction represents an one-compartment (or planar) cell configuration [20, 23, 24, 65, 67, 71, 76, 77]. “Planar solid-state sensors” [53] have been extensively used as primary sensing elements for the fabrication of other gas sensors for sensing catalytically carbon monoxide. In these sensors, one electrode (see Fig. 4.5) is covered with a catalytic material to catalyse the oxidation of the solute gas [20, 23, 40-43, 78]. The oxygen consumed in the catalytic oxidation process results in a lower oxygen concentration at this electrode than that in the absence of oxidizable gas solute. This

kind of electrode is often so-called “pseudo-oxygen electrode”. The voltage therefore depends directly on the bulk concentration of the reducing gas species in the mixture and can thus be calibrated [53].

This sensor type has a planar geometry of electrodes. All three electrodes are located on the same side of a substrate. A galvanic cell

$$p^{B}_{O_2}, p^{B}_{CO} \mid \text{catalyst} \mid p^{I}_{O_2}, p^{I}_{CO}, \text{Pt} \mid \text{stabilized } ZrO_2 \mid \text{Pt}, p^{B}_{O_2}, p^{B}_{CO}, \qquad (4.9)$$

where $p^{B}_{O_2}$, p^{B}_{CO} are the partial pressures of O_2 and CO at the bare electrode (air), respectively, and $p^{I}_{O_2}$, p^{I}_{CO} are the partial pressures of O_2 and CO at the catalyst-covered platinum electrode [65], is an useful high-temperature CO sensor. The cell is used simply by inserting it in the gas stream unlike those without the catalyst coating where one electrode is exposed to the test mixture while the other is exposed to a reference mixture [23, 42, 45].

Okamoto and co-workers have exerted a lot of efforts on investigating the non-ideal behaviour at lower temperatures in order to develop gas sensors for practical uses [20-22]. For example, a CO sensor was developed by covering a Pt electrode with a CO oxidation catalyst. It has been reported [20] to have good CO-sensing characteristics in the temperature range 260-350 °C by covering the electrode of the oxygen sensor with a layer of $H_2PtCl_6/\gamma\text{-}Al_2O_3$ to catalyse the oxidation of carbon monoxide. The construction of this type of the CO gas sensor is shown in Fig. 4.5 [20].

Li et al. [23] reported about a CO sensor in which stabilized zirconia was coated with a $CuO/ZnO/Al_2O_3$ catalyst layer, similar to that reported by Okamoto [18, 23, 53]. $CuO/ZnO/Al_2O_3$ is a well-known catalyst for industrial water-gas regeneration [79] and methanol synthesis [80]. CuO shows better high-temperature adsorption characteristics for oxygen than CO and has no affinity for CO_2 [81]. ZnO has a stabilizing effect on the catalytic activity of CuO and improves its resistance to sulphide poisoning [82]. Al_2O_3 provides better mechanical strength and structural stability to the mixture [53].

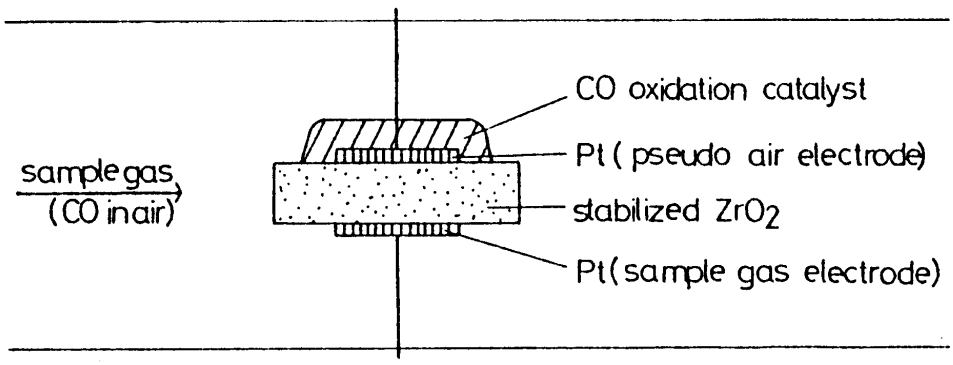

Fig. 4.5: Structure of the planar CO gas sensor operable in air [20]

A typical electrical response of a CO sensor in the presence of CO in a steady flow air stream is shown in Fig. 4.6. The response was almost instantaneous, and the time to reach its steady-state reading increased with decreasing temperatures [23].

It was assumed that the CuO catalyzed oxidation of CO proceeds according to a single-site mechanism whereby the adsorbed CO on the active site (s) of the CuO catalyst surface reacts with O_2 in the gas to form CO_2. The reactions occurring in the oxide layer are described as follows [23]

$$2CO + 2s = 2CO{\cdot}s \text{ – adsorption/desorption,} \quad (4.10)$$

$$2CO{\cdot}s + O_2 = 2CO_2 + 2s \text{ – catalytic oxidation,} \quad (4.11)$$

$$2CO + O_2 = 2CO_2 \text{ – overall.} \quad (4.12)$$

In [53] the sensor response for different CO concentrations and temperatures were determined from the respective sensor current-time curve. A linear relationship was obtained at all temperatures over the CO concentration range 0-0.18 mol%. The linear relationship shows that the catalytic oxidation kinetics are of first order with respect to CO concentration and the O_2 concentration is sufficiently high to maintain saturation with respect to its adsorption on the catalyst surface.

In order to miniaturize and simplify the sensor structure, a chip type device was designed and fabricated by using a small bar of yttria-stabilized zirconia [71]. As an example of a particular chip device, a CO sensor has been constructed by coupling electrodes of SnO_2 and CdO, as shown in Fig. 4.7 (a) [27, 71]. The voltage values of this kind of planar sensor were stable and varied logarithmically with the CO concentration in the range of 20-4000 ppm. In addition, the voltage was not significantly affected by other gases, such as H_2, NO, NO_2, CO_2, O_2, and H_2O, as shown in Fig. 4.7 (b). Due to its good CO sensing characteristics, the YSZ-based device attached with the CdO and SnO_2 electrodes has the potential of a CO sensor to be used in high-temperature combustion exhaust [71].

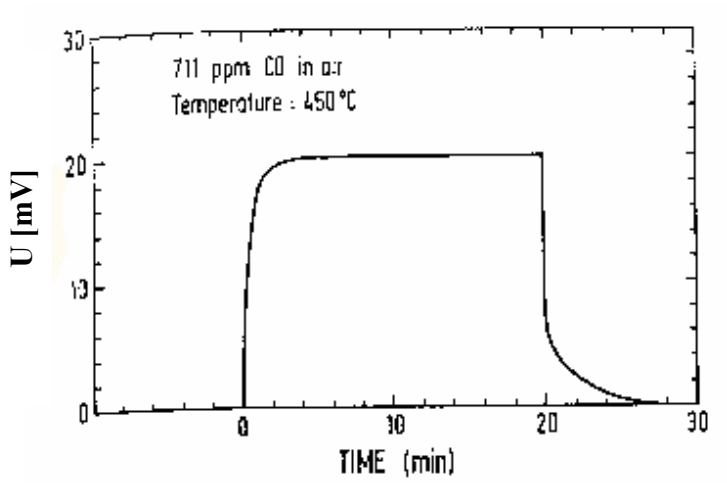

Fig. 4.6: Typical response curve of the CO sensor [23]

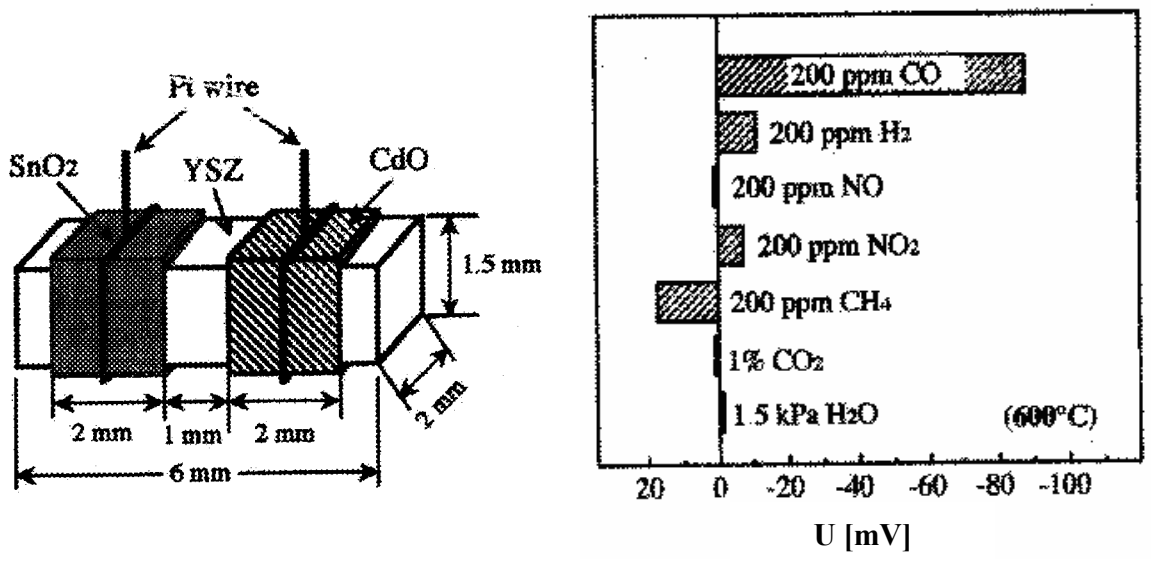

(a) *(b)*

Fig. 4.7: Chip type YSZ-based device attached with CdO and SnO_2 electrodes [71]. (a) Schematic view of device structure, (b) sensitivities to various gases at 600 °C

As another example of a planar sensor the following structure was introduced

$$p_{O_2} + p_{CO}, LaMO_3 \mid YSZ \mid p'_{O_2} \mid \text{catalyst}, \; p_{O_2} + p_{CO}. \qquad (4.13)$$

$LaMO_3$ (M = Mn, Cr, Fe and Co) electrodes were prepared from powders of the constituent oxides through conventional solid-state reactions [26]. It has been revealed [83-86] that perovskite-type oxides $LaMO_3$ (M = V, Cr, Mn, Fe, Co and Ni) show high catalytic activities for the oxidation of CO. In addition, these compounds exhibit high ionic and electronic conductivities and have thus been studied widely for the use as electrode materials of solid oxide fuel cells [26, 87, 88]. It is very important to mention that each sensor has to be individually calibrated unless the fabrication process can be so automated and controlled as to give identical physical characteristics of the oxide coating [23].

4.4.2 Sensors based on cation-conducting solid electrolytes

Apart from zirconia-based sensors, Maruyama et al. [89, 90] studied CO-CO_2 sensors based on Na_2CO_3 [89] and $Na_3Zr_2Si_2PO_{12}$ (NASICON) [90] solid electrolytes. They investigated the voltage dependencies on different CO-CO_2-O_2 mixtures at low oxygen partial pressure. Later on, Petrolekas et al. [91] used the NASICON solid electrolyte in galvanic cell with Pt and Au electrodes for ethylene oxidation. Shimizu and Maeda investigated a NO_x sensor based on the NASICON solid electrolyte and an auxiliary phase of metal oxide [28].

Recently, Otagawa et al. [92] built and studied a planar CO sensor, which was composed of a solid polymer electrolyte (Nafion®) and an amperometrical measuring system (see Fig. 4.8). This sensor

also had a planar geometry of electrodes. In ist basic design, all three electrodes were located on the same side of a substrate. This allowed any geometrical arrangements of the electrodes to be fabricated easily on proton conductive films [93].

The mechanism to monitor the CO concentration in air is also shown in Fig. 4.8 [93].

The reaction scheme on the working electrode is

$$CO + H_2O \rightarrow CO_2 + 2H^+ + 2e^- \quad (4.14)$$

and on the counter electrode

$$2H^+ + 1/2O_2 + 2e^- \rightarrow H_2O \quad (4.15)$$

resulting in a net reaction of

$$CO + 1/2O_2 \rightarrow CO_2. \quad (4.16)$$

CO, CO_2 and O_2 gas permeate through the polymer electrolyte film, while H^+ and H_2O diffuse into the film. The electric current between working and counter electrodes is thought to be proportional to the oxidation rate of CO. In cases where the reaction controlling step is the permeation of CO, the current is thought to be proportional to the concentration of CO. Figure 4.9 shows that the proportional relationship between current and CO concentration was established to be below 700 ppm. As a result, a sensitivity of 0.04 nA/ppm was obtained. Considering that, the minimum sensitivity of the present sensor can be 25 ppm CO. Additionally, in the application of a Nafion® film, the transport behaviour plays a major role [93].

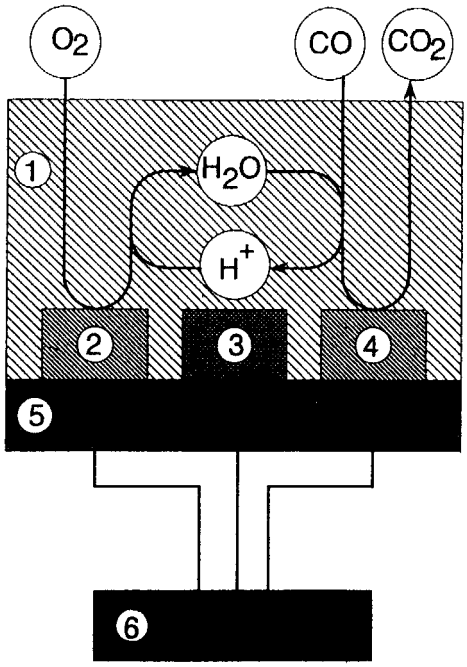

Fig. 4.8: Mechanism to detect CO by its oxidation current: (1) Nafion®; (2) counter Pt electrode; (3) reference Au electrode; (4) working Pt electrode; (5) alumina substrate; (6) potentiostat [93]

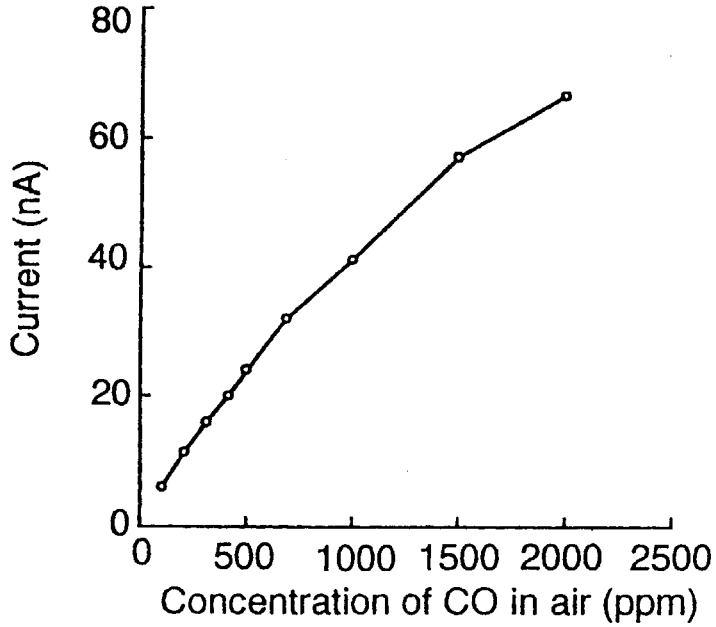

Fig. 4.9: CO oxidation current with various concentrations of CO at 20 °C [93]

4.5 Sensing electrode material used in the solid electrolyte galvanic cells

Solid-electrolyte oxygen sensors have been used in a variety of applications for over three decades [37, 94]. Almost all applications have either involved the monitoring of O_2 in inert environments or the measurement of equilibrium O_2 in reactive environments. For these purposes, platinum is the electrode material of choice due to its excellent O_2 electrode capabilities (e.g., low polarization) as well as its high catalytic activity for driving oxidation reactions to equilibrium [62].

There have been several attempts to use the YSZ-based device as mixed-potential sensor for CO at high temperatures. These attempts have not been so successful, however, because the voltage responses to the reducing gases have remained rather too modest. The main cause seems to be associated with the use of Pt-sensing electrodes due to that, at high temperature, the reducing gases may be oxidized out before reaching the (tpb), whereas operating temperatures lower than about 350 °C cannot be adopted due to the restriction of ionic conductivity of YSZ [18].

4.5.1 Pure metals and metal-doped materials

As it was mentioned above, the noble metal Pt has been widely used as a sensing electrode for the CO mixed-potential type gas sensors using stabilized zirconia [18]. However, the sensors with Pt electrodes exhibited small voltage responses to target gases at operating temperatures above ca. 500 °C and gave poor gas selectivities at temperatures below ca. 400 °C [95].

Despite a very large number of experimental and theoretical studies there still exists a number of unresolved questions regarding the exact mechanism and the origin of hysteresis, steady-state multiplicity, and limit cycle phenomena observed during the reaction under both atmospheric and low-pressure conditions [95]. In order to get over these difficulties, a search for sensing electrode materials was carried out to include other noble metals and noble alloys [18]. NNEP have been reported to occur at various electrode systems and in a broad temperature range (see Table 4.3) [57]. Unfortunately, the catalytic activity of Ag electrodes to CO oxidation, although reduced from that of Pt, is still too high even for qualitative O_2 measurements. And also, there is a high solubility of O_2 in silver [62]. Au paste electrodes were investigated since oxygen is neither soluble in nor adsorbed on Au [96], and Au is less catalytic to oxidation reaction than Pt [97]. Au electrodes were found to be slightly more catalytic than Ag electrodes [62]. The investigation of the electrochemical oxygen pumping on the CO oxidation on an Au electrode-catalyst in the cell with the solid oxygen-conducting electrolyte [63]

$$CO+O_2, Au \mid YSZ \mid Ag, PrO_{2-x}, air \qquad (4.17)$$

has been done. In accordance with the data available in the literature Au is a catalyst for the CO oxidation [98-100] and is an active electrode for the electrochemical oxidation and reduction of oxygen in the cell with a solid oxygen-conducting electrolyte [67, 101, 102].

The observed kinetic data [106, 107] permit us to make some conclusions about the mechanism of CO oxidation on Au. It seems reasonable to suppose that the $CO+O_2$ reaction follows the Eley-Rideal mechanism with the participation of a strongly bound oxygen state, whose surface coverage is close to unity. A strongly bound oxygen state on Au, stable up to 800 °C in vacuum, was detected by various surface science techniques after exposure of Au in O_2 at low pressure (10^{-6} Torr) and temperature above 200-300 °C [108-113]. An alternative Langmuir-Hinshelwood mechanism can also be proposed. For example, it is possible that a weakly bound molecular state of CO as well takes part in the process. According to the data obtained [63], the catalytic properties of Au in contrast to Pt and Pd electrodes [107, 114] did not alter essentially.

Electrode material	Temperature range [°C]	Ref.
Pt	260-350	[20, 36]
Au	550-700	[103, 104]
Ag	500-650	[103]
$MoSi_2$	550	[104]
Pt + (V_2O_2, TiO_2, CuCo, Co_3Co_4)	300-550	[105]

Table 4.3: List of electrode materials at which NNEP have been reported to occur [57]

Vogel et al. found that sensors using Pt-based alloy electrodes gave a higher voltage response to CO even at the high temperature of 550 °C [57]. Bimetallic alloy catalysts exhibit different properties than their single metal counterparts because the presence of foreign metal atoms at the surface changes its electronic and structural nature. In addition to the surface composition, the structure of the alloy also affects its catalytic properties. The increased gas sensitivities of the sensors attached with alloy electrodes were considered to be due to a reduction in the catalytic activity for the gas phase oxidation of CO by alloying Pt with Au, Ag, Cu, Ni and Rh.

In Table 4.4 the voltages developed at electrode materials in the presence of 1000 ppm CO are shown. The Pt/Au and the Mo electrode reveal the largest CO sensitivity. Changes of the voltage monitor these variations of surface properties. In case of the Mo electrode the metal could have been oxidized to MoO_3 with higher catalytic activity. Oxidation of the transition metal component is also assumed to be the reason for the degradation of the Pt/Ni and Pt/Cu electrodes. In the case of the Pt/Rh and the Pt/Ag electrodes the aging could result from diffusion of the metal component at the working electrode into zirconia leaving behind a pure Pt electrode at the surface layer with high catalytic activity [57].

With the exception of the Pt/Au electrode all the materials showed a strong degradation of sensitivity. After 16 days the voltage characteristic for Mo electrodes resembles that of a Pt electrode. The Pt/Ag and Pt/Rh electrodes behaved in a similar way, whereas it was not possible to perform reproducible measurements with Pt/Cu and Pt/Ni electrodes for longer than one day. The Pt/Au electrode did not show this aging effect. After testing a number of electrode materials the Pt/Au electrode has been found to be stable for use in a solid electrolyte sensor cell for the detection of small amounts of combustible gases in the exhaust fumes of a combustion process. Lukacs et al. [73] have tried to investigate the working mechanism of the Pt-Au electrode, i.e. to clarify whether carbon monoxide takes part in an electrochemical reaction step or is oxidized only in a chemical step, i.e. in a heterogeneous catalytic reaction. However, the working mechanism of the Pt-Au electrode at high temperatures is still not completely understood [57].

The thermodynamic and kinetic measurements [61, 115] show that the surface reaction of the Pt-Au|zirconia sensor contains an electrochemical oxidation step of CO which determines the formation of mixed potentials and the polarization resistances at the mixed potentials as well as under anodic or cathodic polarization conditions [73].

	Electrode materials					
	Pt/Au	Pt/Ag	Pt/Rh	Pt/Ni	Pt/Cu	Mo
Voltage (1000 ppm CO) [mV]	81	2	12	5	21	110

Table 4.4: CO sensitivity of the working electrodes prepared in [57]

Hibino et al. [35] have used the Au sensing electrode for the determination of hydrocarbons containing C1-C4 alkanes and alkenes at 600 °C. The voltages for the alkenes became more negative as the concentration increased, whereas those for the alkanes were not significantly affected by changing the concentration. These observed behaviours, especially for the alkenes, cannot be explained using the Nernst equation. For example, assuming that all of the 500 ppm 1-butene gas is burned to CO_2 gas over the Au sensing electrode, the O_2 concentration will change from 10 to 9.7 %. According to the Nernst equation, the voltage will change from –13.9 to –14.4 mV. This can be supported by the result using the Pt sensing electrode, where the voltage for 500 ppm 1-butene is –17.7 mV. Therefore, the Au sensing electrode is found to produce large mixed potentials for the alkenes. As common features for both alkanes and alkenes at the Au sensing electrode, the negative voltage became significant as the number of carbons of the hydrocarbon molecule increased from one to four. Moreover, the mixed potential of the Au sensing electrode is enhanced in the order of alkane, alkene, and alkyne. The non-Nernstian behaviour for the hydrocarbons is closely correlated to their carbon number, structure factor, and unsaturated fraction [35, 67, 69].

It has been found also [67] that the Au electrode showed a large voltage response to propylene, but the Pt electrode had no voltage response to it. The use of a pair of Au and Pt electrodes in a one-compartment cell makes it possible to reduce the influence of the O_2 concentration on the detection of propylene. The mixed potential of the Au sensing electrode for propylene becomes smaller as the O_2 concentration increases [67].

Fifteen kinds of metal oxides were added to the Au working electrode in order to improve its selectivity and sensitivity [69]. The addition of MoO_3 and MnO_2 significantly reduced the voltage for propene. Propene will be almost completely burned to CO_2 over these metal oxides because of their high catalytic activities toward such a reaction. The addition of YSZ the voltage changed for propene only little. This can be explained by the fact that YSZ has a catalytic activity as poor as Au metal [116]. The addition of TiO_2, CeO_2, WO_3, In_2O_3, Eu_2O_3, and SrO showed voltages for propene near the value observed using the Au working electrode. Ta_2O_5 and Nb_2O_5 were the most effective additives in enhancing the voltage for propene. These values correspond to about three times the value of the cell using an Au working electrode. Both Ta_2O_5 and Nb_2O_5 are oxides of V_a metals. V_2O_5, belonging to the same group, unfortunately cannot be examined because of a melting point lower than 600 °C. However, it can be presumed that the best addition effect of Ta_2O_5 and Nb_2O_5 is common property to the oxides of group V_a metals [69].

4.5.2 Oxide materials

The electrical resistance (conductance) of a metal oxide depends sensitively on the oxygen vacancies in its lattice and the gases adsorbed at the surface. Reactive/reducing gases such as hydrocarbons, CO, and H_2 cause a change in the oxygen balance of an oxide when they come in contact with the oxide surface at elevated temperatures [117].

The resistance of the MoO_3 thick film decreased rapidly in the presence of small concentrations of CO in the gas stream and reached a value which was several orders of magnitude lower than that before the introduction of CO into the furnace. When the concentration of CO was increased further, however, the resistance did no longer show a significant change. It is generally accepted that the chemisorption and ionosorption of O^{2-} ions on the surface of oxides creates a thin layer of high electric resistance. When these chemisorbed or ionosorbed oxygen species are consumed by a reducing gas, the net result is an accumulation of free electrons which is manifested in the form of an increase of conductivity. Oxygen ions can be adsorbed if their negative charge is compensated by ionized donors in the bulk of the oxygen in a space-charge region [118-120]. On the other hand, from thermodynamic considerations, a defect structure, consisting of bulk oxygen vacancies and interstitial oxygen ions, acting as donor species is always present at elevated temperatures. A schematic of the defect surface of the sensor is shown in Fig. 4.10 (a). The following defect equilibrium could be written in terms of Kroeger-Vink notations

$$O_O \rightarrow O_i'' + V_O^{\cdot\cdot} \tag{4.18}$$

where O_O is an oxygen atom at the lattice position, O_i'' is an interstitial oxygen with two negative charges and $V_O^{\cdot\cdot}$ is an oxygen vacancy with two positive charges (relative to the lattice) [117].

The reaction of CO with the surface might occur as

$$CO_{(g)} + O_i'' \rightarrow CO_{2(g)} + 2e^- \tag{4.19}$$

or

$$CO_{(g)} + O_O \rightarrow CO_{2(g)} + V_O^{\cdot\cdot} + 2e^- . \tag{4.20}$$

It is evident that by virtue of the reaction (4.19), the equilibrium interstitial oxygen concentration $[O_i'']$, decreases and according to Eq. (4.20), the oxygen vacancy concentration would increase. In either case, this would result in a decrease in the resistance of the sample, by virtue of generation of free electrons and their migration into the conduction band. For a given concentration of CO, there would exist an equilibrium concentration of the oxygen vacancies and as the time progresses, a plateau would reach in the resistance dependence. A hypothetical schematic of the reduced surface is shown in Fig. 4.10 (b). It appears that the experimental results are in better conformity with the reaction of CO as per Eq. (4.19) rather than Eq. (4.20) [117].

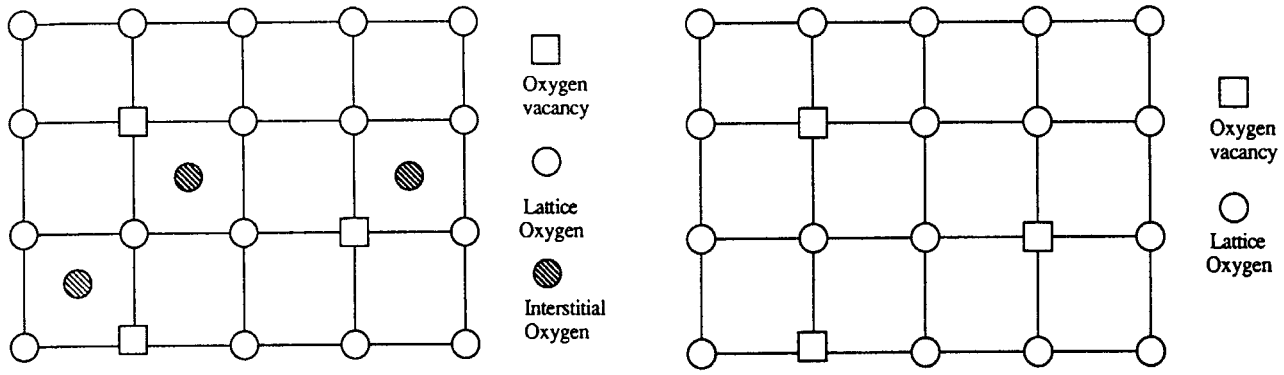

(a) *(b)*

Fig. 4.10: Hypothetical crystal defect structure of (a) the sensor surface and (b) the reduced surface [117]

Recently, a high-performance solid-state compact gas sensor to detect CO was needed for monitoring and controlling the combustion condition and appliances. The sensor used should have high CO sensitivity as well as high CO selectivity against other gases, such as H_2, hydrocarbons, NO_x, and H_2O, coexisting in combustion exhausts. Moreover, the sensor must work at high temperatures. Miura et al. [27] have measured the voltages to 200 ppm CO at 600 °C for devices attached with each of fifteen kinds of single-metal oxides. As a result, it was found that the voltage depended largely on the kind of oxide used and could have large negative values with some oxides, such as ZnO, CdO, In_2O_3, and SnO_2, even at 600 °C. The voltage varies almost linearly with the logarithm of the gas concentration in each case. The largest CO response as well as the largest CO sensitivity was attained with CdO electrode. It seems that the sensing mechanism of the present device may be explained on the basis of the mixed potential model, as was done in other zirconia-based gas sensors [20, 27, 30, 57, 121-126].

Hibino et al. [68] have investigated the sensing properties of various oxide electrode materials in the two-compartment cell at 600 °C. The sample gas containing 0 or 500 ppm carbon monoxide and 10% oxygen was fed to the sensing electrode. Table 4.5 summarizes the voltages observed using the various metal oxide electrodes. In the absence of reducing gas, most of the electrodes gave voltages of ca. –14 mV, which corresponded to the value calculated from the Nernst equation. In the presence of such a gas, electrodes exhibited more negative voltage values for 500 ppm CO [68].

Electrode material	Voltage [mV]	
	0 ppm CO	500 ppm CO
Ta_2O_5	-13	-152
Nb_2O_5	-10	-113
In_2O_3	-15	-117
SnO	-15	-84
Eu_2O_3	-5	-98
NiO	-12	-53
Nd_2O_3	-9	-60
TiO_2	-7	-44
WO_3	-11	-54
Fe_2O_3	-11	-37
CeO_2	-11	-48
RuO_2	-13	-24
MnO_2	-12	-16
Au	-15	-63

Table 4.5: Sensing properties of cells using various metal oxide electrodes for CO at 600 °C [68]

4.5.3 Spinels and perovskites

Besides the pure metal and oxide as sensing electrode materials, materials with more complicated crystal structure were investigated. In this section the sensing properties of some spinels and perovskites described in the literature until now will briefly be discussed.

Table 4.6 shows the voltage data of sensor devices attached to spinel electrode materials to 2000 ppm CO in air. It is clear that ZnM_2O_4 (M = Mn, Co) and $MnFe_2O_4$ attached sensors have a high sensitivity to CO [76].

Table 4.7 shows the voltage data of the sensor devices attached to perovskite electrode materials exposed to 500 ppm CO in air at 500 °C, investigated by Sorita et al. [26]. Because of the large voltage values in air for some devices, increments of voltage due to CO (ΔU) were taken as a measure of sensitivity to CO.

Electrode materials	ΔU (p_{CO}=2 000 ppm) [mV]	CO conversion [%]
$ZnMn_2O_4$	56.6	67.4
$ZnCo_2O_4$[a]	46.8	100
$ZnFe_2O_4$[a]	27.5	52.8
$MnFe_2O_4$[a]	23.9	100

Measurement temperature 400 °C

[a]Measured at 500 °C

Table 4.6: The voltage emf data of sensors and catalytic activity of each spinel electrode material [76]

Electrode materials	ΔU(CO)[a] [mV]	U(air) [mV]
$LaMnO_3$	13.2	2.1
$LaCoO_3$	39.7	-0.2
$LaCrO_3$	12.1	13.8
$LaFeO_3$	37.0	10.7

[a] ΔU = U – U(air).

Table 4.7: Characteristics of $LaMO_3$ (M = Mn, Co, Fe, Cr) electrode materials [26]

It is noted that the voltage of the $LaCrO_3$- or $LaFeO_3$-attached device in air exceeded 10 mV, while the $LaMnO_3$- or $LaCoO_3$-attached one indicated a value very close to 0 mV. This suggests that, on the $LaCrO_3$ or $LaFeO_3$ electrode, the electrochemical reaction of oxygen is too slow under the present conditions to attain the equilibrium electrode potential, since otherwise the voltage level in air should be 0 mV. Because of this non-equilibrium nature, these electrodes were judged to be inadequate for the sensor. The $LaMnO_3$ and $LaCoO_3$ electrodes which could reach the equilibrium state in air, $LaCoO_3$ could not stay well attached to the YSZ after several heat cycles, since its thermal expansion coefficient differed significantly from that of YSZ. Thus, they concluded that $LaMnO_3$ was best adaptable as a sensor [26].

The voltage output of the $LaMnO_3$-attached sensor to (air + 500 ppm CO) decreased at increasing temperatures. The decrease of the output to CO in the interval above 400 °C is considered to result as follows. To generate the voltage output, the electrochemical reaction of CO should take place effectively at a (tpb) between the electrode material, YSZ and gas phase. If non-electrochemical oxidation of CO takes place competitively at an increasing rate with increasing temperature, the number of CO molecules reaching the (tpb) would decrease, accompanied by a decrease in voltage output [26]. The extent of electrochemical reaction occurring at the (tpb) may be crucially important for determining the voltage [127]. At 350 °C, however, it was unreasonably large, indicating that even with this electrode the electrochemical reaction of oxygen becomes too slow to establish the equilibrium in air at this temperature [26].

When compared at the same gas concentration of 2000 ppm, the voltage to CO was 6-18 times higher than that to H_2, CH_4 or C_3H_8. Such large differences in sensitivity seem to reflect that the $LaMnO_3$ electrode catalyses the electrochemical oxidation of CO more selectively than those of the other gases [26].

4.6 Other oxidizable gases analyzed by solid electrolyte galvanic cells

Beside CO various kinds of oxidizable gases to be determined by a solid electrolyte galvanic cell were described [21, 26, 35, 62, 67-69, 75, 77, 128-131]. Various hydrocarbons and their non-Nernstian behaviour for Pt and Au electrodes in presence of C1-C4 alkanes and alkenes [35, 67] or propylene [69] were already described in chapter (4.4.1).

Hibino et al. [35] reported that the zirconia-based sensor using an Au electrode gave large voltage responses for the unsaturated hydrocarbons which were aliphatic as well as aromatic at 600 °C. In this case, such high sensitivities are also considered to be ascribed to the low catalytic activity of the Au electrode for non-electrochemical (gas phase) oxidation of the hydrocarbons [35].

The mixed potential is reduced when a non-electrochemical oxidation of the reductive gas occurs as a parallel reaction [35]. The alkanes did not react with O_2, but the alkenes were oxidized into CO_2 to a greater extent. This shows that the electrochemical and non-electrochemical reactivities of the unsaturated hydrocarbons have an opposite effect on the non-Nernstian behaviour of the sensor as reported for the other reductive gases [20, 23, 27-30, 35, 36, 57, 66, 78, 121-123].

When the sample gas containing 0-500 ppm propylene and 10 vol.% O_2 was fed to various metal electrodes at 600 °C, the Pt, Pd and Ni electrodes had a small or negligible voltage response, but the Au electrode had a large voltage response, which was based on a mixed potential. The mixed potentials of the Au electrode for H_2, CO and CH_4 were very small. As a common feature for all the sensing electrodes, the negative voltage became weaker as the temperature increased [67].

5 Mechanism of functioning

5.1 Solid electrolytes

5.1.1 Yttria-stabilized zirconia (YSZ)

Useful oxide solid electrolytes are solid solutions which have the fluorite crystal structure and abnormally high oxygen-ion conductivities [132]. The fluorite structure is a face-centered-cubic arrangement of cations with the anions occupying all the tetrahedral sites. In this structure each metal cation is surrounded by eight oxygen ions, and each oxygen ion is tetrahedrally coordinated with four metal cations. In the fluorite structure all octahedral interstitial sites are empty. Thus this structure is a rather "open" one, and rapid ion diffusion might be expected along octahedral interstitial sites [132]. Amongst them, ZrO_2- and ThO_2-based electrolytes have been studied most extensively and found suitable for a wide range of applications like fuel cells, oxygen monitors and pumps, and for various thermodynamic and kinetic measurement devices. ZrO_2-based electrolytes have the advantage of higher conductivity at a given temperature and are used in the wide oxygen partial pressure range [133].

There are three well-defined polymorphs of ZrO_2, namely, monoclinic, tetragonal, and cubic structures. The monoclinic phase is stable up to about 1100 °C where it transforms to the tetragonal phase. Finally, at approximately 2370 °C, the compound adopts the cubic fluorite structure [134] (see Fig. 5.1). Addition of some of the aliovalent oxides (such as Y_2O_3, CaO, or MgO) stabilizes the high-temperature fluorite cubic structure down to room temperature and thus avoid the tetragonal-monoclinic transformations. The replacement of Zr^{4+} cations by cations of lower charge (e.g., Y_2O_3) results in the formation of vacant sites in the anionic oxygen sublattice. In the Kröger and Vink notation, one can write this incorporation reaction of Y_2O_3 as

$$Y_2O_3 \xrightarrow{2ZrO_2} 2Y'_{Zr} + V_O^{\cdot\cdot} + 3O_O^x . \qquad (5.1)$$

Thus, the general formula of the solid solutions of Y_2O_3 and ZrO_2 is $Zr_{1-x}Y_xO_{2-x/2}$ [136]. Both the distributions of the stabilizing cations and resulting vacant anion sites are statistical. The oxygen vacancies may move through the lattice, thus providing electric conductivity by the transport of electric charge. In order that the energy required for the movement of oxygen from a vacant site to the next through the lattice is small enough, it is necessary that at least one of the neighboring anion sites is also a vacancy, a requirement that is best provided by a statistical distribution of the vacant sites [135]. The highest conductivity in the system ZrO_2-Y_2O_3 occurs near the lower limit of the cubic phase region. In practice ZrO_2-9 mol.% Y_2O_3 has been regarded as having the highest conductivity in the system [133].

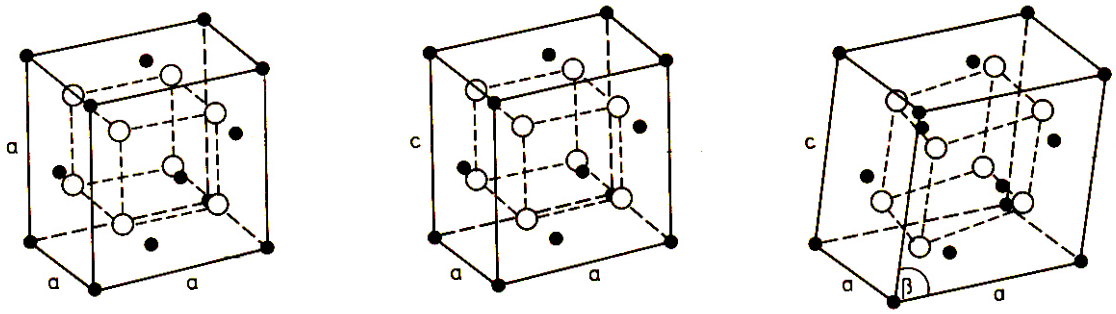

(a) cubic *(b) tetragonal* *(c) monoclinic*

Fig. 5.1: Structures of the cubic, tetragonal and monoclinic ZrO_2 phases [135]

The use of yttria-stabilized zirconia as a solid oxide electrolyte goes back to Nernst, who in 1899 invented the "Nernst light" [137]. This electrolyte was used in the first solid oxide electrolyte fuel cell constructed by Bauer and Pries in 1937 [138]. More than 600 articles concerning the properties and applications of this electrolyte were published in the mean time. Today, YSZ solid electrolyte is widely used as in combustion control high-temperature oxygen sensors [39, 139], especially in automotive engines for the control of the air-to-fuel ratio, atmosphere control in furnaces, oxygen pumps [140], fuel cells [141] and as monitors of the oxygen concentration in molten metals.

5.1.2 Sodium-ß-alumina (NBA)

ß-Alumina is a generic term currently used to refer to Na_2O-Al_2O_3-based compounds derived from the as yet unknown sodium aluminate, $Na_2O{\cdot}11Al_2O_3$ or $NaAl_{11}O_{17}$. All these compounds contain excess Na compared with this composition. ß-Alumina has been discovered by Rancin and Merwin [142] and was originally thought to be a polymorph of Al_2O_3. A second Na_2O-Al_2O_3 compound structually very similar to ß-alumina was found later [143]. Its composition is $Na_2O{\cdot}5Al_2O_3$ or $Na_2Al_{10}O_{16}$ and it has been named ß´´-alumina.

ß-alumina has a hexagonal layered structure [144]. The stoichiometric structure is built up by two spinel blocks bridged by oxygen atoms at widely spaced intervals and related by a two-fold screw axis (see Fig. 5.2, a). In the spinel blocks the oxygen ions form a cubic closest packing in which the Al^{3+} ions occupy octahedral and tetrahedral interstitial sites. The mobile and thus conducting Na^+ ions occupy sites in the relatively unpopulated two-dimensional planes between the spinel blocks which are termed the conducting planes. The general composition of ß-alumina is $Na_{1+x}Al_{11}O_{17+x/2}$, with x ranging from 0.1 to 0.3. The excess sodium content may thus vary between 10 and 30%. The excess Na^+ ions also populate the conducting plane between the spinel blocks, but not all available sites are occupied. The excess positive charge is compensated for by defects and by oxygen ions in the conducting plane. Ionic conductivity due to the movement of the Na^+ ions can therefore only

take place two-dimensionally, i.e. in the plane of the bridging oxygen ions but not through the spinel blocks.

Actually, ß´´-Alumina is not a stable compound in the binary system Na_2O-Al_2O_3, but it can be stabilized by a variaty of third cations [145] which are capable of occupying either the octahedral or tetrahedral sites in the spinel blocks. The structure of the ß´´-alumina contains three spinel blocks related by a three-fold screw axis parallel to the c-axis (see Fig. 5.2, b). The oxygen planes between the blocks are staggered and result in slightly larger spacings through which the sodium ions can migrate. ß´´-Alumina thus has a higher ionic conductivity than ß-alumina. The general formula of ß´´-alumina is $Na_{1+x}M_xAl_{11-x}O_{17}$, in which M represents a divalent cation such as Mg^{2+}, Ni^{2+} or Zn^{2+}. The excess charge of the Na^+ ions is compensated for by substituting the divalent or monovalent cation into a spinel block site normally occupied by Al^{3+}.

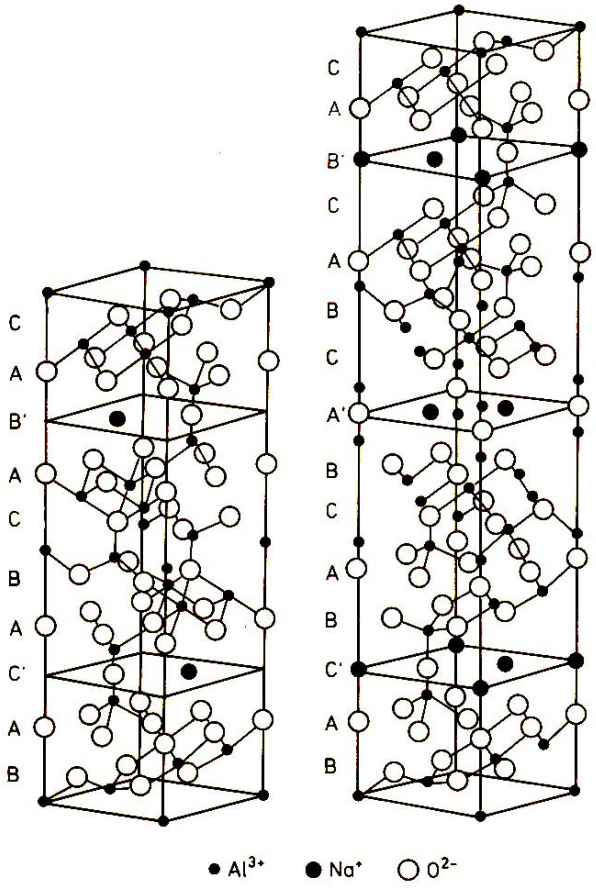

(a) *(b)*

Fig. 5.2: (a) Structure of stoichiometric ß-alumina. A, B and C indicate oxygen layers of the spinel blocks; B´ and C´ show the conducting planes. Each conducting plane of the unit cell contains one Na^+ ion; (b) structure of ß´´-alumina (idealized). A, B and C indicate oxygen layers of the spinel blocks; A´, B´ and C´ show the conducting planes. Each conducting plane of the unit cell contains two Na^+ ions [146]

5.2. Defect chemistry

In 1956 Kröger and Vink [147, 148] proposed the commonly used nomenclature for the description of defects. The point defects are considered as dilute species and the solid as the solvent. Several analogies can be found between intrinsic defect formation and self-dissociation of water:

1. A pair of charge defects is formed, which are responsible for electrical conduction;
2. A mass action law constant using defect activities (or concentration for dilute species) describes the defect equilibrium; and
3. Defect concentrations are normally thermally activated.

In the Kröger-Vink notation, the subscript shows the site of a defect. For instance, the subscript *i* represents an interstitial site. The effective defect charge is written as a superscript, relative to the ideal lattice: a dot ($^{\bullet}$) represents a positive and a prime ($'$) a negative charge. In Na-ß-Al_2O_3, for example, $Na_i^{\bullet}$ represents an interstitial sodium ion and V'_{Na} is a single negatively charged sodium vacancy. Bulk defect chemical reactions must obey mass balance, charge balance (global electrical neutrality), and lattice-site balance.

There are essentially three ways of establishment of equilibrium of defects in ionic crystals.

(i) Intrinsic defect; i.e. the defect present in the bulk of a crystal is in thermodynamic equilibrium. This includes the Frenkel and Schottky defects.

(ii) Defect doping; i.e. the intentional manipulation of defect types and concentration by incorporation of specific impurities into the bulk of the crystal.

(iii) Defect reactions at the interface, e.g. the incorporation of the neutral species from the "outside" into the crystal via defect, or the opposite, the loss of crystal atoms to the ambience generating defects in crystal.

In cation conductors, like Na-ß-Al_2O_3, lattice disorder occurs predominantly in the cation sublattice. The intrinsic lattice defects are Frenkel pairs [149, 150], i.e. metal interstitials and metal vacancies, $M_i^{\bullet}$ and V_M, respectively, while the anions are immobile.

The relevant defect formation reactions in Na-ß-Al_2O_3, along with their mass action relations, assuming dilute solution, are given in Table 5.1, where a_{Na} is sodium activity in the surroundings, V_i and V_{Na} are the interstitial and sodium vacancies, respectively, h is the electron hole, e is the excess electron, [ ] denotes the concentration of ion or electron defects and K_F, K_e, K_p and K_n are the constants of above equilibriums, having the form

$$K(T) = K_0 \exp\left(-\frac{\Delta H}{RT}\right). \qquad (5.2)$$

Type of reaction	Reaction	Law of mass action	Eq.
Intrinsic defect formation	$Na_{Na} + V_i \Leftrightarrow Na_i^{\bullet} + V'_{Na}$	$K_F = \frac{[Na_i^{\bullet}]\cdot[V'_{Na}]}{[Na_{Na}]\cdot[V_i]}$	(5.3)
Interaction with the surroundings	$Na_{Na} \Leftrightarrow Na + V'_{Na} + h^{\bullet}$	$K_p = \frac{[V'_{Na}]\cdot[h^{\bullet}]}{[Na_{Na}]} a_{Na}$	(5.4, a)
	$Na + V'_{Na} \Leftrightarrow Na_{Na} + e'$	$K_n = \frac{[Na_{Na}]\cdot[e']}{[V'_{Na}]} a_{Na}^{-1}$	(5.4, b)
Electrone-hole generation-recombination	$0 \Leftrightarrow e' + h^{\bullet}$	$K_e = [e']\cdot[h^{\bullet}]$	(5.5)

Table 5.1: Defect formation reactions along with mass action law

K_0 includes the entropy term, ΔH is the reaction enthalpy. In addition, the electro-neutrality condition has to be taken into account

$$[V'_{Na}] + [e'] = [h^{\bullet}] + [Na_i^{\bullet}] \,. \qquad (5.6)$$

Equations (5.3) – (5.6) allow to calculate the defect concentration as a function of the sodium chemical potential and temperature.

The defect concentration in solid electrolyte as a function of the chemical potential of the neutral species in the ambience of solid electrolyte is represented with the so-called Brouwer diagram.

5.3. Conductivity

For a material to behave as a solid electrolyte a number of ions should not be restricted to normal lattice positions. They must be free to move from one position to another after application of an electric field (migration), as in an oxygen pump, or under a concentration gradient (diffusion), as in the case of a sensor. In the solid electrolyte, movement differs from the gas or liquid phase in that only one type of ions is free to move. For example, for Na-ß-Al_2O_3 the Na^+ ions are moving with the Al^{3+}, and O^{2-} are fixed. For oxygen conducting solid electrolyte the O^{2-} ions are moving and Zr^{4+} and Y^{3+} are fixed.

Though many conduction mechanisms can be produced only three are regarded as likely in ionic conductors, these are interstitial, interstitialcy and vacancy diffusion. The vacancy mechanism for transport of ions is illustrated in Fig. 5.3. The two dimensional representation of interstitial motion shown in Fig. 5.4 looks very overcrowded, a three dimensional model for the same motion shows the motion to be quite energetically favorable. The third type of motion involves a possible combination of vacancy and interstitial mechanisms, as shown in Fig. 5.5.

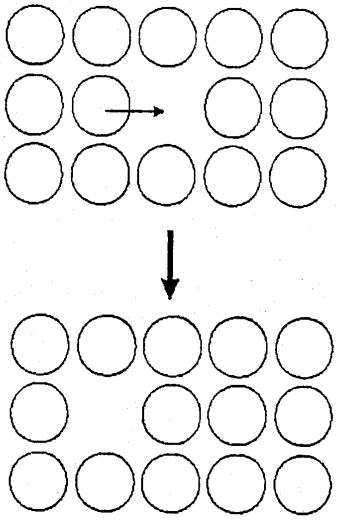

Fig. 5.3: Vacancy mechanism for transport of ions

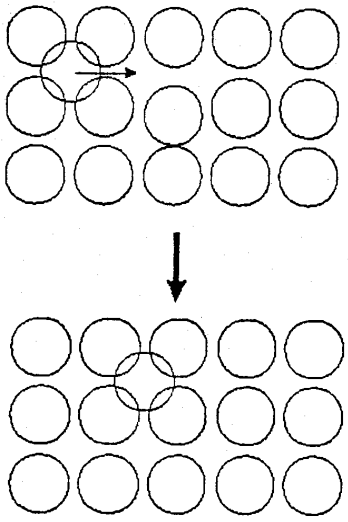

Fig. 5.4: Interstitial mechanism for transoport of ions

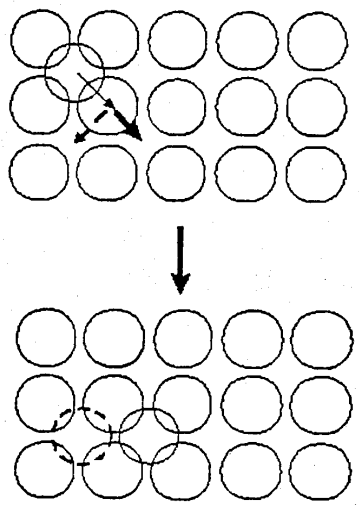

Fig. 5.5: Interstitialcy mechanism showing the two possible locations of ions after movement

Concentrations of ionic and electronic defects discussed in above mentioned chapter are important because electrical charge is transported by movement of these defects. The electrical conductivity (σ) of a solid is related to its defect concentrations by [151, 152]

$$\sigma = \sum_i c_i z_i q_i u_i + n q_e u_e + p q_h u_h = \sum_j \sigma_j \,, \tag{5.7}$$

where c_i, n and p are the ionic, electron and hole concentrations, q is the charge, u is the mobility (i.e., the mean particle velocity per unit potential gradient), and subscripts i, e and h denotes ions, electrons and electron holes, respectively.

The mobility of an electronic carrier is usually significantly larger than that of an ion. This means that ionic motion will only be predominate if the concentration of electron holes is considerably smaller than the concentration of ionic defects.

The quotient of the partial conductivity σ_j of one type of particles *j* to the total conductivity is called the transference number, t_j

$$t_j = \frac{\sigma_j}{\sum_j \sigma_j} = \frac{\sigma_j}{\sigma} . \qquad (5.8)$$

Good solid electrolytes have a transference number for the ions of nearly one and for electrons of nearly zero. Often it is important that the transference number of a special ion is one and that the transference numbers of the other ions are practically zero besides that of the electrons [152].

5.4 Electrode processes

5.4.1. General description

A practical oxygen electrode suited for working at relatively elevated temperatures is a noble metal supported gas electrode, where the metal is present as a thin porous film, whose texture is supposed to remain unaltered with respect to time, temperature and thermal cycling.

The oxygen reduction occurs as an heterogeneous reaction at a (tbp)

$$1/2O_2 \text{ (gas phase)} + 2e \text{ (metal)} \leftrightarrow O^{2-} \text{ (electrolyte)}. \qquad (5.9)$$

Independently of the kind of porous metal used as the support, one recognizes from Fig. 5.6 that the possible rate determining steps for the oxygen reaction are [153]

1. The migration of oxygen vacancies in the electrolyte;
2a. Oxygen diffusion in the gas phase, or
2b. Oxygen diffusion in the pores of the electrode;
3. Oxygen chemisorption and dissociation at the metal surface;
4a. Oxygen diffusion at the metal surface, or
4b. Oxygen diffusion at the grain boundaries of metal;
5. Dissolution and diffusion of oxygen into the metal phase;
6. Oxygen chemisorption and dissociation at the electrolyte surface followed by diffusion;
7. Dissolution and diffusion of oxygen in the electrolyte;
8. Migration of electrons in the electrolyte (high voltage range);
9. Electrochemical reaction, consisting in the transfer of electrons across the elecrode/electrolyte phase boundary.

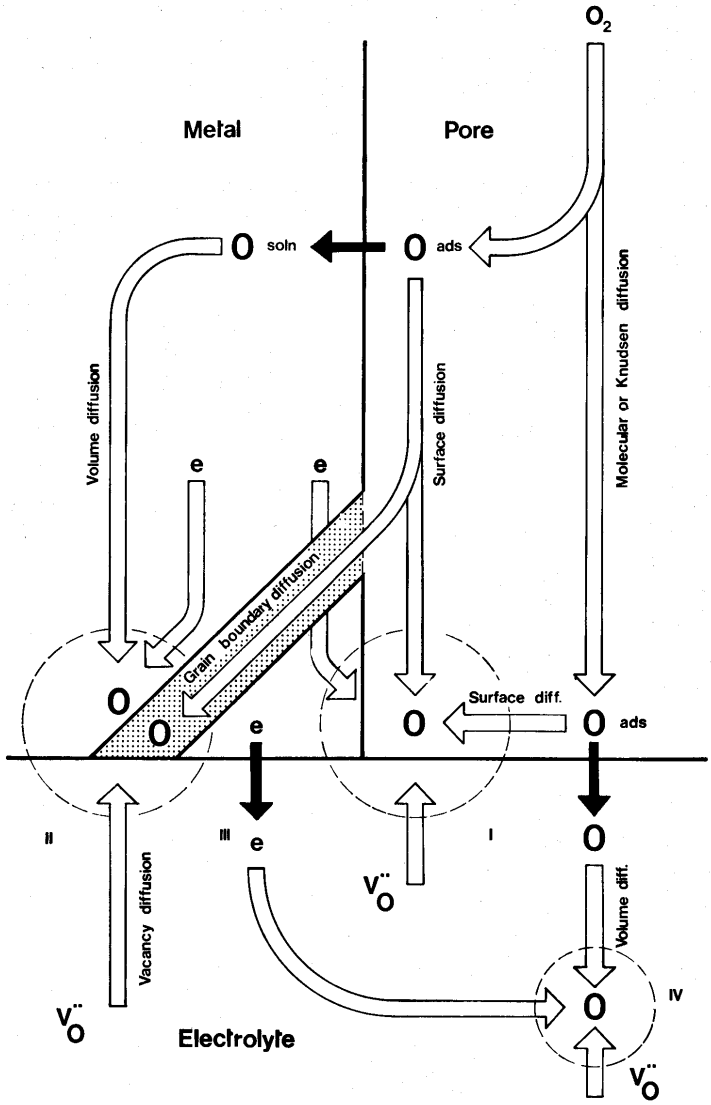

Fig. 5.6: Schematic picture of the single possible rate-determining steps for the oxygen reduction at a metal-supported gas electrode and zirconia based electrolyte. Empty arrows indicate transport processes in the homogeneous phases, solid arrows indicate transport processes across a phase boundary [153]

The rate-limiting step of the electrode processes depends on structure, pretreatment of electrode, temperature, oxygen partial pressure, physicochemical properties of the electrode and electrolyte, and on the configuration of an experimental galvanic cell.

Indepently of the method employed for measuring the electrode resistance, for electrodes of normal porosity the form of the empirical isotherm which fit the electrode resistance values R is

$$\frac{1}{R} = A\left(\frac{p}{B+p}\right)^{w}, \qquad (5.10)$$

where A and B are constants, p is the oxygen pressure and w varies within 0,8 and 0,6 in the case of macroporous electrodes. In isothermal conditions the rate of the electode reaction is proportional to

the concentration of atomic oxygen adsorbed on the pore walls and therefore to the number of active sites at the surface.

In the case of electrodes having a well defined structure of macropores, the rate determining step is a surface diffusion (low temperature) or surface dissociative chemisorption reaction (high temperature). For electrodes having very small pores the rate determining step is the Knudsen molecular diffusion or, possibly, the molecular oxygen surface diffusion [153].

5.4.2. Non-Nernstian Electrode Potential (NNEP)

When the sample gas contains combustible gases such as CO, the galvanic cell can be described as outlined already above as [20]

$$O_2\,(p'_{O_2}) + CO\,(p_{CO}),\ Pt \mid \text{stabilized } ZrO_2 \mid Pt,\ O_2\,(p''_{O_2})\ . \qquad (5.11)$$

At the left electrode-solid electrolyte interface of the galvanic cell the following processes have to be considered for the generation of the sensor voltage [56]

$$O_2(g) + 2G \leftrightarrow 2O_G \text{ – dissociative adsorption of } O_2\ , \qquad (5.12)$$

$$O_G + V''_O + 2e^- \leftrightarrow O^{2-} + G \text{ – oxygen incorporation,} \qquad (5.13)$$

$$CO(g) + O_G \leftrightarrow CO_2(g) \text{ – CO oxidation,} \qquad (5.14)$$

$$CO_G + O^{2-} \leftrightarrow CO_2(g) + G + 2e^- \text{ – electrochemical CO oxidation.} \qquad (5.15)$$

G denotes a free site for adsorption on the electrode surface, V''_O denotes an oxygen ion vacancy, and O^{2-} is an oxygen ion in the zirconia anion sublattice. If no CO is present only the processes (5.12) and (5.13) are possible. Oxygen from the YSZ electrolyte migrates to the three-phase boundary (tpb) where two charge-transfer reactions may take place (see Fig. 5.7). Oxygen supplied electrochemically may form either adsorbed O_2 or adsorbed ionic oxygen. Adsorbed O_2 can decompose to form adsorbed O species, which may desorb. Also, adsorbed O_2 species may be reduced to form the ionic oxygen species. In the presence of carbon monoxide (see Fig. 5.8) the processes (5.14) and (5.15) are enabled. Both adsorbed oxygen and adsorbed ionic oxygen can be scavenged from the surface by carbon monoxide. If there is good mass transfer between the surface and the gas phase, then the gas-phase oxygen partial pressure will still determine the adsorbed oxygen coverage. It is assumed that carbon monoxide is primarily produced from adsorbed oxygen (and not ionic oxygen) and that oxygen desorption can be neglected [154]. The importance of the processes for the sensor voltage is considered differently in the literature. Generally, a sensor voltage depends on the CO/O_2 ratio.

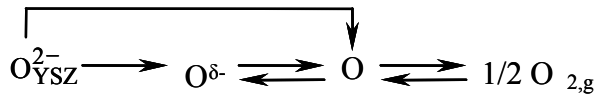

Fig. 5.7: Schematic diagram of reaction network for electrochemical oxygen supply to a surface [154]

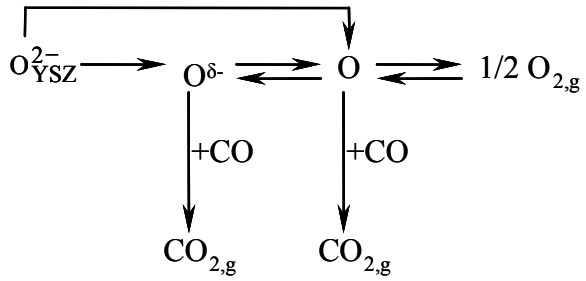

Fig. 5.8: Schematic diagram of reaction network for electrochemical oxygen supply to a surface during carbon monoxide oxidation [154]

The appearance of a NNEP indicates that the oxygen activity at the (tpb) electrode/electrolyte/gas is not in equilibrium with the O_2 partial pressure of the gas near the electrode, if there are O_2 and CO present together at the electrode. In the absence of CO, however, an equilibrium can be established and a Nernstian voltage is developed [57].

Two mechanisms responsible for the formation of a NNEP are being discussed in the literature. The first assumption is a mixed potential at the (tpb) generated by electrochemical reduction of oxygen and electrochemical oxidation of CO [20, 36, 57, 155]. According to the second model the adsorption of CO molecules at the electrode reduces the number of oxygen adsorption sites and thus the oxygen activity at the electrode decreases [156]. As a consequence of both, a NNEP strongly depends on physical and chemical surface properties like surface mobility, number of adsorption sites or catalytic activity, i.e. in other words, on the reaction kinetics at the electrode surface [56, 57].

5.4.2.1 Theory of mixed potential

If two electrochemical reactions (5.13) and (5.15) take place simultaneously on an electrode, the electrode potential is determined by the rates of both electrochemical reactions involved and is called mixed-potential. Sensors in which the effects of both interactions are important are often called “mixed potential sensors”.

The concept of mixed-potential for stabilized zirconia-based sensors was first introduced to explain the non-ideal behaviour of an oxygen sensor in the mixed gases of air and fuel (oxidizable gases) by Fleming [36]. Fleming [36] proposed that this model is based on the reactions (5.12), (5.13) and (5.15) assuming that reactions (5.13) and (5.15) are occurring independently at different (tpb) sites.

The open-circuit voltage generated by cell (5.1), with electrochemical reactions (5.13) and (5.15), is given by [36]

$$U_{O_2} = U^0_{O_2} + \frac{RT}{4F} \ln\left(\frac{p''_{O_2}}{p'_{O_2}}\right) \tag{5.16}$$

and

$$U_{CO} = U^0_{CO} + \frac{RT}{2F} \ln\left[\frac{(p'_{O_2})^{1/2} \cdot p_{CO}}{p_{CO_2}}\right] . \tag{5.17}$$

The standard cell potential, $U^0_{O_2}$, in Eq. (5.16) is determined by the difference of electrochemical potentials of the electrons, $\tilde{\mu}^0_{e^-}$, between electrodes [141]. When all constituent phases of the cell (5.11) (gas, metal electrode, and solid electrolyte) are in thermodynamic equilibrium, electrochemical potentials, $\tilde{\mu}^0_{e^-}$, are the same at both electrodes thus $U^0_{O_2}$ is equal zero. The standard cell potential, U^0_{CO}, is given by

$$U^0_{CO} = \frac{(\tilde{\mu}^0_{CO} - \tilde{\mu}^0_{CO_2} + 1/2\tilde{\mu}^0_{O_2})}{2F} . \tag{5.18}$$

where the electrochemical potentials, $\tilde{\mu}^0$, are equal to the Gibbs chemical free energies of the gases CO, CO_2, and O_2 determined at the temperature of interest.

Attention now is given to the electrode/electrolyte interface region of the working electrode. As depicted in Fig. 5.9, the bulk working electrode usually has a labyrinth structure with interspersed pores permitting gas/electrolyte contact. Locations where the (tpb) sites exist are shown in Fig. 5.9. Electrochemical reactions (5.13) and (5.15) can only occur at or near (tpb) because these reactions require the simultaneous presence of gases, electrons, and oxygen ions [36].

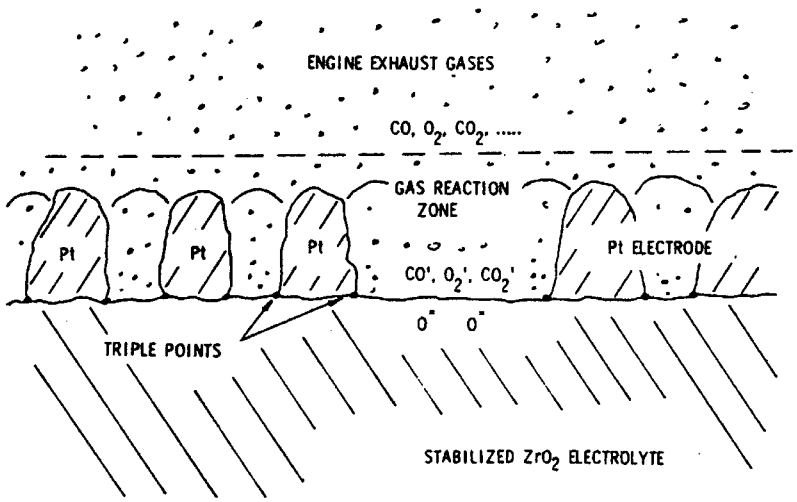

Fig. 5.9: Schematic representation of physical structure of electrode/electrolyte region [36]

The fraction of the (tpb) sites occupied by adsorbed CO is calculated using the Langmuir adsorption isotherm [157]. When CO and O_2 molecules occupy single sites in adsorption, the Langmuir expression for the fraction, θ_{CO}, of (tpb) sites occupied by CO can be written as

$$\theta_{CO} = \frac{K_{CO} p_{CO}}{1 + K_{CO} p_{CO} + K_{O_2} p_{O_2}} , \tag{5.19}$$

where K_{CO} and K_{O_2} are adsorption constants for CO and O_2. For both gas species, CO and O_2, the adsorption constant K is estimated from kinetic gas theory using the following equations

$$K = K^0 \exp\left(\frac{Q}{RT}\right) \tag{5.20}$$

and

$$K^0 = \frac{\sigma \Psi^0}{\nu n_s} , \tag{5.21}$$

where Q is the heat of adsorption, σ is the condensation coefficient of sticking probability, Ψ^0 is the flux of gas molecules at a pressure equal to 1 atm colliding with unit area of surface per unit time, ν is the frequency of gas molecule vibration, and n_s is the number of (tpb) sites at which CO and O_2 compete for adsorption [157].

Similarly, the fraction of sites, θ_{O_2}, supporting the O_2 cell reaction (5.13) is given by the fraction of sites where CO is not adsorbed, namely

$$\theta_{O_2} = 1 - \theta_{CO} . \tag{5.22}$$

The output voltage of the carbon monoxide gas sensor due to simultaneous existence of O_2 and CO cell reactions (5.13) and (5.15) is determined by

$$U = \theta_{O_2} U_{O_2} + \theta_{CO} U_{CO} . \tag{5.23}$$

The combination of Eqs. (5.16), (5.17) and (5.23) gives the desired final result

$$U = \theta_{O_2} \left\{ U^0_{O_2} + \frac{RT}{4F} \ln\left(\frac{p''_{O_2}}{p'_{O_2}}\right) \right\} + \theta_{CO} \left\{ U^0_{CO} + \frac{RT}{2F} \ln\left[\frac{(p'_{O_2})^{1/2} \cdot p_{CO}}{p_{CO_2}}\right] \right\} . \tag{5.24}$$

where θ_{O_2} and θ_{CO} are given by Eqs. (5.19) and (5.22) [36].

After Fleming, the theory of mixed potential has been described in more detail by Okamoto et al. [20, 58-61, 158]. They discussed the behaviour of the galvanic cell (5.11) in low temperature region (around 350 °C), where the voltage becomes anomalously high. Particularly in the region where $p_{CO}/p_{O_2} < 2$, an anomalously high voltage is observed [20, 36, 58, 59, 70]. This anomalous voltage has been accounted for the competition between O_2 and CO gases for (tpb) sites on the anode electrode [11, 27]. The result for voltage measurements when $p_{CO}/p_{O_2} < 2$ at 350 °C is shown in

Fig. 5.10. The observed values are quite different from the ones calculated using Nernst equation. Hypothetically, the whole p_{CO}/p_{O_2} interval can be divided to three regions. The anomalous voltage is about 100 mV when $p_{CO}/p_{O_2} \leq 0.1$ [region (I)], while it is more than 700 mV for $p_{CO}/p_{O_2} \geq 0.7$ [region (III)]. In the region $0.1 \leq p_{CO}/p_{O_2} \leq 0.7$ [region (II)], the voltage increases sharply with oscillating values, providing the voltage range shown in Fig. 5.10 [20]. The variation of amounts of oxygen (N_O or N_{O_2}) and CO (N_{CO}) over the whole gas composition range is shown in Fig. 5.11. This figure is based on results obtained in [60] as well as those reported in [58, 59, 159].

The mechanism responsible for the appearance of an anomalous voltage was described in [20, 58, 59]. According to this, at the air electrode, only oxygen is adsorbed on Pt leading to the reaction (5.13) which gives the equilibrium electrode potential. On the other hand, both oxygen and CO are adsorbed on Pt at lower temperatures at the sample gas electrode. The reactions (5.13) and (5.15) occur where CO_2(g) is gaseous and hardly adsorbed on Pt [160]. They provide a mixed electrode potential. Thus, the observed voltage at lower temperatures is the difference between this mixed electrode potential and the equilibrium electrode potential [20, 59].

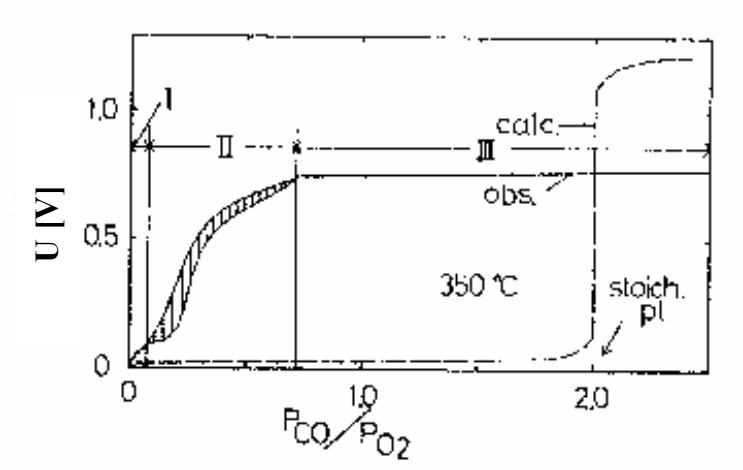

Fig. 5.10: Anomalous voltage of an O_2 gas sensor (4.24) when $pCO/p_{O_2} \leq 2$ [20]

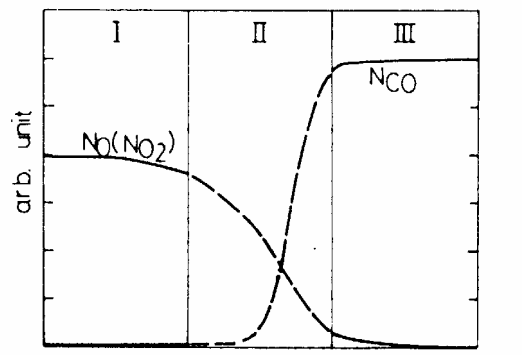

Fig. 5.11: Schematic diagram for N_O (or N_{O_2}) and N_{CO} [60]

The relation between the voltage and the p_{CO}/p_{O_2} ratio at lower temperatures (see Fig. 5.10) is quite complicated. However it seems to indicate a surface adsorption state during the CO oxidation on Pt. The CO oxidation on Pt proceeds via either the Eley-Rideal mechanism

$$O_G + CO(g) \rightarrow CO_2(g) , \qquad (5.25)$$

or the Langmuir-Hinshelwood mechanism [20, 62, 161-165]

$$O_G + CO_G \rightarrow CO_2(g) . \qquad (5.26)$$

A CO gas sensor detects very small amounts of CO in air and thus is related to the anomalous voltage in region (I). Therefore, this region should be examined in more detail to clarify the behavior of the CO gas sensor [20]. In region (I) (see Fig. 5.10), the main species adsorbed on Pt is anticipated to be oxygen [20]. The amount of CO on Pt would be very small. The voltage is also higher than that calculated, but it is comparatively low [58] and no surface CO (N_{CO}) was detected by means of infrared spectroscopy [59].

In region (I) the reaction proceeds via the simple Langmuir-Hinshelwood mechanism (see Eq. 5.26). Here, oxygen adsorption is considered to be dissociative [58, 59, 159, 166]. This is because in this region the surface CO concentration is so small that the reaction system can be approximately regarded as that of oxygen/Pt, where it is established that oxygen adsorbs dissociatively [167-170]. CO-supply is a rate-determining step. Oxygen adsorption on Pt is almost saturated in region (I), while many vacant sites remain for CO [159]. If the adsorbed CO mobility is sufficiently high on Pt, then N_{CO} should be nearly zero and independent of p_{O_2}, because of the near saturation adsorption of oxygen.

If the adsorbed CO mobility is low, N_{CO} depends on p_{O_2} for the following reason. Oxygen is in dynamic adsorption-desorption equilibrium and gaseous oxygen can be adsorbed to the adjacent adsorbed CO, accompanied with oxygen desorption from another site. Then, the adjacent adsorbed CO and oxygen readily react [60].

In region (III), the Pt surface will be largely covered with CO [20]. The amounts of CO adsorbed on Pt did not change and the voltage is very high and almost constant [58]. In this region elementary steps for CO oxidation are according to Eley-Rideal mechanism (see Eq. 5.25) [60, 62].

In region (II), however, both reactions (5.25) and (5.26) occur and the amount of CO adsorbed on Pt is not constant [161] leading to the oscillation of the voltage. In this way, the anomalous voltage of an O_2 gas sensor is considered to have a direct relation to the amounts of the CO and oxygen adsorbed on Pt during the CO oxidation [20, 58]. The value N_{CO} oscillates, at least in the presence of a sufficient amount of oxygen [59]. Therefore, the rate-determining step moves from CO-supply to surface reaction between adsorbed species, with experimental conditions approaching those in region (II) [60].

The above discussion is illustrated in Fig. 5.12 from the electrochemical point of view already. If the voltage is determined only by oxygen activity on Pt, the anodic and cathodic currents due to reaction (5.13) are the same, thus generating an electrode potential at E_0 in the figure. Therefore, i_0 is uniquely determined by the electrode potential whether CO is present or not, because i_0 is determined by N_O and N_G, which do not increase or decrease simultaneously. On the other hand, two electrochemical reactions (5.13) and (5.15) give a mixed electrode potential at E_m in Fig. 5.12, at which potential the sum of anodic currents due to reactions (5.13) and (5.15) equals the cathodic current owing to reaction (5.13), since the backward reaction for reaction (5.15) can be ignored under the experimental conditions. In this case, i_0 may change with a given E_m according to the presence or absence of CO [61].

Can et al. [66] have measured the steady-state polarization curves in the stream of CO-O_2-Ar gas mixtures. Above 600 °C, the polarization current does not change for the CO concentration up to 400 ppm. However, at temperatures below 550 °C, at the same concentration of CO, the polarization current varies in the region within ≤ +/-50 mV of the equilibrium potential. When CO existed in a stream, on the sensing electrode of the sensor, the electrode reaction of the adsorbed oxygen atoms, O_G, on the porous Pt surface and CO oxidation reaction both proceeded at the same time. The variation in O_2 polarization current of the sensor in the presence of CO is essentially due to the same mechanism as the mixed potential mechanism [66, 171, 172].

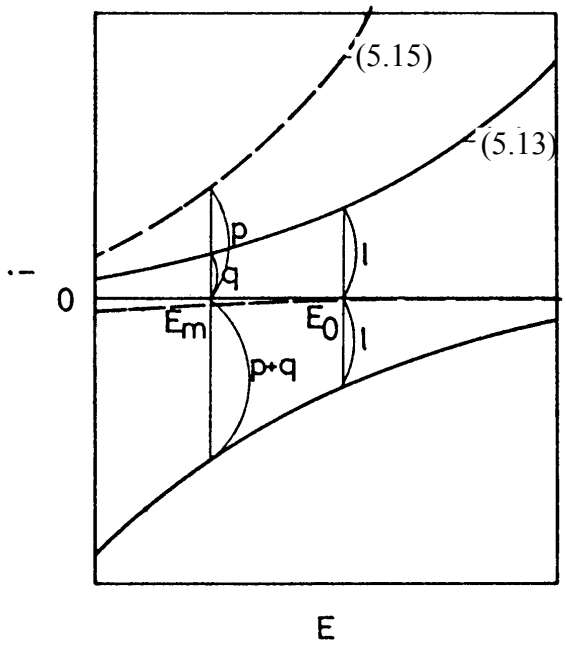

Fig. 5.12: Schematic illustration for the mechanism of voltage determination [61]

After considering the mixed potential sensor with Pt electrodes, other sensors were developed in order to understand the mechanism of CO oxidation. Williams et al. [155] reported that the Pt|YSZ|Au sensor developed a voltage in the presence of CO at temperature less than 500 °C. However, they were unable to obtain a response at higher temperatures. The model proposed in the literature to explain the mixed potential response of a Pt|solid electrolyte|Au device is illustrated in Fig. 5.13 (a) [155]. Here, E(O) is the reference potential at p_{O_2} = 1 atm, E(O_2) is the equilibrium potential of the base gas in absence of any reducing gas, and E(CO/CO_2) is the equilibrium potential of the reducing gas mixture in the absence of oxygen. The mixed potential on a particular electrode is fixed by the intersection of the polarization curves for oxygen reduction and reducing gas oxidation, respectively. Under the condition that $p_{CO} << p_{O_2}$ the mixed potential curves resemble the schematic proposed in Fig. 5.13 (b).

This model is similar to models proposed for the mixed potential behavior of oxide-based CO [71] and NO_x [121] sensors. The low concentration of the reducing gases (< 500 ppm) can be expected to limit the electrochemical oxidation current on the Au and Pt electrodes to I(Au) and I(Pt), respectively. At steady state, this current [I(Au) and I(Pt)] should equal the oxygen reduction current on the Au and Pt electrodes, and hence, the potential on the electrodes is given by E_m(Au) and E_m(Pt), respectively. This model is consistent with the sign of the mixed potential and also the fact that E_m(Pt) is close to equilibrium at 600 °C. This model implies that the oxygen reduction kinetics of an electrode is as important as the CO oxidation kinetics in determining the mixed potential of such electrodes.

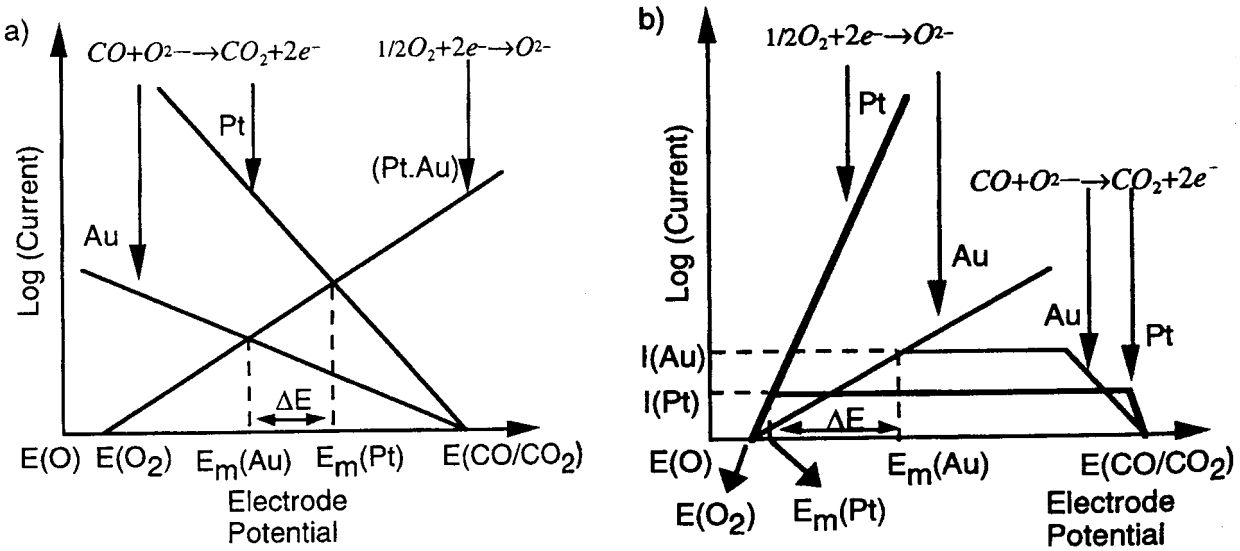

Fig. 5.13: (a) Schematic proposed by Williams et al. [155] for a Pt|YSZ|Au sensor at T≤500 °C. (b) Schematic proposed for operation of Pt|solid electrolyte|Au sensors at T=600 °C in O_2 (1 %). The relatively low concentrations of CO at the electrode surface limit the kinetics for the electrochemical oxidation of CO

Hibino et al. [35] have recently reported that the potential at the gold electrode is significantly different from the equilibrium potential in the presence of reducing gases at temperatures up to 600 °C. They also reported that the platinum electrode was close to equilibrium even in the presence of reducing gases at 600 °C [35, 74].

Conversely, voltage measurements by use of a solid electrolyte concentration cell are especially useful in the study of very small amounts of adsorption during the reaction, because the mixed electrode potential is sensitive to reactants [59].

The same mechanism can be proposed for the characterization of hydrocarbons also. It is considered [20, 23, 27, 30, 36, 57, 66, 78, 121-123] that in the presence of oxygen and hydrocarbons, the following electrochemical reactions occur at the sensing electrode [35]

$$O_2 + 4e^- \rightarrow 2O^{2-} , \qquad (5.27)$$

$$C_xH_y + (2x+y/2)O^{2-} \rightarrow xCO_2 + y/2H_2O + (4x+y)e^- . \qquad (5.28)$$

These reactions proceed at an equal rate due to the formation of a local cell, and thus result in a mixed potential at the sensing electrode [35].

5.4.2.2 Theory of preferential CO adsorption

In contrast to the model of mixed potential, where two electrochemical reactions proceed simultaneously on the electrode, it has been proposed that an anomalous high voltage is caused by an imperfect catalytic activity of a platinum electrode [20, 36, 58, 70]. It is thought to reflect either the adsorption states of CO and oxygen on Pt [20, 58, 70] or oxygen activity on Pt [62, 122, 123] during the reaction [59]. The adsorption of oxidizable molecules (CO) at the electrode reduces the number of oxygen adsorption sites and thus the oxygen activity at the electrode decreases [156]. In outline, the model could be considered as follows. The zirconia sensing element contains mobile oxygen vacancies $V_{\ddot{O}}$ (effective charge +2e). The coupling between the electrical and the chemical parts of the sensing system was assumed to be through the reaction at the (tpb) lines in which adsorbed oxygen atoms, O_G, and electrons, e^-, on the electrode combine with charged oxygen vacancies, $V_{\ddot{O}}$, producing oxygen ions, O^{2-}, in the oxide, according to Eq. (5.13). The adsorbed reducing species on the electrode, CO_G, in that scheme, changes the concentration of charged oxygen vacancies indirectly by chemically reacting with and modifying the concentration of O_G. As a consequence, the NNEP strongly depends on physical and chemical surface properties like surface mobility, number of adsorption sites or catalytic activity, i.e. in other words, on the reaction kinetics at the electrode surface [56, 57].

The mechanisms of the catalytic oxidation of combustible gases in general and CO in particular have been investigated and reported numerous times [62, 162, 163]. The primary mechanisms for CO oxidation on metallic catalyst surfaces include: (i) the Langmuir-Hinshelwood mechanism and (ii) the Eley-Rideal mechanism, which were described in the previous chapter in more detail.

Vayenas et al. [95, 173, 174] proposed a model based on reaction (5.12), (5.13) and (5.14). They assume that the intrinsic rate of oxygen adsorption [reaction (5.12)] is comparable with the intrinsic rate of the oxidation step [reaction (5.14)] resulting in a decrease of oxygen surface activity. They obtained a sensor voltage proportional to $\log(CO/O_2)$.

The chemical reactions taking place on the platinum surface can be divided into three distinct groups: adsorption-desorption reactions, chemical oxidation-reduction reactions, and the electrochemical reaction that generates the voltage response of the electrode. The following three adsorption-desorption reactions can be considered [175]

$$2G + (O_2)_{gas} \leftrightarrow 2O_G\,, \tag{5.29}$$

$$G + (CO)_{gas} \leftrightarrow CO_G\,. \tag{5.30}$$

$$CO_G + O_G \leftrightarrow CO_2 + 2G - \text{oxidation reaction.} \tag{5.31}$$

The electrochemical reaction can be represented as

$$O_G + 2e^- \leftrightarrow G + O^{2-}\,. \tag{5.32}$$

If molecules of CO are present in the gas stream, CO may adsorb on electrode surface and may occupy the (tpb) where oxygen equilibrium reaction takes place. As a result the situation will be able to appear when (tpb) free sites will be not enough for achievement of oxygen equilibrium and the voltage will deviate from the theoretical values [175].

It follows that the open-circuit potential depends on the concentration of adsorbed oxygen, which in turn depends on the oxygen concentration at the surface of the electrode, as well as on the rates of the various reactions listed above [175].

6 Measuring principles

6.1 Cell voltage measurements

6.1.1 Determination of the voltage and the CO sensitivity by means of the two-compartment galvanic cells

The characterization of the CO sensitivity for $Pt_{1-x}Au_x$ sensing electrodes was done by means of the two-compartment galvanic cell which is represented as follows (cell (I))

$$Pt\,|\,Pt_{1-x}Au_x,Ar,CO(p_{CO}=5\text{-}5\cdot10^4\,Pa),O_2(p'_{O_2}=1\cdot10^3\,Pa)\,|\,YSZ\,|\,O_2(p''_{O_2}=1\cdot10^5\text{-}1\cdot10^{-33}\,Pa),Pt\ , \qquad (6.1)$$

where YSZ was employed as an oxygen ion-conducting solid electrolyte.

The over-all voltage of the two-compartment galvanic cell determined by the Nernst equation is given as follows

$$U=\frac{RT}{4F}\ln\left(\frac{p'_{O_2}}{p''_{O_2}}\right), \qquad (6.2)$$

where p'_{O_2} and p''_{O_2} represent oxygen partial pressures at the working and reference electrodes, respectively.

The oxygen partial pressure at the working electrode was constant in all the investigations and was equal to $1\cdot10^3$ Pa. For the reference electrodes pure molecular oxygen and H_2/H_2O equilibrium gas mixtures were used. In case of using pure molecular oxygen the oxygen partial pressure of the reference electrode was constant at all the investigated temperatures and was equal to $1\cdot10^5$ Pa. In contrasr to that at using a H_2/H_2O mixture the oxygen partial pressure depends on temperature and on the standard Gibbs free energy of formation of the water according to the reaction

$$H_2+\frac{1}{2}O_2 \xleftrightarrow{\Delta_f G^0_{H_2O}} H_2O\,. \qquad (6.3)$$

Then, the oxygen partial pressure for the H_2/H_2O equilibrium gas mixture is calculated by means of the following equations using the thermodynamic data from the literature [176, 177]

$$\Delta_f G^0_{H_2O}=-RT\cdot\ln\frac{p_{H_2O}}{p_{H_2}\cdot p_{O_2}^{1/2}}, \qquad (6.4)$$

where $\Delta_f G^0_{H_2O}$ is the standard Gibbs free energy of the reaction (6.3), and p_{H_2O} and p_{H_2} are the partial pressures of water vapour and pure molecular hydrogen, respectively.

6.1.2 Determination of the voltage and the CO sensitivity by means of the bi-electrolyte galvanic cells

The alternative way for the characterization and determination of the presence of CO in the surrounding atmosphere is based on the previous knowledge about the CO_2 sensor which is represented by the following galvanic cell [178-180]

$$\text{Au}, O_2, CO_2, Na_2CO_3(\text{Au}) \mid \text{Na-}(\beta+\beta'')\text{-}Al_2O_3 \mid \text{YSZ} \mid O_2, (CO_2), \text{Au} . \qquad (6.5)$$

This galvanic cell can be regarded as a combination of a sodium and an oxygen concentration cell. For the conversion of CO to CO_2 the sodium carbonate counter electrode is partially covered by a thin catalyst layer.

Initially, the planar bi-electrolyte galvanic cell (cell (II)) constructed under this investigation was written as follows

II III I

$$\text{Pt}|\text{Au},O_2,\text{CO},Na_2CO_3(\text{Au})\text{-catalyst} \mid \text{Na-}(\beta+\beta'')\text{-}Al_2O_3 \mid \text{YSZ} \mid O_2, \text{CO}, Pt_{1-x}Au_x\ (x=0, 0.2)|\text{Pt}. \qquad (6.6)$$

a''_{Na} a'''_{Na}

$p_{CO}(p_{CO_2})$, p''_{O_2} p'''_{O_2} p_{CO}, p'_{O_2}

$\underbrace{p''_{O_2} \quad p'''_{O_2}}_{U_1}\ \underbrace{p'''_{O_2} \quad p'_{O_2}}_{U_2}$

$\underbrace{U_1 \quad U_2}_{U}$

The overall voltage (U) is the sum of the voltages generated due to chemical potential differences that are established between the interfaces of both of these concentration cells [179, 180]. The gas phase of the outer electrodes and the oxygen partial pressure of both sides of the cell (I) are different, i.e. $p''_{O_2} \neq p'_{O_2}$, due to the oxidation reacton of CO

$$CO + ½O_2 = CO_2. \qquad (6.7)$$

According to Eq. (6.7) the oxygen partial pressure at the interface (II) can be determined as

$$p''_{O_2} = p'_{O_2} - \frac{1}{2} p_{CO} . \qquad (6.8)$$

For the theoretical consideration one has to assume that CO is fully oxidized to CO_2 by means of the catalyst, i.e. $p_{CO} = p_{CO_2}$. According to this assumption, on the counter electrode side [interface (II)] the sodium activity, a''_{Na}, is determined by the equilibrium between CO_2, O_2, and Na_2CO_3 [164], according to

$$Na_2CO_3 \leftrightarrow 2Na + CO_2 + ½O_2 \qquad (6.9)$$

and

$$\ln a''_{Na} = \frac{\Delta_f G^0_{Na_2CO_3} - \Delta_f G^0_{CO_2}}{2RT} - \frac{1}{2}\ln p_{CO} - \frac{1}{4}\ln p''_{O_2} = \frac{\Delta_f G^0_{Na_2CO_3} - \Delta_f G^0_{CO_2}}{2RT} - \frac{1}{2}\ln p_{CO} - \frac{1}{4}\ln\left(p'_{O_2} - \frac{1}{2}p_{CO}\right), \tag{6.10}$$

where $\Delta_f G^0_{Na_2CO_3}$ and $\Delta_f G^0_{CO_2}$ stand for the standard free enthalpies of formation of Na_2CO_3 and CO_2, respectively.

The activity a'''_{Na} at the interface between the two electrolytes [interface (III)] may be regarded as fixed by the sodium oxide dissolved in the outermost layers of the NBA phase adjacent to YSZ. According to the dissociation equilibrium of the sodium oxide

$$Na_2O \leftrightarrow 2Na + ½O_2\,, \tag{6.11}$$

the magnitude of a'''_{Na} depends on the magnitude of the oxide activity, a'''_{Na_2O}, and of the oxygen chemical potential, p'''_{O_2}, established at this interface. Thus,

$$\ln a'''_{Na} = \frac{\Delta_f G^0_{Na_2O}}{2RT} + \frac{1}{2}\ln a'''_{Na_2O} - \frac{1}{4}\ln p'''_{O_2}\,. \tag{6.12}$$

Using Eqs. (6.10) and (6.12) and provided that there is no electron conduction to be taken into account, the voltage U_1 of the sodium concentration cell yields

$$U_1 = \frac{\Delta_f G^0_{Na_2CO_3} - \Delta_f G^0_{Na_2O} - \Delta_f G^0_{CO_2}}{2F} - \frac{RT}{2F}\cdot\left[\ln a'''_{Na_2O} + \ln p_{CO} + \frac{1}{2}\ln\frac{\left(p'_{O_2} - \frac{1}{2}p_{CO}\right)}{p'''_{O_2}}\right]. \tag{6.13}$$

At the interface (I) the reaction takes place with the participation of the oxygen ions into the YSZ solid electrolytes, electrons, and oxygen in surrounding atmosphere

$$O_2 + 4e^- \leftrightarrow 2O^{2-}\,. \tag{6.14}$$

Voltage of the oxygen concentration cell is calculated by the Nernst equation as follows

$$U_2 = \frac{RT}{4F}\cdot\ln\frac{p'_{O_2}}{p'''_{O_2}}\,. \tag{6.15}$$

In view of Eqs. (6.13) and (6.15) the overall voltage of the cell (II) (see Eq. 6.6) is

$$U = U_1 + U_2 = \frac{\Delta_f G^0_{Na_2CO_3} - \Delta_f G^0_{Na_2O} - \Delta_f G^0_{CO_2}}{2F} - \frac{RT}{2F}\cdot\left[\ln a'''_{Na_2O} + \ln p_{CO} + \frac{1}{2}\ln\frac{\left(p'_{O_2} - \frac{1}{2}p_{CO}\right)}{p'_{O_2}}\right]. \tag{6.16}$$

From a thermodynamic point of view, the oxygen chemical potential p'''_{O_2} must be considered as not fixed. It is floating and may change within a certain range of magnitudes which is expected to lie on a medium level. Equation (6.16), however, reveals that, whatever p'''_{O_2} might be, in the overall cell

voltage it is not involved. While the partial voltages U_1 and U_2 would change if p'''_{O_2} changed, U remains constant [179].

In the bi-electrolyte cell (II) the short-circuited NBA pellet can be also used for fixing sodium activity from both the sides of NBA. Then, this cell can be written as

Pt | Au,O_2,CO,Na_2CO_3(Au)-catalyst | Na-(ß+ß´´)-Al_2O_3(Au) | YSZ | O_2,CO,$Pt_{1-x}Au_x$ | Pt (6.17)

and is termed cell (III). Since the sodium activities at the interfaces (II) and (III) are equal to each other, e.i. $a''_{Na} = a'''_{Na}$, the theoretical voltage of cell (III) can be calculated by the Nernst equation only (see Eq. 6.15). However, finally, after all the mathematical operations using Eqs. (6-7)-(6.15) the theoretical voltages for the bi-electrolyte cell (III) will be also determined by Eq. (6.16).

Consequently, the voltage of the bi-electrolyte cells (II) and (III) is well defined depending on the temperature, the CO partial pressure of the surrounding atmosphere and the oxygen partial pressure from both the sides of the cells.

For a better understanding of the influence of CO to the processes proceeding on the working electrode and to make clear the theoretical consideration of the bi-electrolyte concept, the bi-electrolyte cells (II) and (III) (see Eqs. 6.6 and 6.17) have been further developed by separating the gas compartments between the counter and the working electrodes. Consequently, two different constructions of this kind of the bi-electrolyte cell have been prepared. In the first case a non-short-circuited NBA pellet is used (cell (IV))

Pt | Au,O_2(p''_{O_2}),CO,Na_2CO_3(Au)-catalyst | NBA | YSZ | O_2(p''''_{O_2}),Pt | Pt , (6.18)

whereas in the second case a short-circuited one is applied (cell (V))

Pt | Au,O_2(p''_{O_2}),CO,Na_2CO_3(Au)-catalyst | NBA(Au) | YSZ | O_2(p''''_{O_2}),Pt | Pt. (6.19)

As it can be seen, in the bi-electrolyte cells (IV) and (V) CO participates in the thermodynamic equilibrium on the counter electrode only. In these cells the oxygen partial pressures of the counter electrode side remains without changes and can be determined by Eq. (6.8). The oxygen partial pressure on the working electrode (p''''_{O_2}) was kept constant under all the investigations and was equal to $1 \cdot 10^5$ Pa.

Since the processes on the counter and working electrodes are the same (see Eqs. 6.9-6.14), finally, the theoretical voltages for the bi-electrolyte cells (IV) and (V), with substitution of p'_{O_2} to p''''_{O_2} in Eq. (6.15), can be determined as

$$U = \frac{\Delta_f G^0_{Na_2CO_3} - \Delta_f G^0_{Na_2O} - \Delta_f G^0_{CO_2}}{2F} - \frac{RT}{2F} \cdot \left[\ln a'''_{Na_2O} + \ln p_{CO} + \frac{1}{2} \ln \frac{\left(p'_{O_2} - \frac{1}{2} p_{CO} \right)}{p''''_{O_2}} \right]. \quad (6.20)$$

For the calculation of the theoretical voltages the thermodynamic data from the JANAF database for the individual chemical compounds have been used [181-183].

For the determination of the sodium oxide activity into the Na-(β+β´´)-Al_2O_3 solid electrolyte the temperature dependence (250-650 °C) obtained in [184]

$$\log a_{Na_2O}(\beta+\beta'') = -\frac{12810 \pm 50K}{T} + 2.737 \pm 0.080\,, \qquad (5.22)$$

has been taken.

6.2 Impedance spectroscopy measurements

Impedance spectroscopy (IS) is an useful method for characterizing the electrical and electrochemical properties of materials and their interfaces with electronically conducting electrodes. Electrical measurements to evaluate the electrochemical behavior of electrode and/or electrolyte materials are usually made with cells having two identical electrodes applied to the faces of a sample. However, if devices such as chemical sensors are investigated, this simple geometry is often not feasible. Vacuum, a neutral atmosphere such as argon or an oxidizing atmosphere are variously used. The most common and standard approach of using IS is to measure impedance directly in the frequency domain by applying a signal-frequency voltage to the interface and measuring the real and imaginary parts of the complex resistance [185]. The role of IS in the development and characterization of solid state chemical sensors is rapidly expanding. Solid state chemical sensors are electrochemical cells designed to measure the concentration or pressure of chemical species in gases and the most successful ones use usually zirconia-based electrolytes to measure oxygen concentrations [185].

In the present study, this technique was used to examine the effect of presence of CO in the vicinity of the (tpb) on the properties of the various $Pt_{1-x}Au_x$ sensing electrode materials used in the two-compartment solid electrolyte galvanic cell (I). In particular, it could be possible to characterize the influence of the oxidizable gas on electrochemical processes proceeding on the sensing electrodes under different reference electrode potentials while the oxygen partial pressure from the sensing electrode side is kept constant.

The impedance spectroscopy investigations were done in the two-compartment cell cell (I) for each of the sensing electrodes. The $Pt_{1-x}Au_x$ electrodes were taken as working electrodes whereas the Pt electrode inside the YSZ tube was used simultaneously as a reference and counter electrode.

A typical impedance spectrum of a zirconia-based oxygen sensor is characterized by two semicircles in coordinates Z´ and Z´´ (Nyquist plot) as shown in Fig. 6.1 (a) [186, 187].

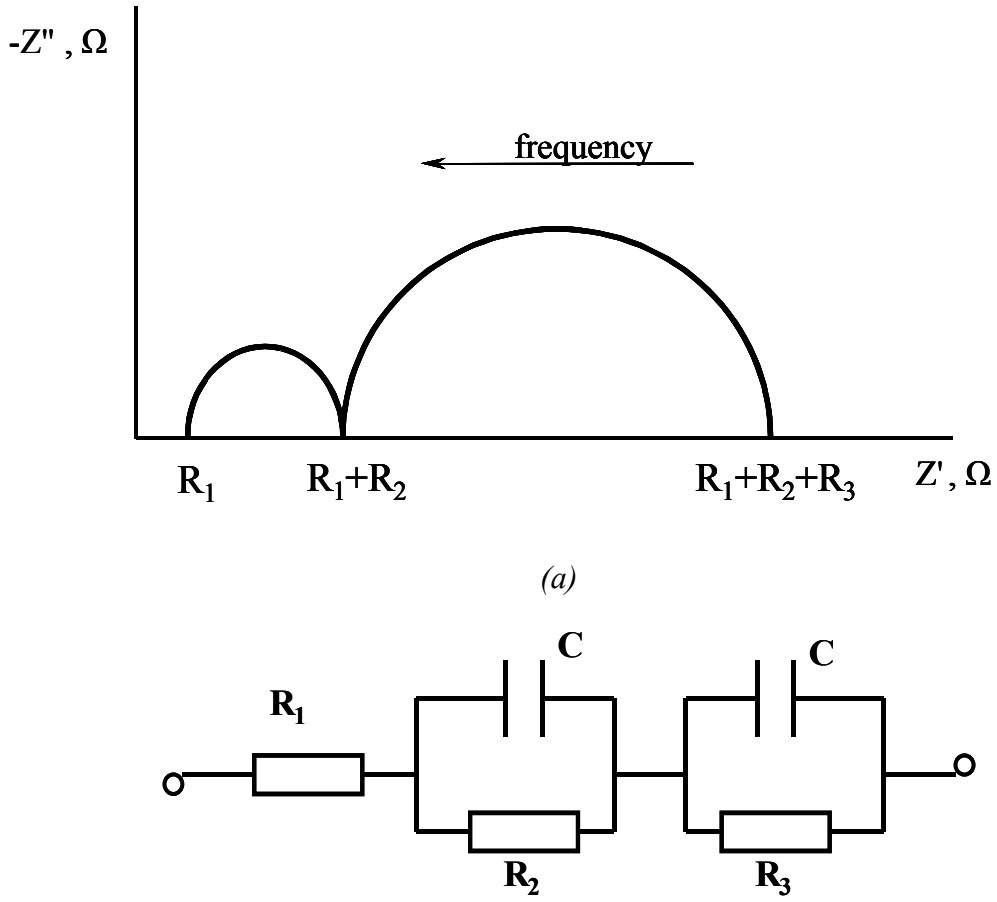

Fig. 6.1: A typical impedance spectrum (a) and corresponding equivalent circuit (b) for a zirconia-based oxygen sensor [186, 187]

The intersection of the low-frequency semicircle at the extreme right side of the abscissa is determined by the resistance arising from the electrode reaction on the three-phase boundary electrode/electrolyte/gas phase and is represented in the equivalent circuit, which is shown in Fig. 6.1 (b) by R_3. The values of R_1 and R_2 in Fig. 6.1 (b) represent the bulk and grain boundary resistance, respectively.

7 Experimental part

7.1 Characterization techniques

7.1.1 X-ray analysis and scanning electron microscopy

X-ray diffraction data for all the synthesized powders were obtained at room temperature on Siemens D5000 X-ray diffractometer (Siemens AG, Germany) using Ni-filtered Cu $K\alpha_{1+}\alpha_2$ radiation (λ = 1.54056 Å) in flat plane *θ/2θ* geometry. Data were collected in the range 10-80 ° *2θ*, in steps of 0.01 °, with a scan time of 2 s per step. The X-ray patterns were identified by means of JCPDS X-ray database [188] using EVA 5.0 Diffrac plus program (Bruker Analytic X-Ray Systems, USA).

The microstructure and the phase composition of $Pt_{1-x}Au_x$ alloys were investigated by scanning electron microscopy (SEM) (Zeiss DSM982 GEMINI) coupled with energy dispersive X-ray analysis (EDX) (Oxford-Instrument ISIS 300).

7.1.2 Chemical analysis

For the determination of very small amounts of CO it should be excluded that the sensing electrodes contain traces of C, H or N after removal of the organic binders.

For this purpose an elementary chemical analysis of the prepared powders was done by means of thermal conductivity detector “Elemental vario EL” (Elemental GmbH, Germany) after burning all organic components in a pure oxygen atmosphere ($p_{O_2} = 1 \cdot 10^5$ Pa). The detection limit of this method is 1 μg with a relative error of 1%.

7.2 Sensor components

7.2.1 Yttria-stabilized zirconia and Na-(ß+ß´´)-alumina solid electrolytes

Two kinds of yttria-stabilized zirconia (YSZ) ceramics were applied as an oxygen ion-conducting solid electrolyte. First, a commercially available one-end-closed 8 mol.% Y_2O_3 stabilized ZrO_2 (Lamtec GmbH, Germany) tube was used prepared from ZrO_2 and Y_2O_3 powders (Tosoh Corporation, Japan). This tube had a working length of 25 mm and a diameter of 8 mm with 1 mm wall thickness. The density of the YSZ tube was 6.05 g/cm^3 (98.2 % of the theoretical one). Second, commercially available YSZ pellets were taken (Friatec AG, Germany) with a dimension of 10 mm in diameter and 1 mm in thickness.

Solid electrolyte	Chemical composition	Amounts of the compounds [wt.%]
ZrO_2-Y_2O_3 (YSZ)	ZrO_2	91.987
	Y_2O_3	8.07
	Al_2O_3	max. 0.005
	SiO_2	0.005
	Fe_2O_3	max. 0.002
	Na_2O	0.021
Na-(ß+ß´´)-Al_2O_3 (NBA)	Al_2O_3	87.48
	Na_2O	9.14
	MgO	3.32
	Others	0.06

Table 7.1: Chemical compositions of the YSZ and NBA commercial materials

As a sodium ion-conducting solid electrolyte commercially available Na-(ß+ß´´)-Al_2O_3 (NBA) pellets (ABB [189], Germany) were used. These ceramic pellets were cut from the NBA tube and were 10 mm in diameter and 1 mm in thickness. After cutting the pellets were polished. The chemical compositions of the YSZ and NBA materials are represented in Table 7.1.

7.2.2 Electrode preparation

Solid state electrochemical cells are usually constructed by combining a membrane of the solid electrolyte with a pair of electrodes.

7.2.2.1 $Pt_{1-x}Au_x$ sensing electrodes

The different $Pt_{1-x}Au_x$ alloy sensing electrodes (x=0, 0.2, 0.5, 0.8, and 1) were prepared by chemical reduction of their corresponding metal compounds dissolved in ethylene glycol according to the following equations

$$H_2AuCl_4 \cdot 3H_2O \rightarrow 2HCl + Cl_2\uparrow + 3H_2O + Au\downarrow \text{ and} \quad (7.1)$$

$$H_2PtCl_6 \cdot 6H_2O \rightarrow 2HCl + 2Cl_2\uparrow + 6H_2O + Pt\downarrow . \quad (7.2)$$

In addition to its role as solvent, the ethylene glycol also acts as a reducing agent.

Synthesis of $Pt_{1-x}Au_x$ alloy particles from an ethylene glycol solution of their corresponding acids depends greatly on the operation mode. The formation of a true solution of Pt and Au seems to require conditions that allow the simultaneous reduction of both metal species and the deposition of both metal atoms into the same crystal lattice [190].

$Pt_{1-x}Au_x$ alloy particles (with different wt.% ratios) were synthesized, according to [190], in a three-necked round flask (1) by heating an ethylene glycol solution (~150 ml) of $H_2PtCl_6 \cdot 6H_2O$ and $HAuCl_4 \cdot 3H_2O$ (Merck Eurolab GmbH, Germany), taken in appropriate stoichiometric amounts, to 120 °C at a rate of 1 K/min as shown in Fig. 7.1. The Au and Pt acids were dissolved together in ethylene glycol at room temperature under magnetic stirring (2 and 3, respectively), and then the solution was slowly heated to the final reaction temperature via a heating mantle connected to a Eurotherm 902 S regulator (Eurotherm Regler GmbH, Germany) (4) by Ni/Ni-10%Cr thermocouple. The temperature was controlled in parallel by thermometer (5). The preparation was stopped after 1 h reaction at 120 °C. The suspension was then cooled in tap water. A clear supernatant was obtained since the solid settles and deposits on the bottom of the flask. The supernatant was separated from the solid precipitate by decantation. The solid product recovered was washed with water and acetone, and left to dry in air.

Difficulties occurred upon preparation of the pure Au particles. Unfortunately, the Au powder did not precipitate from the ethylene glycol solution. After several attempts glycerin-1-monooleat ($C_{21}H_{40}O_4$) was successfully used for the preparation of the fine pure gold particles using the same procedure of synthesis, which is described above.

The obtained powders were smeared onto the YSZ surface using amylacetate as an organic binder and were calcined at 950 °C for 15 min in order to obtain the final $Pt_{1-x}Au_x$ sensing electrode materials. As an example, Fig. 7.2 shows the X-ray powder diffraction pattern of $Pt_{0.8}Au_{0.2}$ alloy after annealing at 950 °C for 15 min. In this diffractogram the position of the Pt and Au peaks are given by the solid and dashed lines, respectively.

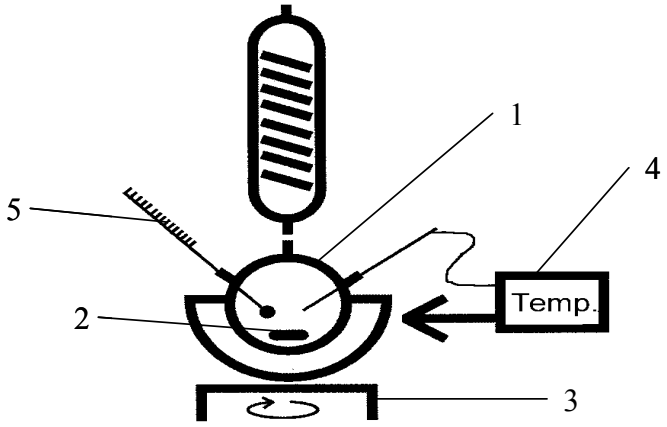

Fig. 7.1: Schematic view of experimental set-up for synthesis of $Pt_{1-x}Au_x$ sensing electrode materials (elucidations in the text)

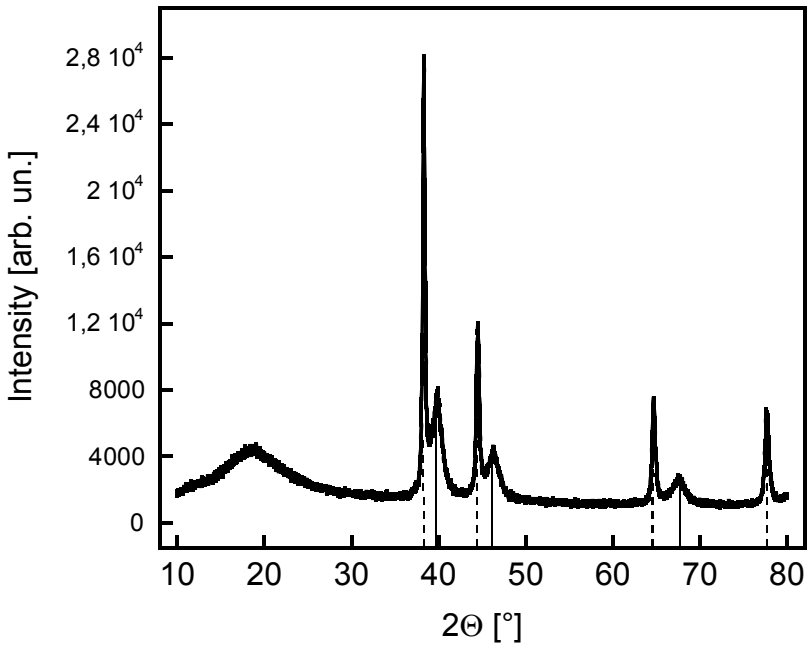

Fig. 7.2: X-ray powder diffractogram pattern of $Pt_{0.8}Au_{0.2}$ sensing electrode after annealing at 950 °C for 15 min (solid lines - Pt, dashed lines - Au)

The other $Pt_{1-x}Au_x$ alloy compositions have the same X-ray patterns with intensities of the peaks depending on *x*. For better comparison the X-ray powder diffractograms for pure Pt and Au metals are shown in Figs. 10.1 and 10.2 of Appendix A, respectively.

From Fig. 7.2 it is very well visible that the reduction of both metal species by ethylene glycol is simultaneous, thus leading to co-precipitation of platinum and gold metals from the solution. Finally, this result indicates that all the sensing electrode materials consist simultaneously of Pt and Au metals.

After preparation of the $Pt_{1-x}Au_x$ sensing electrodes on the surface of YSZ solid electrolyte the sensing electrode surfaces were characterized by scanning electron microscopy (SEM). Figure 7.3 (a) and (b) represents SEM images which show the morphology of the two different $Pt_{1-x}Au_x$ sensing electrodes prepared for the investigations.

On these images the white and light-grey colours represents the metal Pt or $Pt_{1-x}Au_x$ alloy, respectively, whereas the black one is the surface of the YSZ solid electrolyte. According to these figures, it is possible to conclude that the $Pt_{1-x}Au_x$ sensing electrodes have high enough (tpb) sites for occurrence of electrochemical reaction with participation of O_2 or CO.

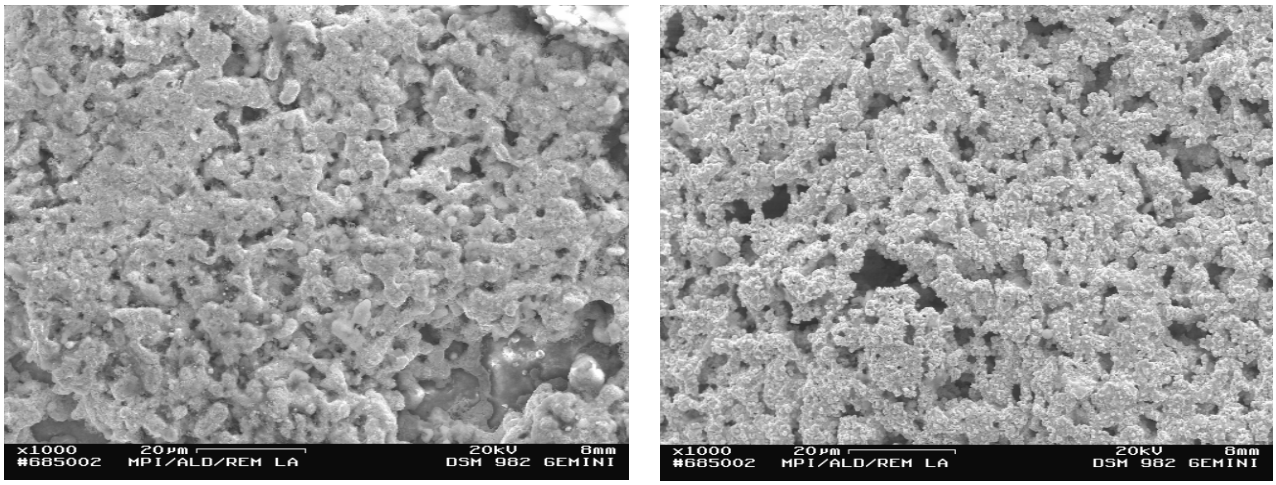

(a) *(b)*

Fig. 7.3: SEM images of (a) Pt and (b) $Pt_{0.8}Au_{0.2}$ sensing electrodes

7.2.2.2 Na_2CO_3(Au) reference electrode

Initially, the commercial available Na_2CO_3 powder (Merck GmbH, Germany) was „fried" at 300 °C over night for removal of the water from the sample.

After that the Na_2CO_3 pellets were prepared by isostatically pressing a mixture of Na_2CO_3 powder with statistically distributed gold wires (thickness of the gold wire was 250 µm) for 1 min at a pressure of 800 kN. The green body was afterwards sintered for 1 h at 750 °C in air. Subsequently, its surfaces were polished to flatness (diameter: 10 mm; thickness: 1 mm). Owing to the dispersed gold wires, the room temperature resistance of the samples was less than 1 Ω.

7.3 Cell arrangements

All the experiments for the characterization of the CO sensitivity of the $Pt_{1-x}Au_x$ sensing electrodes were carried out under certain conditions: (i) the oxygen partial pressure in the working gas is much higher than the CO concentration and (ii) the temperature range varied from 400 to 700 °C. At higher temperatures, according to the literature survey, the CO sensitivity is close to zero due to oxidation of CO by bulk O_2. At temperatures lower than 400 °C various kinetic restrictions appear and very long time is required for the achievement of steady state values.

7.3.1 Two-compartment cell configuration (I)

In this investigation two-compartment galvanic cells (cell (I)) with $Pt_{1-x}Au_x$ (x=0, 0.2, 0.5, 0.8, and 1) as the sensing electrode materials for characterization of those sensing properties in presence of CO in the gas stream were used.

A schematic view of the one-end-closed YSZ tube together with the electrodes used in two-compartment galvanic cell (I) is shown in Fig. 7.4. The platinum-gold sensing electrodes (2) with amylacetate as an organic binder were smeared by brush as thin as possible onto the outer surface of the stabilized zirconia tube (1). For the preparation of the reference electrode on the inner surface of the tube the commercially available Pt paste (5) (DEMETRON GmbH, Germany) was smeared with 2-ethoxyethanol as an organic binder. Then the cell together with electrodes was put into the tubular furnace and heated up to 950-1000 °C with a heating rate of 5 K/min and maintaining this temperature for 15 min for removal of the organic binder. The temperature of annealing depended on the composition of the $Pt_{1-x}Au_x$ sensing electrodes. After that the assembly was placed into an alumina ceramic tube (Friatec AG, Germany) (4) and sealed by means of a gold ring (3). For the sealing the gas compartments from each other the cell was heated up to 800 °C with a heating rate of 5 K/min and after that it was heated up to 1000 °C with the heating rate of 2 K/min, maintained at this temperature for 30 min and then cooled down to the working temperature region with the same rate. Around the temperature of 1000 °C gold becomes soft that provided hermetically sealed gas compartments.

Pt wires and Pt mesh (W.C: Heraeus GmbH&Co. K.G., Germany) attached to the electrodes were used as the output terminal and the electrical collector (6), respectively. For controlling the operating temperature the Pt/Pt-Rh(10 %) thermocouple (7) was used inside the galvanic cell.

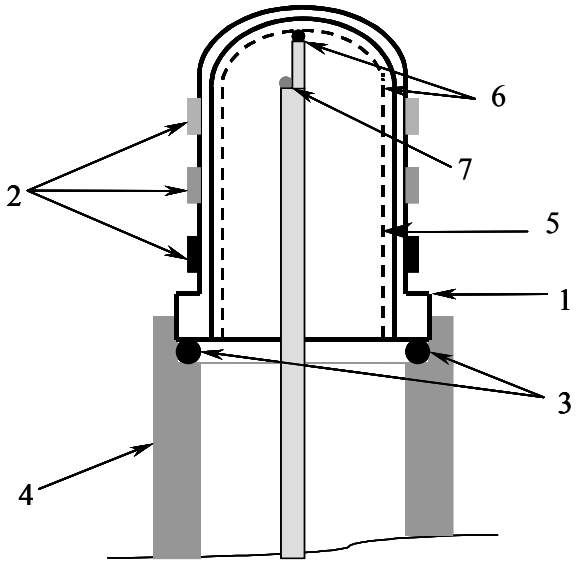

Fig. 7.4: Schematic view of the YSZ solid electrolyte tube with the electrodes used in the two-compartment galvanic cell (I) (elucidations in the text)

The whole construction of the two-compartment cell configuration used for the present study is shown in Fig. 7.5. The central part of the apparatus is the alumina tube with a high-temperature stabilized zirconia tube and three different electrodes, serving simultaneously as the sensing electrode. It is placed in a quartz glas device mainly consisting of the one-end-closed tube and a basis component. The construction of the measuring cell and separation of the gas compartments is described above in detail. The sealing of the cell was achieved by the quartz glas tube which was strongly connected with the basis of the quartz glas device by means of the metal springs.

The alumina tube with the measuring cell was placed into the quartz device and sealed additionally by means of APIEZON W40 (Apiezon Products Limited, Great Britain). Inside the alumina tube the capillary for flowing a reference gas to the reaction zone and thin four-holes alumina tube with Pt-10%Rh/Pt-thermocouple for temperature control and reference electrode contact (Pt) were input, which were folded additionally by metal spring in the bottom of the quartz cell. Pt wires with a thickness of 0.25 mm hermetically isolated by thin alumina tubes in the middle of the cell and by APIEZON W40 paste in the bottom of the cell were used as the contacts and current leads.

Pure O_2 and a H_2/H_2O equilibrium gas mixture were applied as a reference electrodes. Pure molecular hydrogen was bubbled through the distilled water immediately before passing through the measuring cell and after that the H_2/H_2O mixture was flushed through a capillary inside of the alumina tube to the reaction zone of the cell.

The cell was then placed in the quartz glas tube with connectors for inlet and outlet for the measuring gas. The measuring gas flows to the reaction zone through a thin quartz glas capillary. The cooling water was circulated permanently in the basis component of the quartz glas tube.

7.3.2 Bi-electrolyte galvanic cells (II) – (V)

The schematic views of the pellet arrangements used in the bi-electrolyte cells (II)-(V) are shown in Figs. 7.6-7.8. On the surface of the polished YSZ pellet the $Pt_{1-x}Au_x$ (x=0, 0.2) working electrode was smeared by brush as thin layer with amylacetate as an organic binder. After that the pellet was heated up to 1000 °C in the tubular furnace with a heating rate of 5 K/min and was maintained at this temperature for 15 min for removal of all organic components and in order to prepare the fine working electrode.

The short circuiting of the NBA pellet was done by gold sputtering on both surfaces and lateral side of that simultaneously in form of a thin film (few nanometers). Gold sputtering was carried out by plasma sputtering BALZERS UNION SCD-040 (Lichtenstein) with a gold target in vacuum atmosphere (carrier gas - Ar) at room temperature. The constant current was 50 mA and the duration 60 sec.

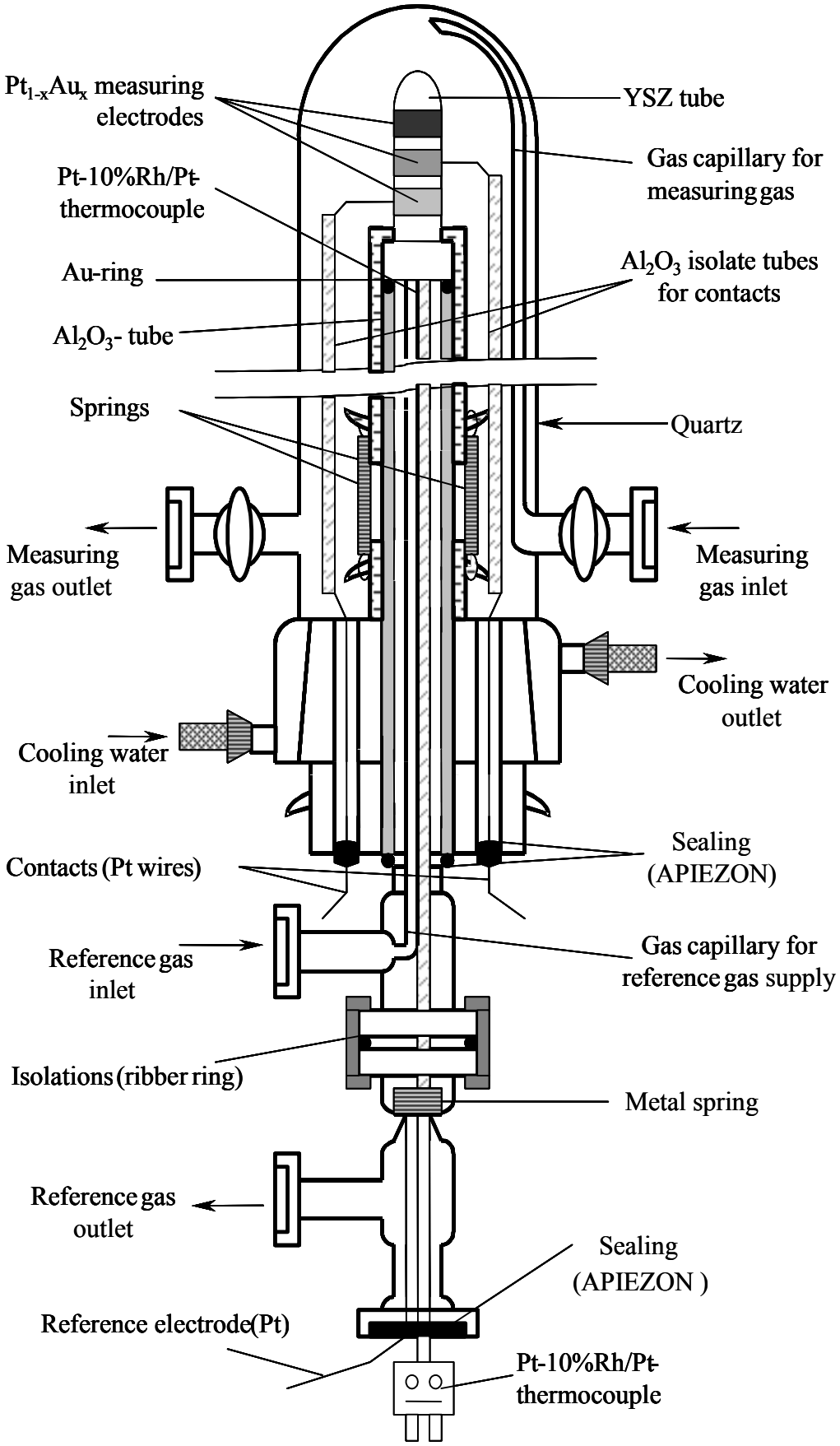

Fig. 7.5: Schematic view of the two-compartment galvanic cell configuration (I)

The preparation of the counter electrode, Na_2CO_3(Au), with catalyst layer included several steps. Firstly, on the surface of the short-circuited polished Na_2CO_3(Au) pellet having a room temperature resistance less than 1 Ω the gold net (W.C. Heraeus GmbH&Co. K.G., Germany) was placed.

A catalyst powder "Hopkalit HTK15" (MSA AUER GmbH, Germany) was used, which consists of manganese oxide (MnO_2) and copper oxide (CuO). The technical characteristics of the catalyst powder are represented in Table 7.2.

With the practical preparation of the bi-electrolyte galvanic cells a very important question is the choice of an organic binder for the synthesis of thin catalyst layer on the counter electrode because in the frame of the investigation very small concentrations (or even traces) of CO in gas phase has been characterized. However, the bulk catalyst could still have residual concentrations of carbon and hydrogen after annealing the catalyst layer using organic binders. It could lead distorted results or wrong values of voltage. In order to preclude this several attempts of annealing catalyst layer have been carried out before using different kinds of organic binders. Initially, ethylene glycol, butanediol, and amylacetate were chosen as organic binders. The choice of organic binder was based on the fired temperature of the counter electrode (Na_2CO_3), which must not exceed 700-750 °C.

In case of using ethylene glycol as an organic binder there was very poor adhesion after sintering between the catalyst layer and the surface of the counter electrode. In other words, the catalyst layer had very bad mechanical properties and could not be used in the practical application. Table 7.3 shows the results of the elemental chemical analysis of the carbon and hydrogen content of the catalyst powders after their annealing at 700 °C for 1h using another two kinds of organic binders.

As it is seen from Table 7.3, in case of using butanediol as an organic binder there are still some small amounts of carbon after annealing of the catalyst. It means that the bulk catalyst powder still contains a certain concentration of carbon as well. However, the analysis of the catalyst powder after sintering using amylacetate has shown that there are no as traces of hydrogen as traces of carbon.

Characteristics of catalyst	Parameter
Chemical composition	MnO_2, CuO
Oxidation time	0.5 s
Particles size	1…2 mm
Bulk density	ca. 1.15 g/cm^3
Oxidation surface	ca. 200 m^2/g

Table 7.2: Technical characteristics of the catalyst powder "Hopkalit HTK15"

Organic binder	Element	Analysis of probes, x_i [wt.%]	Amounts [wt.%]
Butanediol	C	0.0, 0.0, 0.0, **0.13**, 0.0, **0.26**	< **0.2**
	H	0.0, 0.0, 0.0, 0.0, 0.0, 0.0	< 0.1
Amylacetate	C	0.0, 0.0, 0.0, 0.0, 0.0, 0.0	< 0.1
	H	0.0, 0.0, 0.0, 0.0, 0.0, 0.0	< 0.1

Table 7.3: Elemental chemical analysis of the catalyst powders on carbon and hydrogen after annealing at 700 °C for 1h using different organic binders

This allows to assume that the obtained catalyst layer does not contain residual traces of organics and that it could be successfully used in the bi-electrolyte galvanic cells for the oxidation of CO to CO_2 from the counter electrode side.

After that, the catalyst particles were finely distributed into amylacetate solution in order to prepare the catalyst paste. The paste was smeared on the top of the gold net by brush. In the case of the bi-electrolyte cells (II) and (IV) half of the gold net was covered by a thin catalyst layer (see top views in Figs. 7.6-7.7). This principle allows to achieve the thermodynamic equilibrium on the counter electrode very fast. CO oxidizes immediately to CO_2 in the vicinity of (tpb) sites where the thermodynamic equilibrium exists. Under excess oxygen and in the middle temperature range it leads to the assumption that the concentration of carbon dioxide in the reaction zone is actually equal to the CO concentration in the bulk gas phase. If catalyst layer covers the counter electrode completely, CO could react with oxygen on the catalyst surface directly producing CO_2, which removes further from the reaction zone by gas stream. Under this condition the concentration of CO_2 near the surface of the counter electrode will be unknown, or it could even be equal to zero, which makes it impossible to achieve thermodynamic equilibrium on the counter electrode.

For the bi-electrolyte cells (III) and (V) the catalyst dots were prepared in order to increase the rate of oxidation of CO to CO_2, to optimize the oxidation process, and, finally, to reach the steady-state voltages much faster (see top view in Fig. 7.8).

Na_2CO_3(Au) pellet kept together with a gold net and catalyst layer (or dots) was put into the tubular furnace and heated up to 700 °C with a heating rate of 2 K/min. Such a slow heating rate was chosen in order to preclude the carrying away of catalyst particles from the surface of the gold net.

In the case of the bi-electrolyte cells (II) and (III) three polished pellets, namely, YSZ, Na-(β+β´´)-Al_2O_3 (short-circuited or not), and with Na_2CO_3(Au) catalyst layer/dots short-circuited, were attached together to each other and put into a quartz glas tube (see Fig. 7.9, a). For the preparation of the bi-electrolyte cells (IV) and (V) the two gas compartments were preliminaryly sealed by means of the gold ring. For the sealing the polished YSZ pellet with the working electrode smeared

onto the surface of the electrolyte were attached together with the gold ring and alumina tube by springs, and then, the cells were heated up to 800 °C with a rate of 5 K/min. After that the cells were heated up to 1000 °C with a rate of 2 K/min, were maintained at this temperature for 30 min, and then, were cooled down to room temperature at the same rates. Around the temperature of 1000 °C gold becomes soft, which provided hermetically sealed gas compartments.

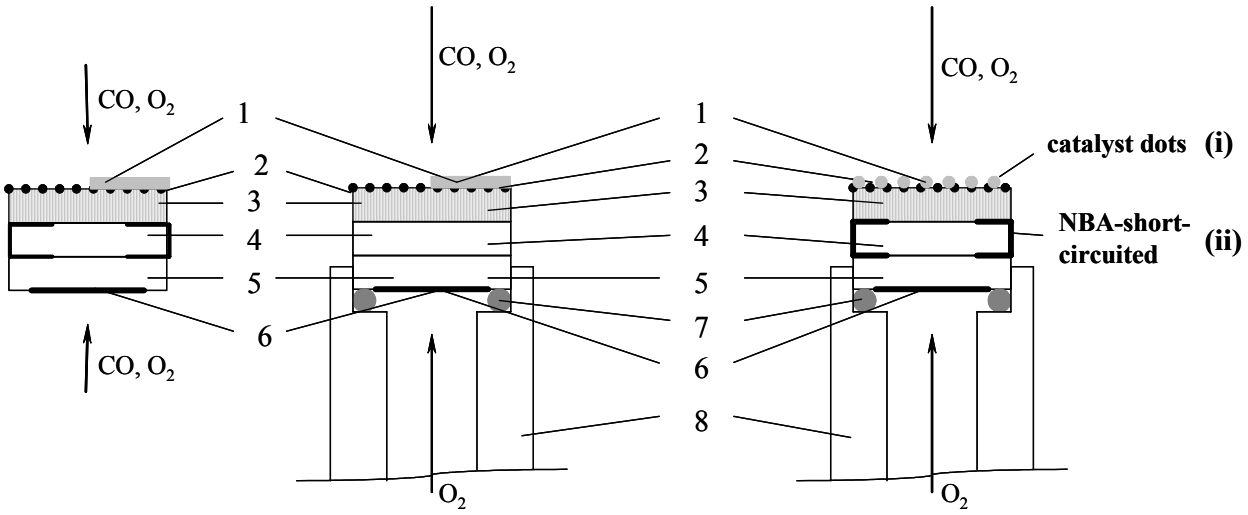

(a) cross view

(a) cross view

(a) cross view

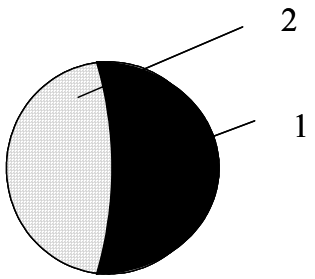

(b) top view

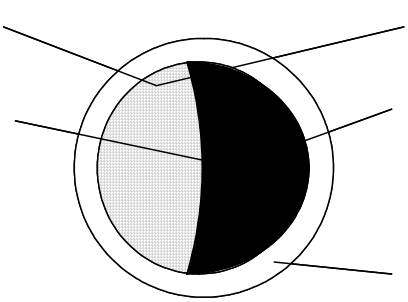

(b) top view

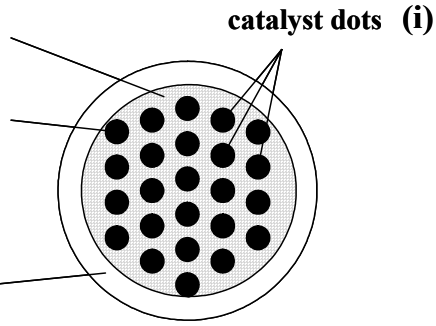

(b) top view

Fig. 7.6: The pellets arrangement for the bi-electrolyte cell (II) or (III)

Fig. 7.7: The pellets arrangement for the bi-electrolyte cell (IV)

Fig. 7.8: The pellets arrangement for the bi-electrolyte cell (V)

Used abbreviations: 1 – Catalyst (MnO_2, CuO); 2 – Au-net; 3 – Na_2CO_3(Au)-electrode; 4 – Na-(β+β‘‘)-Al_2O_3 (short-circuited or not); 5 – $ZrO_2(Y_2O_3)$; 6 – Pt (or $Pt_{1-x}Au_x$)-electrode; 7 – Au-ring; 8 – Alumina-tube

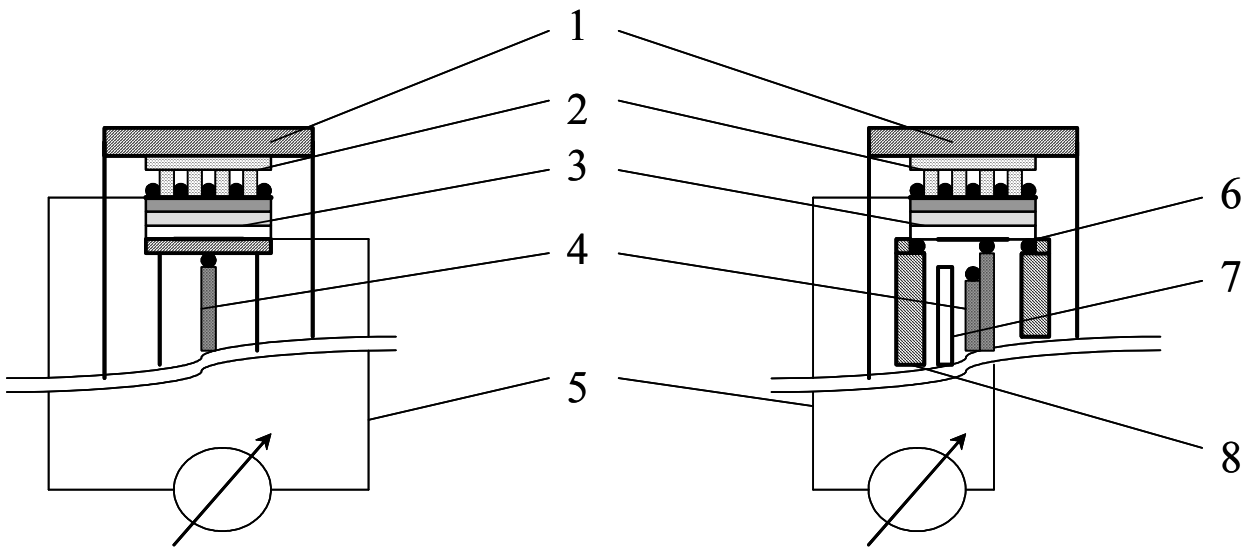

Fig. 7.9: General schematic views of configuration of the bi-electrolyte galvanic cells (a) - II and III, (b) – IV and V

Used abbreviations: 1 – Quartz sample holder; 2 – Alumina protect pellet with deep canals; 3 – Measuring cell; 4 – Pt-10%Rh/Pt-thermocouple; 5 – Contacts (Pt wires); 6 – Au-ring; 7 – Gas capillary; 8 – Alumina-tube

Finally, three polished pellets were attached to each other and put into the quartz tube (see cross views in Figs. 7.7-7.8). Pt wires and Pt mesh attached to the electrodes were used as the output terminal and the electrical collector, respectively.

The general schematic views of the central part of the bi-electrolyte cells (II) – (V) are represented in Fig. 7.9. The measuring cells were put between two quartz glas tubes. On the top of the catalyst an additional alumina pellet was put, which had deep (at least, 1 mm) open canals for the diffusion of the measuring gas and serving the initial catalyst and counter electrode surfaces in safety. Excepting the cell arrangemets it had the same components as described above in the chapter (7.3.1) for the galvanic cell (I).

7.4 Measuring setup

7.4.1 Preparation of the gas mixtures

Gas sensing experiments were carried out with gas mixtures which were prepared by premixing CO with Ar 6.0 and O_2 5.0 from compressed gas bottles. For the measuring (or detectable) gas different CO concentrations (0 - 40 000 ppm) and various O_2 concentrations (1 - 5 vol.%) were used, which

were diluted in highly purify Ar. The list of used gases and their purity are shown in Table 7.3. For the reference gas, pure O_2 or H_2 were used and composition of which are shown in Table 7.3. In case of using H_2, the gas was bubbled through distillated water before entering to the reaction zone of the cell. In the last column of Table 7.3 the O_2 partial pressure of the gases are represented. It is seen that according to the experimental conditions the gases have very small amounts of oxygen which can be neglected. All gases are commercially available (Messer Griesheim GmbH and Westfalen AG, Germany).

The gas composition was determined by controlling the flow rate of each gas. The concentration of the gases were established and controlled by the calibrated mass flow controllers Tylan RO-3070 (Tylan General GmbH, Germany). A general view of the scheme for preparing measuring gas mixtures is shown in Fig. 7.10.

At switching on the electrical switcher (Steuerungstechnik Staiger GmbH, Germany) the gases from the cylinders go through the mass flow controllers where the definite amounts of gas concentrations were established. After mixing all the gases the gas mixture was admitted to the measuring cell.

Type of gas	Gas abbreviation	Gas composition		p_{O_2}, Pa
		Gas	vol.%	
Measuring gas	Ar 6.0	Ar	99.9999	≤ 0.1 (≤ 1 ppm)
	O_2 5.0	O_2	99.999	$1 \cdot 10^5$
	CO 1 000 ppm, rest Ar 5.0	CO	0.102	≤ 1 (≤ 10 ppm)
		Ar	99.898	
	CO 100 000 ppm, rest Ar 5.0	CO	9.82	≤ 1 (≤ 10 ppm)
		Ar	90.18	
Reference gas	O_2 5.0	O_2	99.999	$1 \cdot 10^5$
	Ar 5.0	Ar	99.999	≤ 1 (≤ 10 ppm)
	H_2 5.0	H_2	99.999	< 0.1 (< 1 ppm)

Table 7.3: Technical characteristics of gases (Messer Griesheim GmbH and Westfalen AG, Germany) used under our study

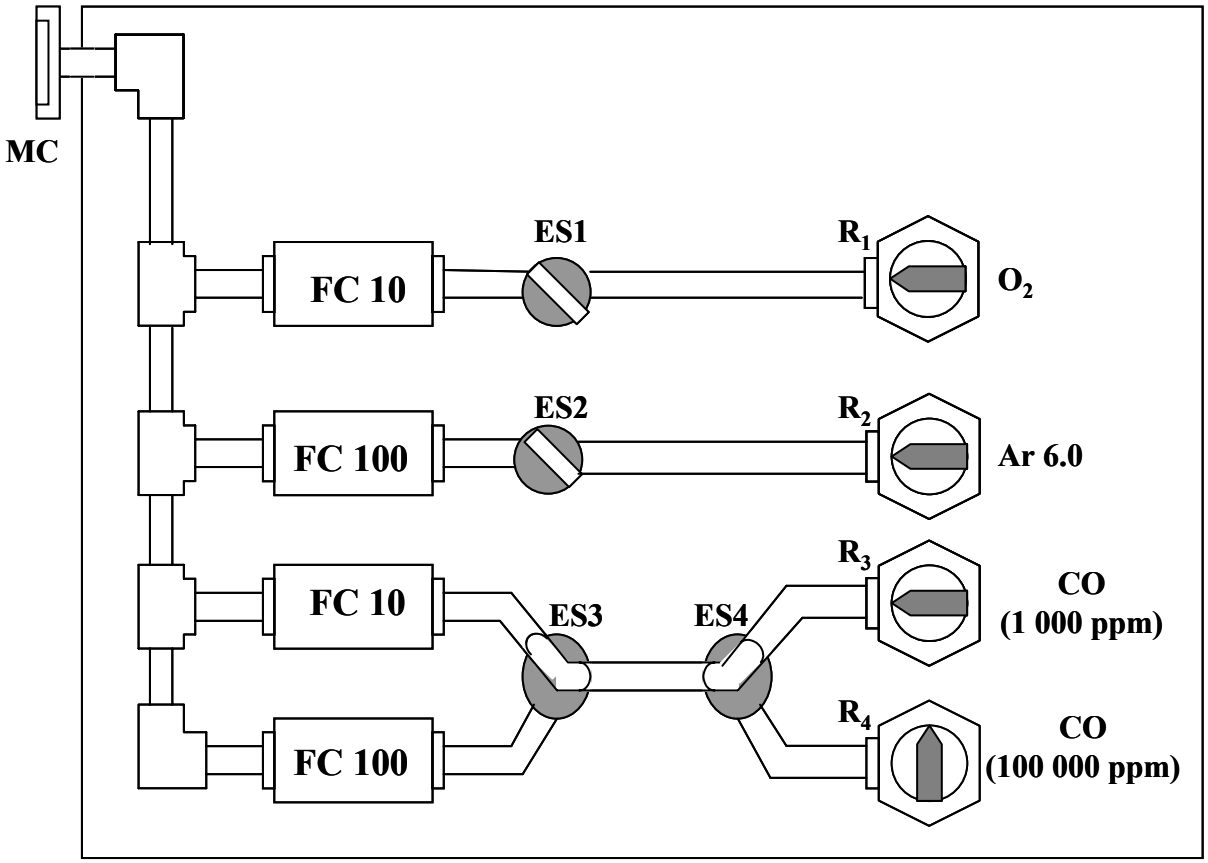

Description of the abbreviations:

R_1-R_4 – reducing agents for used gases (Messer Griesheim GmbH, Germany);

ES1-ES4 – electrical switcher for respective gas component (Steuerungstechnik Staiger GmbH, Germany);

FC10/100 – mass flow controllers (MILLIPORE GmbH, Germany):

10 – 10 cm^3/min,

100 – 100 cm^3/min;

MC – metal connection with the measuring cell (Swagelok GmbH, Germany).

Fig. 7.10: General view of the gas flow system

All the connections between different equipments were prepared from steel and copper tubes, commercially available metallic connectors (Swagelok GmbH, Germany), and special rubber isolated rings.

The total gas flow rate was maintained at 3 l/h (25 °C) for all the experiments. The gas flow rates of the reference and measuring gases were equal to each other.

7.4.2 Controlling setup

The general view of the control equipments used is represented in Fig. 7.11. The quartz glas reactor with the measuring cells inside was connected to the gas lines, which were described in detail above, and was put into the tubular furnace (HTM Reetz GmbH, Germany) in order that the measuring cell was kept in the zone of constant temperature. The temperature inside the tubular furnace was controlled by the Pt-10%Rh/Pt thermocouple, which was connected with a temperature regulator Eurotherm 902 P (or 902 S) (Eurotherm Regler GmbH, Germany).

For the determination of the voltage the cells were connected to the high-resistance electrometers with an input resistance of about 10^{14} Ω. In case of investigating the two-compartment cells two KEITHLEY 2000 (Kiethley Instruments GmbH, Germany) and two Hewlett Packard 34401A (Hewlett-Packard GmbH, Germany) electrometers were used whereas for investigating the bi-electrolyte galvanic cells the measurements of the open-circuit voltage were done by means of KEITHLEY 614/617 electrometers (Kiethley Instruments GmbH, Germany), respectively.

All the obtained results of voltages and also all the experimental conditions, namely, temperature, amounts and flow rates of gases, etc., were installed, controlled and saved permanently by personal computer and LABVIEW software version 5.0.1 (National Instruments™ Corporation, USA).

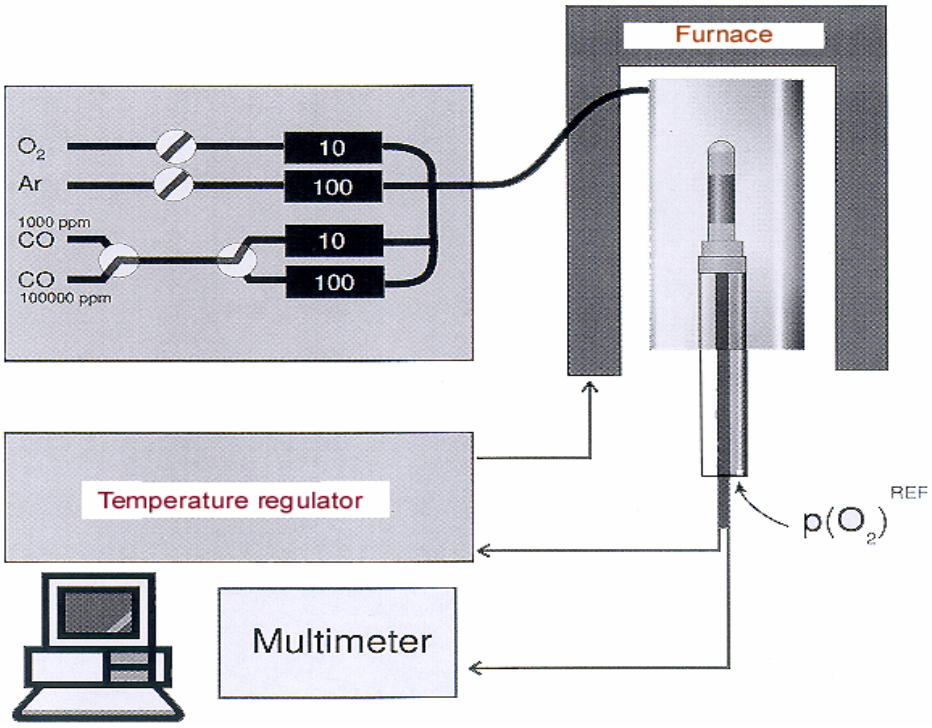

Fig. 7.11: Schematic measurement setup for characterization of the CO sensitivity

7.5 Impedance spectroscopy measurements

The measurements of resistance of the processes occurring on the sensing electrodes were performed by means of ac impedance spectroscopy using a Solartron 1255 system (BELLTEC Ing. Buero Glocke, Germany) in the frequency range from $1 \cdot 10^{-5}$ to $1 \cdot 10^{5}$ Hz in the temperature range of 400-700 °C. The signal amplitude was 10 mV. All the experimental data obtained by Potentiostat/Galvanostat 273 A (EG&G Princeton Applied Research, USA) were imported to a personal computer. The control of the experiment was carried out by impedance spectroscopy software (Impedance Spectroscopy, EG&G Princeton Applied Research, USA). The fitting of the results was done by means of the «Equivalent Circuit» program (software „Equivalent Circuit“, written by Bernard A. Boukamp; The Netherlands).

The concentration of CO was varied between 0 and 900 ppm while the oxygen partial pressure was kept constant and equal to $1 \cdot 10^{3}$ Pa.

Impedance spectroscopy measurements for each cell configuration were performed over two heating and cooling cycles from high to low temperatures.

8 Results and Discussion

8.1 Characterization of the CO sensitivity of $Pt_{1-x}Au_x$ electrodes using two-compartment cell (I)

8.1.1 Sensitivity under high reference electrode potential

Most of the investigations published in literature [20, 35, 36, 49, 56-60, 63, 66, 67, 69, 70, 73, 154] using two-compartment galvanic cells have been done under the condition that the reference electrode potential is higher than that of working electrode, i.e. $p''_{O_2} > p'_{O_2}$. In accordance to this, initial experiments were carried out under the same condition using pure molecular oxygen as a reference gas ($p''_{O_2} = 1 \cdot 10^5$ Pa) and a partial pressure at the working electrode being two order of magnitude smaller ($p'_{O_2} = 1 \cdot 10^3$ Pa).

8.1.1.1 Confirmation of Nernst behaviour

One of the main difficulties of practical application of the two-compartment galvanic cells is reaching a hermetic sealing between the two gas compartments. Due to that, initially, potentiometric measurements were carried out at different temperatures and oxygen partial pressures for confirmation of the validity of Nernst law in the absence of CO.

The dependence of voltage on temperature and oxygen partial pressure of the electrodes investigated is shown in Figs. 8.1 and 8.2, respectively. They are linear and the slopes of the experimental lines are close to the theoretical ones. It is necessary to note that the achievement of steady state voltages for the galvanic cells depends essentially on the operating temperature. At high temperatures the theoretical voltages are reached after 30-40 min whereas at low temperatures 2-3 h were required.

8.1.1.2 Time dependence of the voltage

For the confirmation of the fact that the present results have steady state values, preliminary special long-time measurements have been carried out for all two-compartment galvanic cells. Figure 8.3 shows the dependence of voltage on time at 500 °C in presence of 200 ppm CO in the working gas phase. It is well visible that at that temperature and after approximately 24 h the voltage values reach the steady state and further remain invariable.

Figures 8.4 (a)-(c) show the dependence of the voltage on time for the galvanic cells with three various sensing electrodes at 500 °C and at different CO concentrations in working gas, respectively. Again the voltage stays constant after a certain time under all conditions studied.

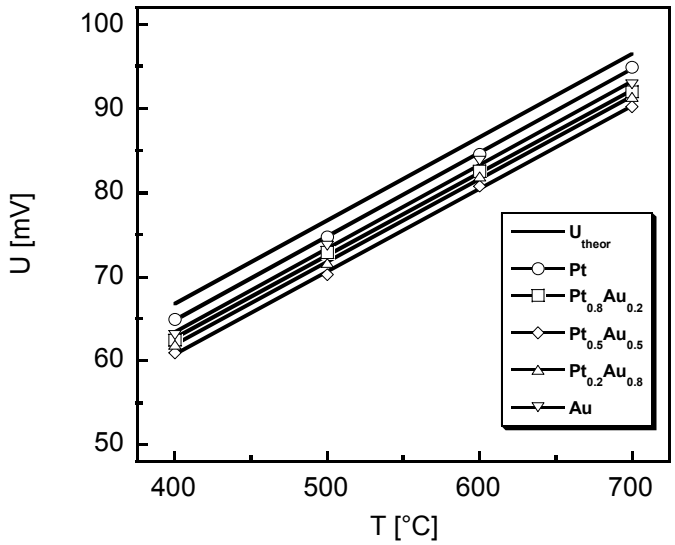

Fig. 8.1: Dependence of the voltage on temperature for all the galvanic cells with different sensing electrodes (no CO)

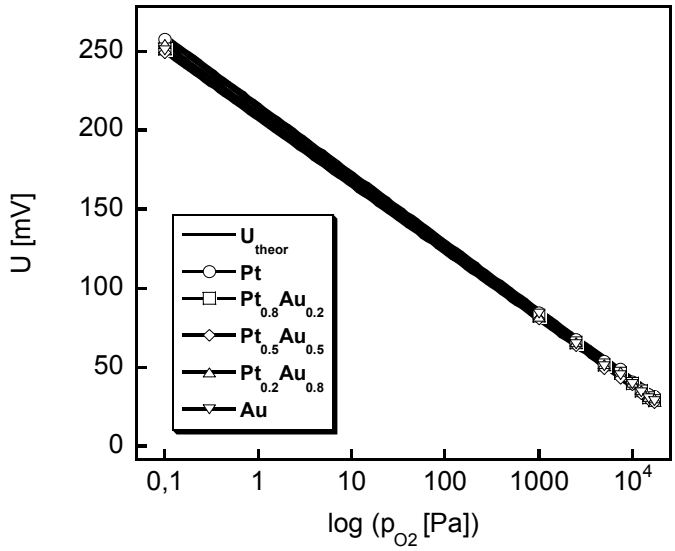

Fig. 8.2: Dependence of the voltage on the oxygen partial pressure in the working gas for all galvanic cells with different sensing electrodes at 600 °C (no CO)

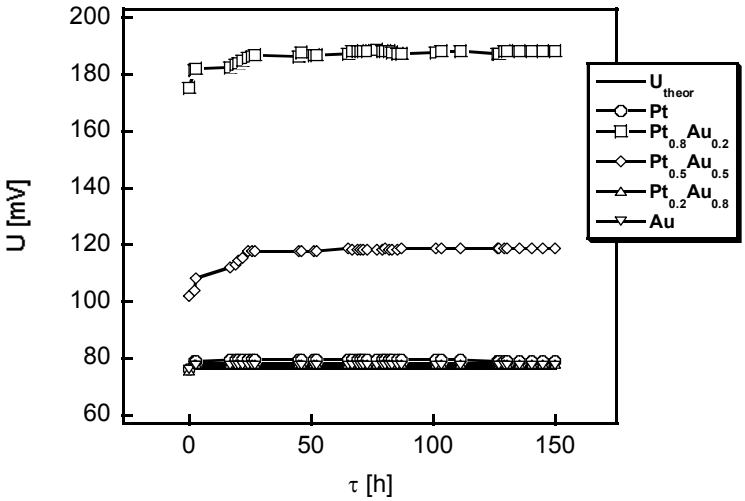

Fig. 8.3: Time dependence of the voltage at 500 °C and at 200 ppm of CO in the working gas

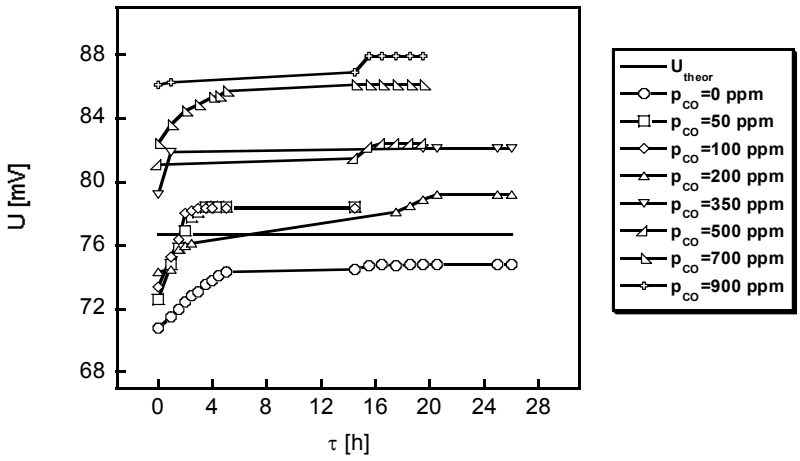

(a)

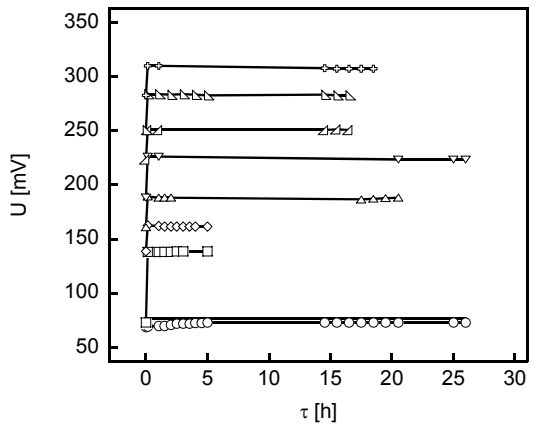

(b)

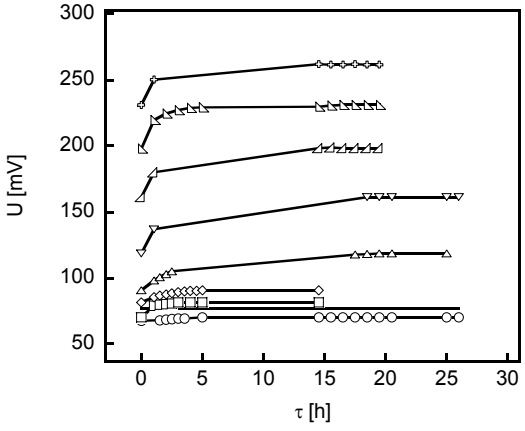

(c)

Fig. 8.4: Dependence of the voltage on time at 500 °C and at different CO concentrations for the galvanic cell (I) with (a) Pt, (b) $Pt_{0.8}Au_{0.2}$, and (c) $Pt_{0.5}Au_{0.5}$ sensing electrodes

In the case of the $Pt_{0.8}Au_{0.2}$ sensing electrode voltage increases sharply (jump-like behaviour) at changing CO concentration. The voltage reaches the new values very quickly and further remains constant (see Fig. 8.4, b). The galvanic cell with the $Pt_{0.5}Au_{0.5}$ sensing electrode exhibits a different behaviour (see Fig 8.4, c). In this case at changing CO concentration the voltage response begins to increase very slowly with time and reaches the steady state values only after a rather long time. This behavior allows to suppose that there are different kinetics of attaining the steady state values of voltage for the galvanic cells with the various sensing electrodes. It seems that the behavior of the galvanic cell with $Pt_{0.8}Au_{0.2}$ sensing electrode is the most stable one in time.

8.1.1.3 Voltage response to CO in gas stream

The dependence of voltage of the CO concentration ranging from 0 to $3 \cdot 10^4$ Pa at 500 °C is shown in Fig. 8.5 for all the galvanic cells with Pt-Au alloys sensing electrodes. The theoretical values were calculated by means of Nernst equation (see Eq. 6.2) where the oxygen partial pressure in the working gas (p'_{O_2}) have been determined in accordance with the following reaction

$$½O_2 + CO \leftrightarrow CO_2 \,. \qquad (8.1)$$

According to that, the so-called "stoichiometric point" where theoretical voltage increases sharply, is at a constant O_2 partial pressure of $1 \cdot 10^3$ Pa (10 000 ppm) and at a CO partial pressure of $2 \cdot 10^3$ Pa (20 000 ppm).

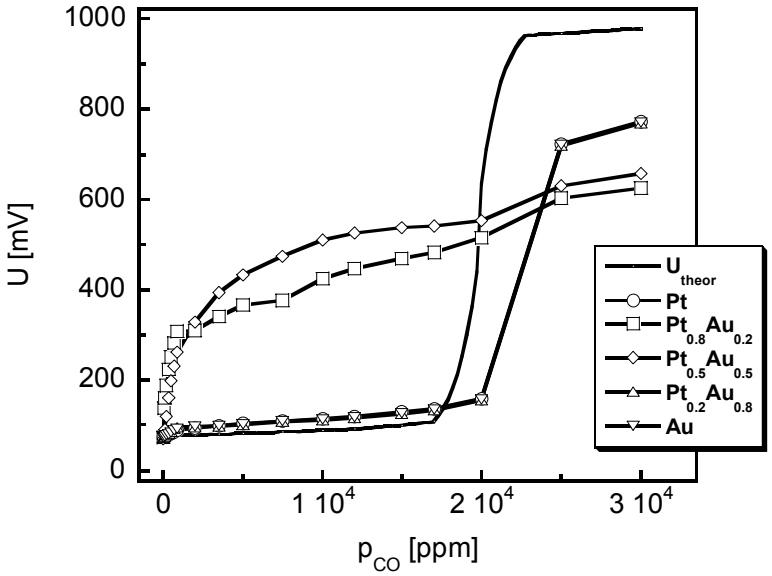

Fig. 8.5: Dependence of the voltage on CO concentration for all the investigated two-compartment galvanic cell (I) at 500 °C

It should be noted that the behaviour of galvanic cells with $Pt_{0.2}Au_{0.8}$ and pure Au sensing electrodes repeated practically the behaviour of the cell with the Pt electrode. The dependence of voltage for these three kinds of galvanic cells are close to the theoretical curve in the whole CO concentration range.

On the other hand, the voltage response of galvanic cells with $Pt_{0.8}Au_{0.2}$ and $Au_{0.5}Au_{0.5}$ sensing electrodes differ greatly from that expected theoretically. Particularly, when the O_2 partial pressure in the working gas is much higher than the CO concentration, i.e. $p'_{O_2} >> p_{CO}$. Since the values of the voltage for the galvanic cells with $Pt_{0.2}Au_{0.8}$ and pure Au sensing electrodes are comparable to those for Pt electrode, further voltage dependence was considered on CO concentration in the investigated temperature range for three galvanic cells with different sensing electrodes only, namely Pt, $Pt_{0.8}Au_{0.2}$, and $Pt_{0.5}Au_{0.5}$, which are shown in Figs. 8.6 (a)-(c). The solid lines represent experimental obtained results, whereas dashed and dashed-dot lines are theoretical ones.

It should be noted that in accordance to these results the voltages for the galvanic cell with Pt electrode (see Fig. 8.6, a) are close to theoretical ones at all the temperatures investigated.

It is necessary to discuss the response of galvanic cells with $Pt_{0.8}Au_{0.2}$ and $Pt_{0.5}Au_{0.5}$ sensing electrodes in more detail (see Figs. 8.6, b and c). It is very well visible that at each temperature the experimentally obtained results differ greatly from those expected theoretically. The whole interval of CO concentrations could be conventionally divided into three regions. In the first region, where the CO partial pressure changes from 0 to $1 \cdot 10^2$ Pa (0 to 1 000 ppm) and the oxygen partial pressure is much higher than that of CO ($p'_{O_2} >> p_{CO}$), the voltage response of these galvanic cells increase very sharply and exceed essentially the theoretical one. At further increasing CO concentrations, in the second region, where $p'_{O_2} \geq p_{CO}$, the voltage values increase weakly already, however, they still exceed theoretical magnitudes. In the third region, after passing through the “stoichiometric point”, the voltages of these two galvanic cells prolong to remain almost constant practically, but they differ from the theoretical one again.

Based on these results, the region (I) offers great interest where the voltage increases sharply and distinct strongly from the theoretical one in presence of CO traces in the working gas. In other words, the two-compartment galvanic cells with the $Pt_{1-x}Au_x$ (x=0.2, and 0.5) sensing electrodes reveal non-Nernstian behavior. It means that the Pt-Au alloy sensing electrodes show non-Nernstian electrode potential, which is described in chapter (5.1) in more detail.

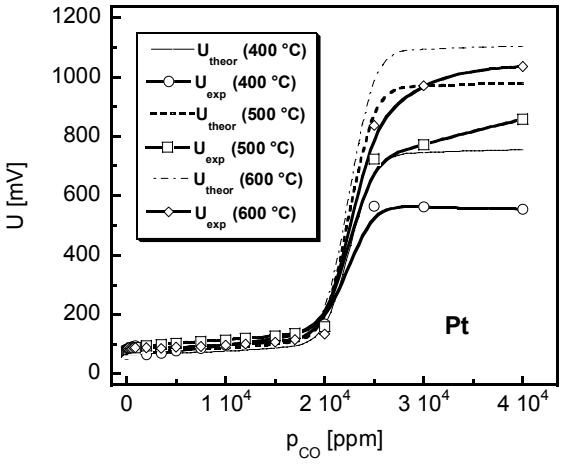

(a)

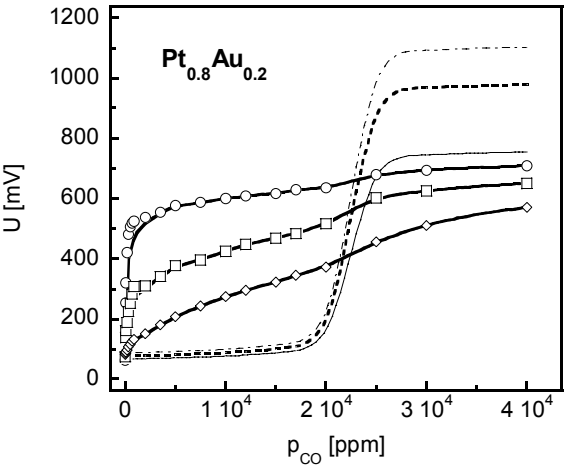

(b)

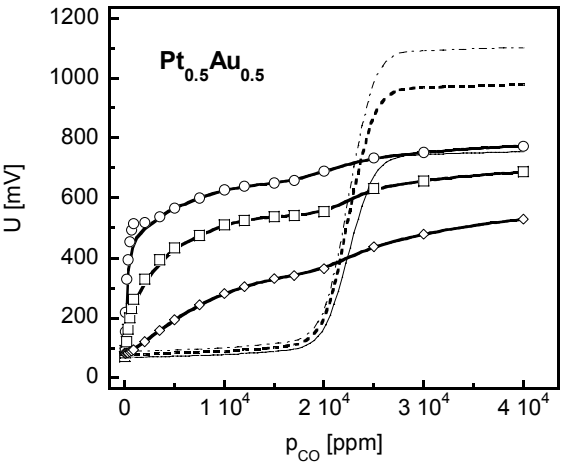

(c)

Fig. 8.6: Dependence of the voltage on CO concentration for the two-compartment galvanic cell (I) with (a) Pt, (b) $Pt_{0.8}Au_{0.2}$, and (c) $Pt_{0.5}Au_{0.5}$ sensing electrodes

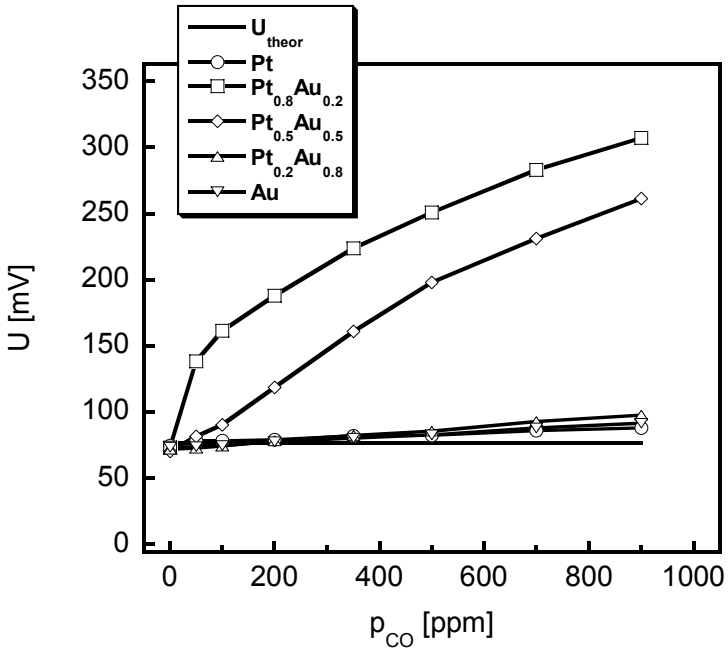

Fig. 8.7: Dependences of the voltage on CO concentration in the region (I) for all the investigated galvanic cells at 500 °C under high reference electrode potential

Further for characterization of the CO sensitivity of the Pt-Au alloy sensing electrodes we will consider the region (I) only, where CO concentration varies from 0 to 1 000 ppm, which is shown in Fig. 8.7 for all the investigated cell configurations at 500 °C in more detail, due to maximum deviations of the voltage from the theoretical one, calculating by Nernst equation.

8.1.1.4 CO sensitivity versus CO concentration, temperature and composition of the sensing electrode

The CO sensitivity of the two-compartment galvanic cells with the Pt-Au alloy sensing electrodes was defined by the absolute difference between the experimental voltage at a finite CO concentration and that under zero CO content.

The dependence of CO sensitivity on CO concentration in the working gas for all types of sensing electrodes under high reference electrode potential at the first run of experiment are shown in Figs. 8.8 (a)-(d) at all investigated temperatures, respectively. It can be seen that the galvanic cells with $Pt_{0.8}Au_{0.2}$ and $Pt_{0.5}Au_{0.5}$ sensing electrodes exhibit the highest CO sensitivity at all the experimental temperatures in comparison with the other electrodes investigated, which have very low values or such even close to the zero line. The highest CO sensitivity for the cells with the $Pt_{0.8}Au_{0.2}$ and $Pt_{0.5}Au_{0.5}$ sensing electrodes is observed at lowest temperature (400 °C) (see Fig. 8.8, a). With

raising temperature the CO sensitivity for all the galvanic cells decreases substantially (see Figs. 8.8, b-d). Finally, at 700 °C the CO sensitivity becomes very low and magnitudes do not exceed 10 mV (see Fig. 8.8, d). Due to that the CO sensitivity of the cells at temperatures higher than 600 °C will have not been discussed any more.

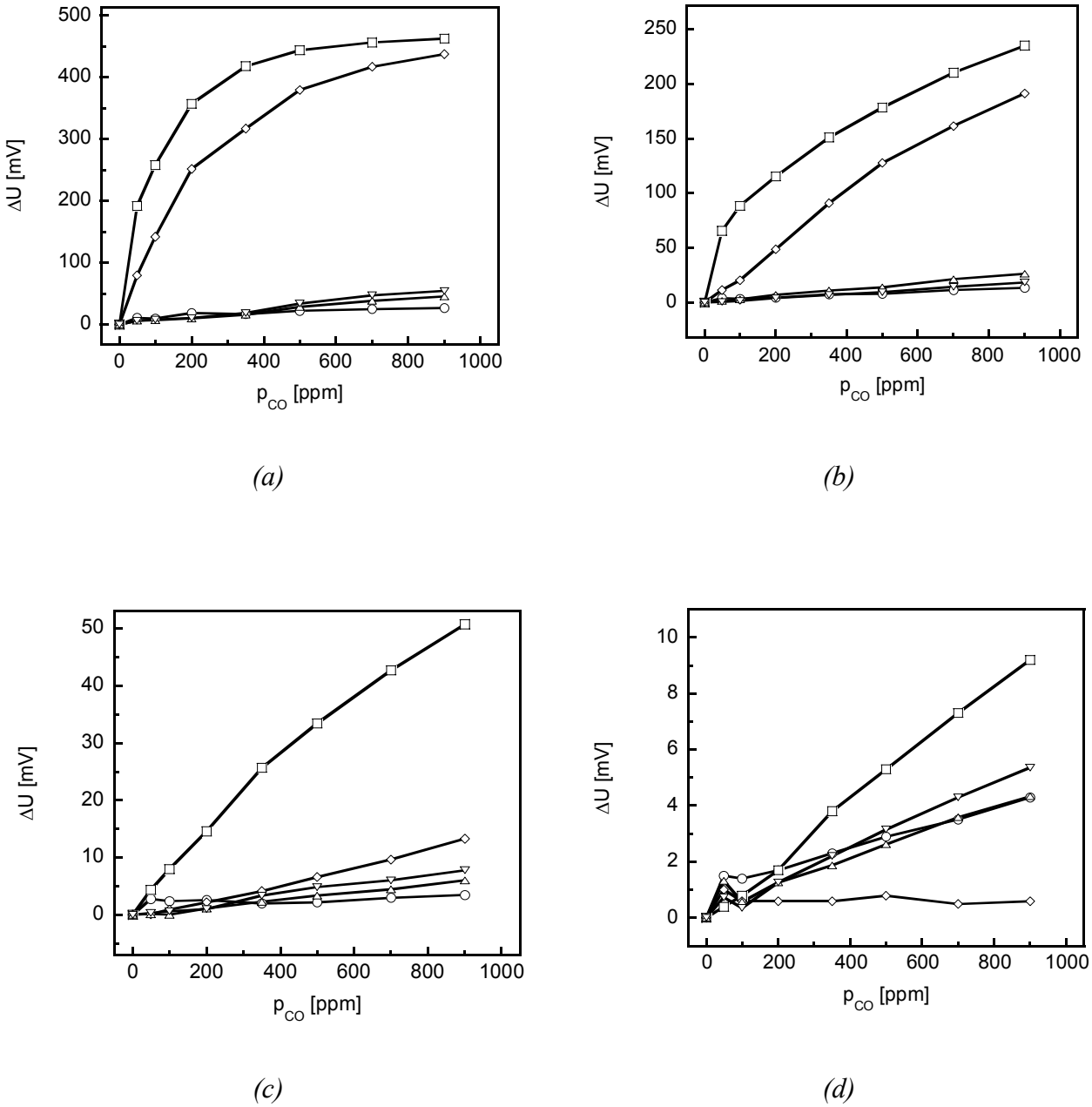

Fig. 8.8: Dependence of the CO sensitivity on CO concentration for all the investigated galvanic cells (I) at the first run of experiment at (a) 400 °C, (b) 500 °C, (c) 600 °C, and (d) 700 °C. ○ - Pt, □ - $Pt_{0.8}Au_{0.2}$, ◊ - $Pt_{0.5}Au_{0.5}$, △ - $Pt_{0.2}Au_{0.8}$, ▽ - Au

One of the main problems at characterization of the very small amounts of CO by galvanic cells with metallic electrodes is as already discussed non-reversibility and non-reproducibility of the experimental obtained results. Due to that the additional two runs of experiments for characterization of the CO sensitivity have been carried out. The results are shown in Figs. 8.9 (a)-(c) at three different temperatures, respectively.

Comparing these results with the data of the first run (see Fig. 8.8, a-c) it is well visible that the CO sensitivities obtained by the first and second runs have non-reproducible behavior. It can be also seen that at the second and third runs the CO sensitivity of all the galvanic cells has essentially smaller values than those at the first cycle of measuring. However, the dependences of CO sensitivity and their absolute values are comparable at the second and third cycles of experiments for each of the sensing electrode compositions (see Figs. 8.9, a-c). The results allow to suppose that reproducibility of the CO sensitivity is reached at all the investigated temperatures.

Reasons of such deviation between the first and second run could be explained by changing either the nominal composition of the Pt-Au electrodes or their morphology, for example, reducing the amounts of (tpb) sites. According to the literature [95], it is known that during the investigation of CO oxidation by solid electrolyte galvanic cells on the surface of polycrystalline platinum there is chemisorbed oxygen, which is not in equilibrium with oxygen electrode reaction. Due to that it is possible to assume the formation of platinum oxide (PtO_2) or Pt-O bonds on the surface of electrode, especially at high oxygen partial pressure, and some fraction of the sensing electrode can be blocked. Consequently, it can lead to a changing of the morphology and nominal composition of the sensing electrode and, finally, voltage response of the galvanic cell will change also.

Another reason of changing the response could be due to the maintaining of the galvanic cell for very long time at relatively high temperatures. Under this condition it is possible to assume that individual metal particles sinter together with formation of agglomerates or even fully dense fraction of the sensing electrode on the surface of the solid electrolyte. It leads to reducing the amounts of (tpb) sites, where electrochemical equilibrium is achieved, in comparison with the initial state. It can also change the response of voltage of the investigated galvanic cells.

Summing up all the obtained results of characterization of the CO sensitivity using the galvanic cells with $Pt_{1-x}Au_x$ sensing electrodes under high reference electrode potential it is necessary to note that the most preferable temperature range for the determination of CO traces in a gas stream is 400-500 °C. All the results of CO sensitivity on the composition of the sensing electrodes at 400 and 500 °C are shown in Figs. 8.10 and 8.11 for the first (a), and the second and third (b) run of experiments, respectively.

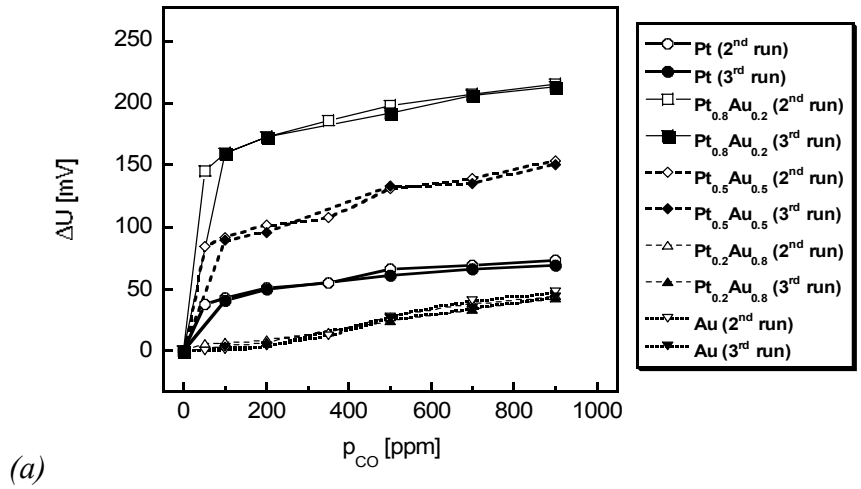

(a)

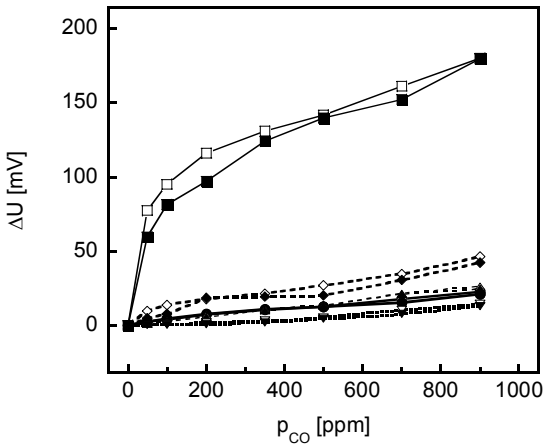

(b)

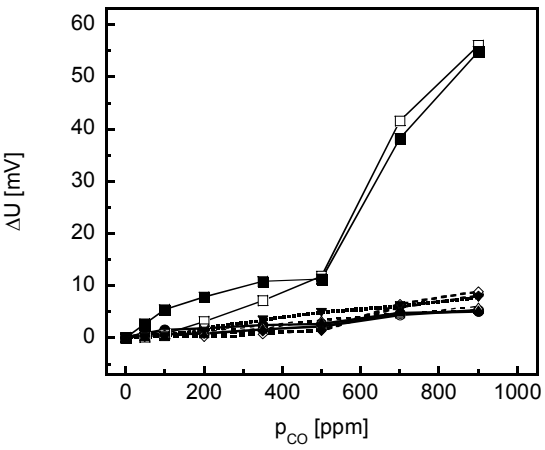

(c)

Fig. 8.9: Dependence of the CO sensitivity for the cells (I) at the second and third runs of experiments at (a) 400 °C, (b) 500 °C, and (c) 600 °C. ○ - Pt, □ - $Pt_{0.8}Au_{0.2}$, ◊ - $Pt_{0.5}Au_{0.5}$, △ - $Pt_{0.2}Au_{0.8}$, ▽ - Au

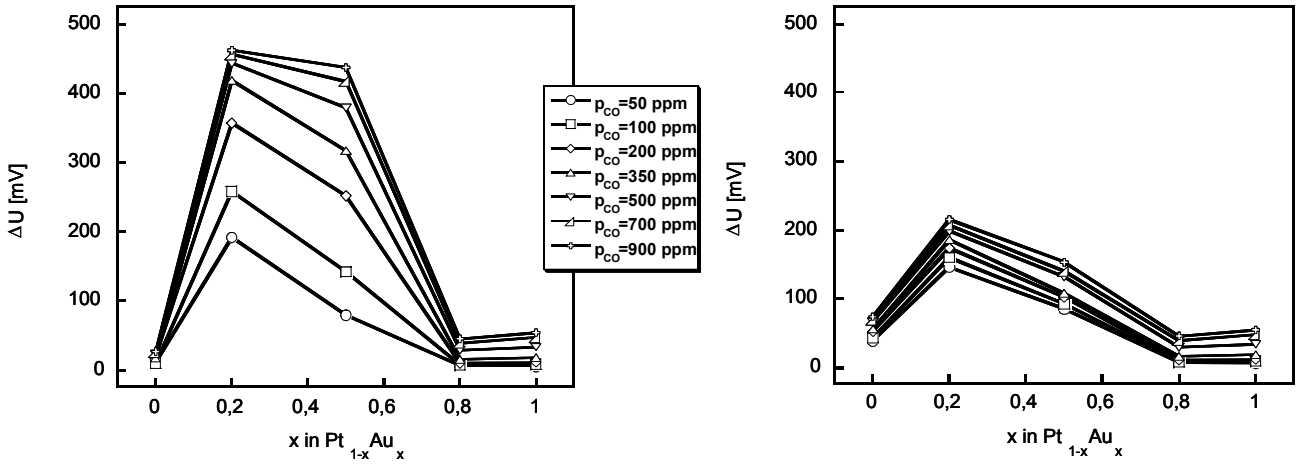

Fig. 8.10: Dependence of the CO sensitivity on x in the $Pt_{1-x}Au_x$ at 400 °C for (a) the first and (b) the second/third runs of experiments

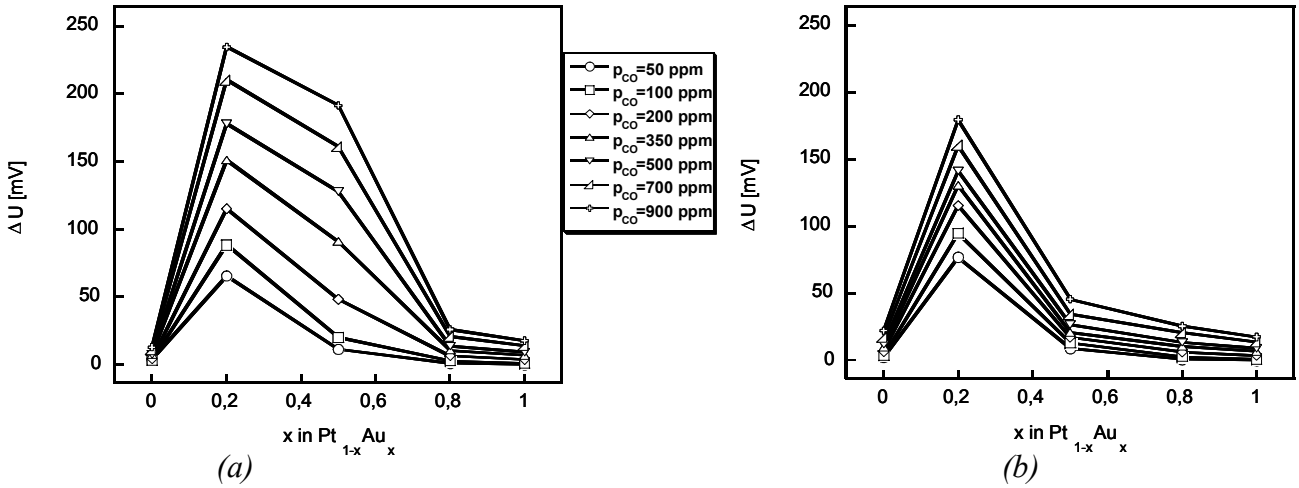

Fig. 8.11: Dependence of the CO sensitivity on x in the $Pt_{1-x}Au_x$ at 500 °C for (a) the first and (b) the second/third runs of experiments

In accordance to these results, the CO sensitivity has a maximum at x=0.2. The CO sensitivity for pure metals is comparable to each other and has minimum values. These results mean that $Pt_{0.8}Au_{0.2}$ sensing electrode is the best composition for practical applications in two-compartment galvanic cells (I) under high reference electrode potential and in the middle temperature range (~400-500 °C) for characterization of the small CO concentrations in gas stream.

The second preliminary conclusion proceeding from these results is that it is necessary to be very careful at estimating the experimental obtained CO sensitivities because the experimental conditions, morphology of electrodes and their pretreatment directly before experiments could make

very important influence as on the voltage response of galvanic cells sensing electrodes composed of Pt and/or Au as on the CO sensitivity of these materials.

8.1.2 CO sensitivity under low reference electrode potential

As mentioned above most of investigations of characterization of the CO sensitivity have been done under the high reference electrode potential. But if we consider the electrode reactions on the working electrode (see Eqs. 5.12-5.15 in chapter (5.4.2)) it is possible to see that electronic conductivity could influence also the process of CO oxidation by means of oxygen transport through a solid electrolyte.

A schematic view of the oxygen gradient through the potentiometric solid electrolyte galvanic cell at changing reference electrode potential is shown in Fig. 8.12. It can be assumed that the oxygen transport through a solid electrolyte could influence the processes proceeding on a working electrode and, therefore, to influence the CO response and the CO sensitivity of the $Pt_{1-x}Au_x$ sensing electrode materials. The change of the reference gas from higher oxygen partial pressures to lower ones allows to change polarity of the electrochemical cell, so to change oxygen gradient and oxygen transport through an YSZ electrolyte (see Fig. 8.12).

For understanding the influence of the reference electrode potential the investigations were carried out with a H_2/H_2O mixture as a reference gas. The calculation of the oxygen partial pressure at the reference electrode side using a H_2/H_2O equilibrium mixture is described in chapter (6.1.1). The oxygen partial pressure of the sensing electrode sides is kept unchanged.

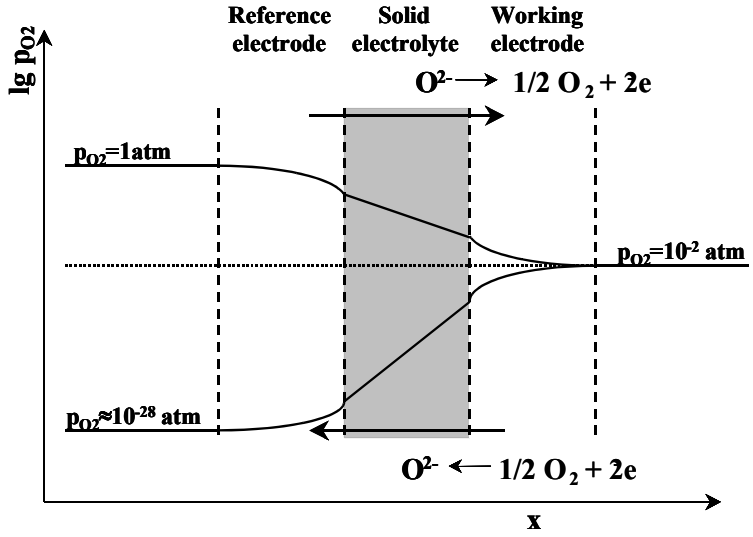

Fig. 8.12: Schematic view of the oxygen gradient through the potentiometric solid electrolyte galvanic cell (I) at changing reference electrode potential

8.1.2.1 Voltage response to transition from higher reference electrode potential to lower one

Figure 8.13 shows the dependence of the voltage on time at 400 °C for all the used galvanic cells at transition from high reference electrode potential to low one. Solid and dashed lines represent calculated theoretical voltages using H_2/H_2O equilibrium mixture and pure molecular oxygen as a reference gas, respectively.

The galvanic cells (I) with sensing electrodes of pure Pt, pure Au, and $Pt_{0.2}Au_{0.8}$ exhibit exact Nernst behavior whereas the voltage of cells with the two other alloy electrodes reaches at this temperature higher steady state magnitudes than those expected theoretically.

The same tendency keeps with raising temperature also. Figures 8.14 (a) and (b) illustrate the behavior of the investigated galvanic cells under low reference electrode potential at increasing temperature from 400 to 500 °C and from 500 to 600 °C, respectively. According to these dependences, the magnitudes of voltage for the galvanic cells with $Pt_{0.8}Au_{0.2}$ and $Pt_{0.5}Au_{0.5}$ sensing electrodes are still higher than theoretical ones (see Fig. 8.14, a). Only at high temperatures (600 °C) the values of the voltage approache more or less theoretical ones (see Fig. 8.14, b).

Nevertheless, it should be noted that all these dependencies obtained have reproducible character at repeating cycles by changing the reference electrode potential from high magnitude to low one. The voltages attain steady state values and remain constant with time. It confirms that all the obtained results have reversible behavior using H_2/H_2O equilibrium mixture as a reference gas in the galvanic cells with sensing electrode materials consisting of Pt and/or Au.

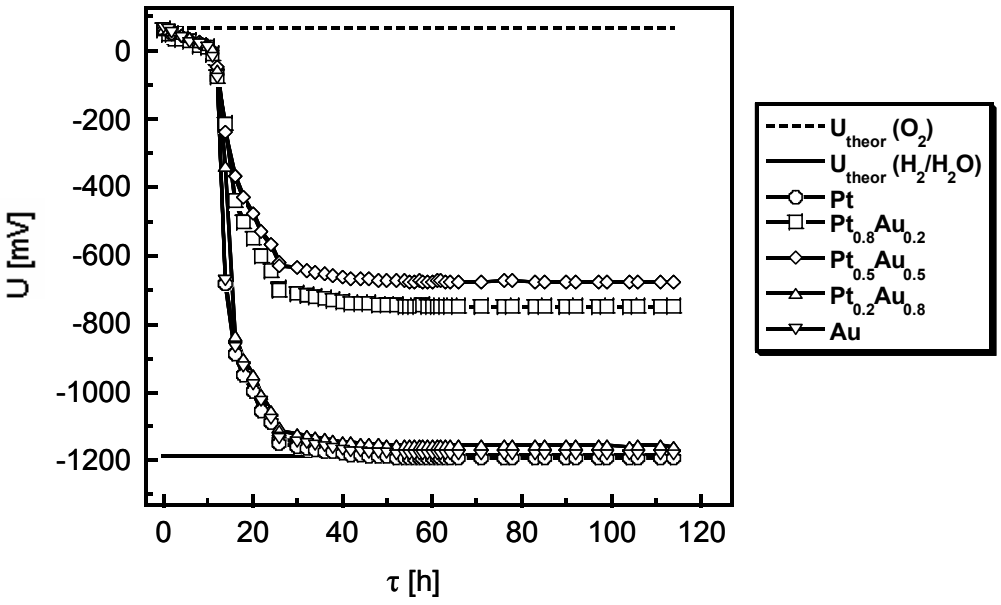

Fig. 8.13: Dependence of the voltage on time at transition from high reference electrode potential to low one at 400 °C

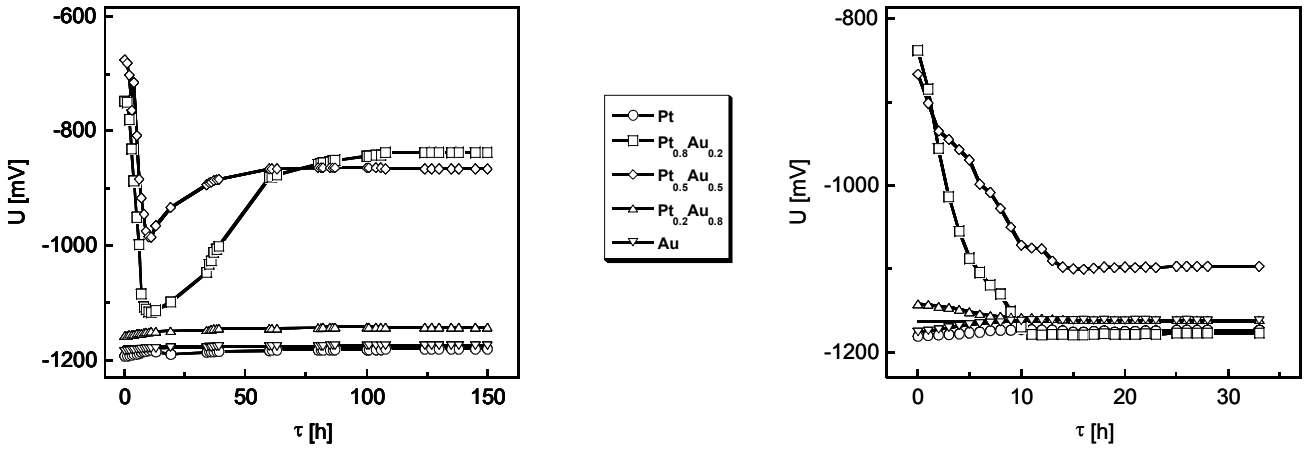

(a) *(b)*

Fig. 8.14: Dependence of the voltage on time for the investigated galvanic cells (I) under low reference electrode potential at temperature transitions (a) from 400 to 500 °C and (b) from 500 to 600 °C

8.1.2.2 Time dependence of voltage

As mentioned above the achievement of steady state values has very important meaning at characterization of the CO sensitivity by solid electrolyte galvanic cells with metal sensing electrodes. Figures 8.15 (a) and (b) show one of the examples of voltage dependence on time for all

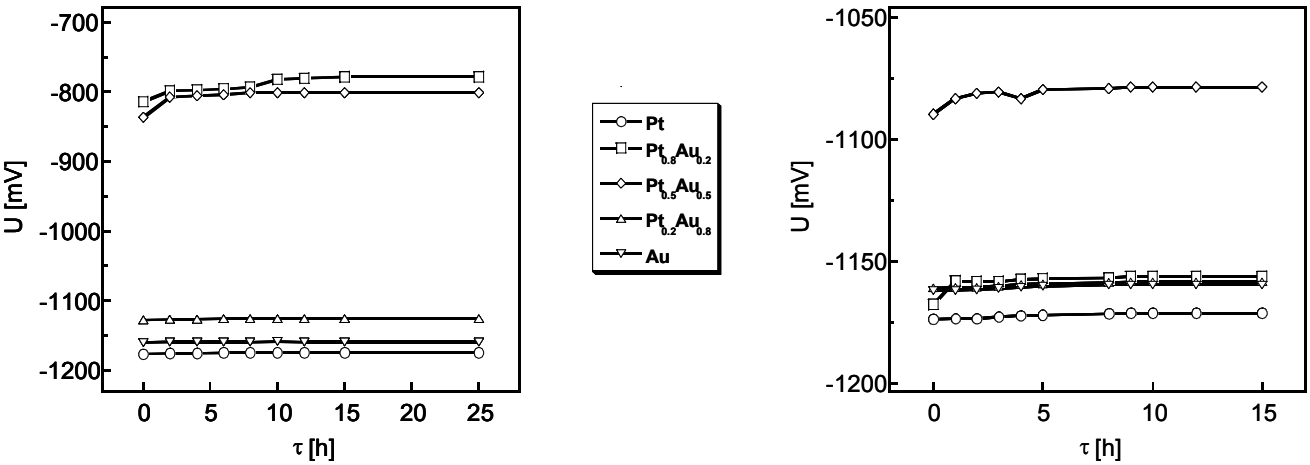

(a) *(b)*

Fig. 8.15: Time dependence of the voltage at constant CO concentration (200 ppm) in the working gas under low reference electrode potential at (a) 500 and (b) 600 °C

the studied galvanic cells at 200 ppm CO in the working gas using a low reference electrode potential at 500 and 600 °C, respectivrely.

The steady state values are reached after several hours and further they remain constant. The other time dependence at different CO concentration in the working gas have identical behavior as shown in Fig. 8.15. The time, which is necessary for the achievement of steady state magnitudes of voltage, depends on the operating temperature only.

8.1.2.3 Voltage response to CO concentration

Figure 8.16 (a) shows the experimental obtained voltages with respect to CO concentration in the working gas at 600 °C for all the studied galvanic cells under low reference electrode potential. The dashed line represents the theoretical voltages calculated by Nernst equation. Excepting higher magnitudes of the voltage for the galvanic cells with $Pt_{0.8}Au_{0.2}$ and $Pt_{0.5}Au_{0.5}$ sensing electrodes at zero CO content it could be noted that the dependence has similar behavior with that determined under high reference electrode potential (see Fig. 8.5). The dependence of voltage on CO concentration in the region (I) is shown in Fig. 8.16 (b) in more detail. It confirms that the galvanic cells with $Pt_{0.8}Au_{0.2}$ and $Pt_{0.5}Au_{0.5}$ sensing electrodes exhibit non-Nernstian behavior in all the investigated CO concentration range.

According to the experimental obtained results it could be preliminary concluded that $Pt_{0.8}Au_{0.2}$ and $Pt_{0.5}Au_{0.5}$ sensing electrodes reveal the Non-Nernstian Electrode Potential independent of the experimental conditions and in contrast to pure metal sensing electrode materials.

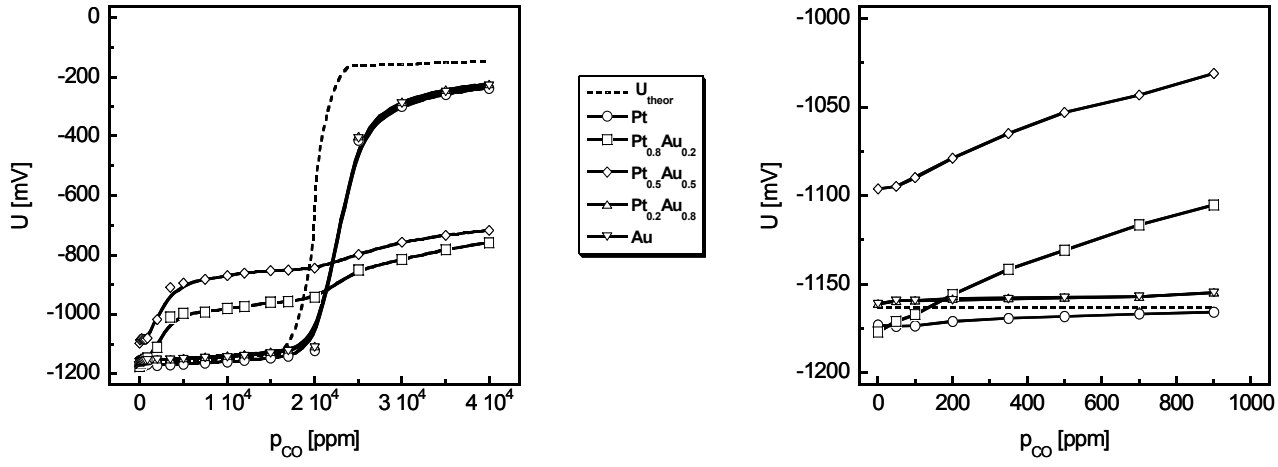

(a) *(b)*

Fig. 8.16: The voltage response to CO concentration at 600 °C under low reference electrode potential (a) in all investigated CO concentration range and (b) when CO partial pressure changes from 0 to 100 Pa (1 000 ppm)

8.1.2.4 CO sensitivity versus CO concentration, temperature and composition of the sensing electrode

Figures 8.17 (a)-(c) represent the obtained results of CO sensitivity at 400, 500, and 600 °C, respectively, for all the $Pt_{1-x}Au_x$ sensing electrodes under low reference electrode potential at the first cycle of measurements. The results show that the galvanic cell with pure Pt sensing electrode has maximum CO sensitivity already at low temperature (400 °C) (see Fig. 8.17, a). At this temperature the more interesting feature is the behaviour of galvanic cells with the $Pt_{1-x}Au_x$ sensing electrodes. The CO sensitivity for these sensing electrodes increases weakly at introducing CO into the gas stream and further the response does not practically depend on CO concentration in the working gas. The values of CO sensitivity at 400 °C remain very low and they do not exceed 30-40 mV. With raising temperature the CO sensitivity for the cells with $Pt_{0.8}Au_{0.2}$ and $Pt_{0.5}Au_{0.5}$ sensing electrodes increases (see Fig. 8.17, b and c). At 500 and 600 °C these galvanic cells exhibit high enough CO sensitivity, the values of which are comparable to each other reaching the maximum CO sensitivity at 500 °C. The galvanic cells with remaining sensing electrodes, namely, pure Pt, pure Au and $Pt_{0.2}Au_{0.8}$, have very low CO sensitivity in this temperature range.

An almost opposite situation takes place at repeating the potentiometric measurements by the studied galvanic cells under low reference electrode potential at low temperature especially. Figures 8.18 (a)-(c) show the dependences of CO sensitivity on CO concentration for all the galvanic cells after the second and third run of experiments at 400, 500, and 600 °C, respectively. Open symbols and solid lines represent the second run of experiment whereas solid symbols and dashed lines represent the third one. Based on these dependences, it could be concluded that at repeated cycles of the measurements the CO sensitivity becomes reproducible.

Comparison of these results with those obtained at the first run of experiments at 400 °C (see Figs. 8.17, a and 8.18, a) has shown that the CO sensitivity for the cell with pure Pt sensing electrode changes weakly. However, the values of CO sensitivity for the cells with $Pt_{0.8}Au_{0.2}$ and $Pt_{0.5}Au_{0.5}$ sensing electrodes increase dramatically under repeated cycles of investigations. The difference between CO sensitivities for these sensing electrodes and that for other sensing materials is around 100 mV (see Fig. 8.18, a). This fact could have been very well illustrated by the dependence of the CO sensitivity on composition (x) of the sensing electrodes at 400 °C after the first, and the second and third runs of experiments, which are shown in Figs. 8.19 (a) and (b), respectively.

It could be seen that the dependence at two different cycles of experiments has completely different behavior. However, selective further measurements by the investigated galvanic cells under low reference electrode potential confirm that the results of second/third runs by characterization of the CO sensitivity are reproducible.

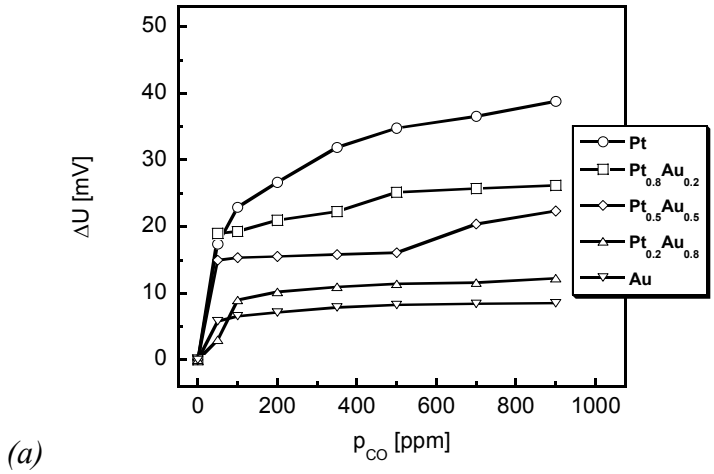

(a)

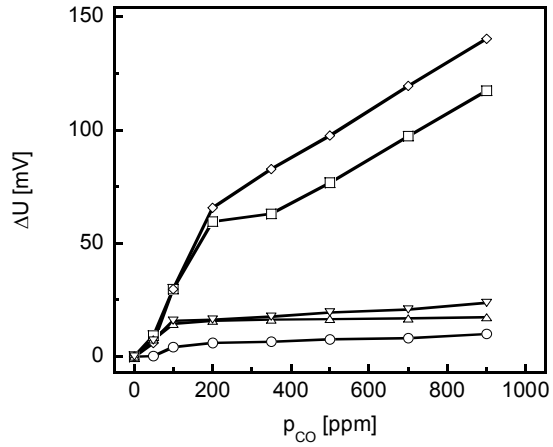

(b)

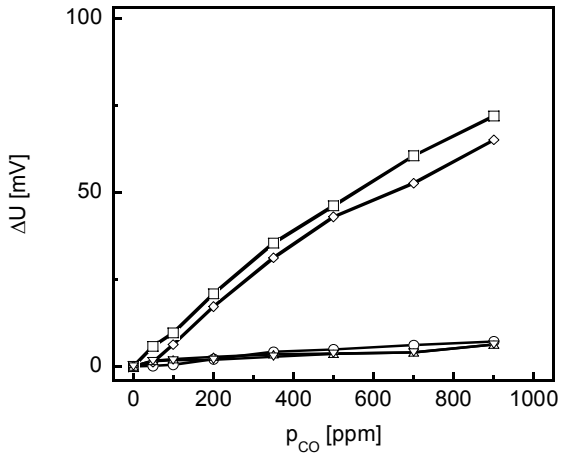

(c)

Fig. 8.17: The CO sensitivity of galvanic cells (I) with the $Pt_{1-x}Au_x$ sensing electrodes at (a) 400, (b) 500, and (c) 600 °C under low reference electrode potential after the first run of experiments

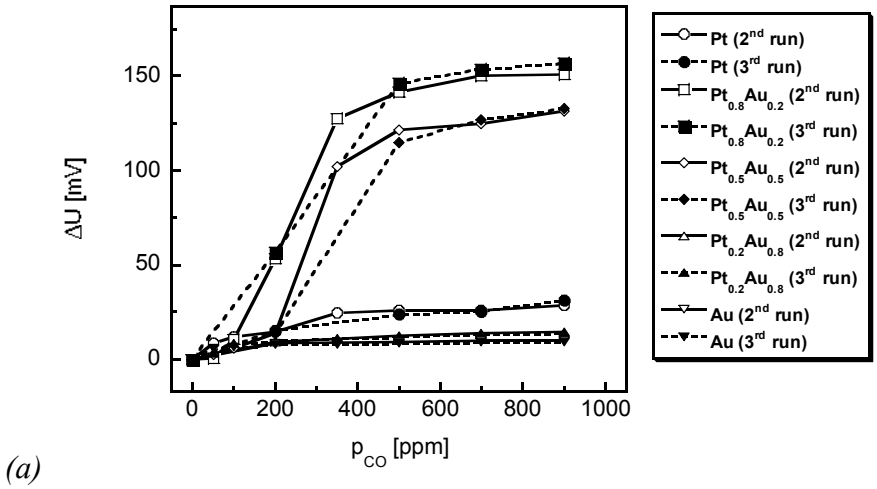

(a)

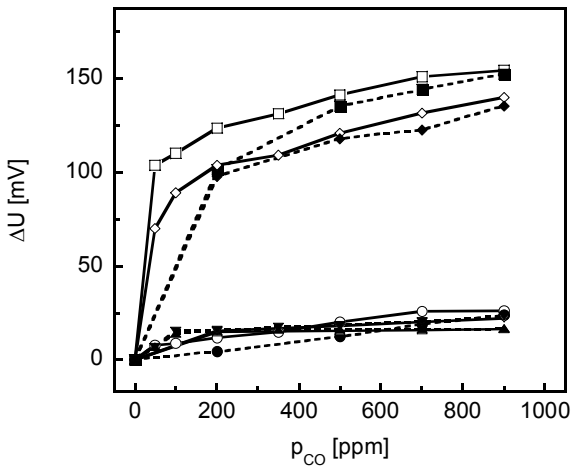

(b)

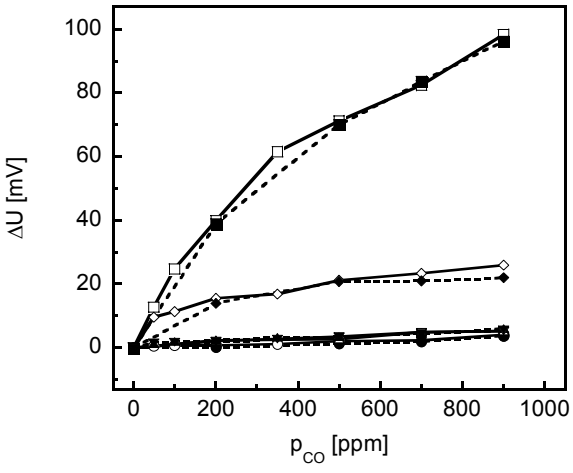

(c)

Fig. 8.18: The CO sensitivity on CO concentration after the second/third runs of measurements under low reference electrode potential at (a) 400, (b) 500, and (c) 600 °C

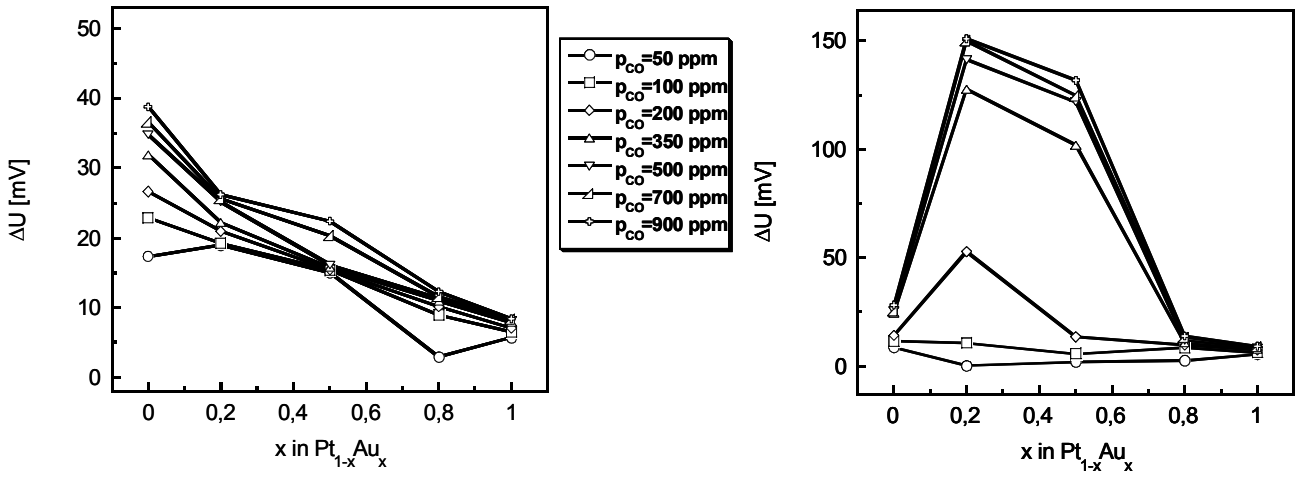

Fig. 8.19: Dependence of the CO sensitivity on (x) in the $Pt_{1-x}Au_x$ sensing electrodes at 400 °C after (a) the first run and (b) the second/third runs of experiments

Great difference between the values of CO sensitivity for the cells with $Pt_{0.8}Au_{0.2}$ and $Pt_{0.5}Au_{0.5}$ sensing electrodes on one side and those for the other electrode materials to the other exists with raising temperature. At 400 and 500 °C the dependence of CO sensitivity on CO concentration shows similar behavior (see Fig. 8.18, b), whereas, at higher temperatures (600 °C) only the galvanic cell with $Pt_{0.8}Au_{0.2}$ sensing electrode exhibits sensor properties in presence of CO (see Fig. 8.18, c), which do exceed 20 mV and keeping value high enough for reliable sensing.

Moreover, it should be noted that at several investigations of the galvanic cells with the $Pt_{1-x}Au_x$ sensing electrodes under low reference electrode potential, the values of CO sensitivity at all the cycles of experiments are reproducible in the whole investigated temperature range excepting 400 °C. The galvanic cell with $Pt_{0.8}Au_{0.2}$ sensing electrode exhibits the maximum CO sensitivity. It confirms the previous obtained results in the galvanic cells under high reference electrode potential that $Pt_{0.8}Au_{0.2}$ electrode is the best electrode material in comparison with the other Pt-Au alloys and pure metals for the characterization of CO in gas stream by the two-compartment solid electrolyte galvanic cells.

8.1.3 Comparison of the obtained CO sensitivities under high and low reference electrode potentials

All the obtained results of CO sensitivity for the $Pt_{1-x}Au_x$ sensing electrodes using the two-compartment galvanic cell configuration under two different kinds of reference electrode potentials are summed up in Figs. 10.3-10.7 of Appendix B.

According to these results, the following features of behavior of the galvanic cells with the $Pt_{1-x}Au_x$ sensing electrodes should be noted. Firstly, there is very big difference between the values of CO sensitivity using different reference electrode potentials at the first run of experiment. The values of CO sensitivity for the $Pt_{1-x}Au_x$ sensing electrodes are much higher under high reference electrode potential than those under low ones. At repeated cycles of experiment the CO sensitivity obtained does not distinguish considerably, however, a difference between the absolute values still exists. Moreover, in accordance with the dependence shown in Figs. 10.3-10.7, it is seen that the CO sensitivity obtained under high reference electrode potential is always higher than that under the low one independent of the numbers of experiments. Based on this, it is possible to assume that oxygen gradient through the solid electrolyte (or, other words, reference electrode potential) could play an important role at characterization of the CO sensitivity for the $Pt_{1-x}Au_x$ sensing electrodes by the two-compartment galvanic cell.

Secondly, as it could be seen from the obtained results, the CO sensitivity for the $Pt_{1-x}Au_x$ sensing electrodes after the first and the second run of experiments is not reproducible and it is increasing or decreasing depending on the experimental conditions. However, the CO sensitivity for the sensing electrodes exhibits the reproducible behaviour at the further cycles of measurements. It is seen that the CO sensitivity for all the $Pt_{1-x}Au_x$ sensing electrodes is well reproducible after the second, third, and also at further investigations (see Figs. 10.3-10.7 of Appendix B). The most probable reason of such behaviour is the changing of the morphology of the sensing electrode under long-time maintaining of the galvanic cell at relatively high temperatures. The particles of the electrode material could sinter at high temperatures with the formation of large agglomerates or even fully dense fraction of the electrode. That leads to reducing the amounts of (tpb) sites, where electrochemical equilibrium exists, and, finally, a decrease of the sensitivity of the electrode material. This assumption could be partially confirmed by the investigation of the microstructure of $Pt_{0.8}Au_{0.2}$ sensing electrode after the long-time exploitation in the two-compartment galvanic cell (I). Figure 8.20 represents the microstructure of $Pt_{0.8}Au_{0.2}$ sensing electrode after two years under experiment. As it is seen the sensing electrode surface has two typical regions. One of them has net-like structure (see Fig. 8.21), whereas the other one is fully dense (see Fig. 8.22). Nevertheless, it should be stressed that the sensing electrodes have had almost homogeneous microstructure before the beginning of experiments (see Fig. 7.3, b).

Figures 8.20-8.22 confirm partially the assumption about changing morphology of the sensing electrodes, however, it is difficult to say exactly at which time the changes proceed. According to the SEM investigations of the electrodes after the long-time maintaining in the galvanic cells, the changing morphology is more clearly observed for the alloy sensing electrodes, whereas for the pure metal electrodes the morphology remains actually unchanged.

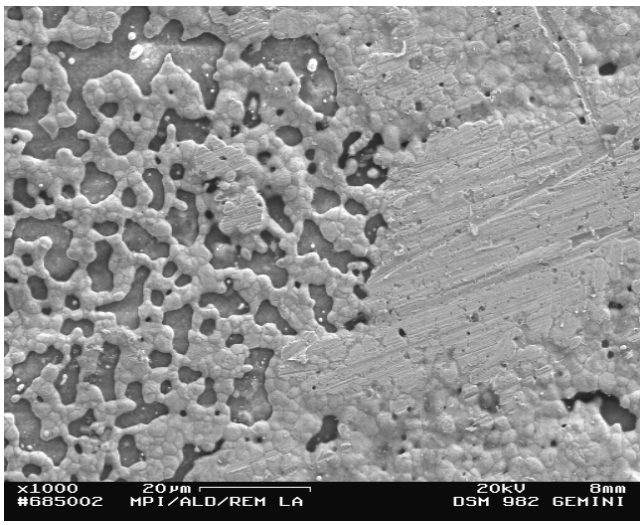

Fig. 8.20: SEM micrograph of $Pt_{0.8}Au_{0.2}$ sensing electrode surface after two years of experimental investigations

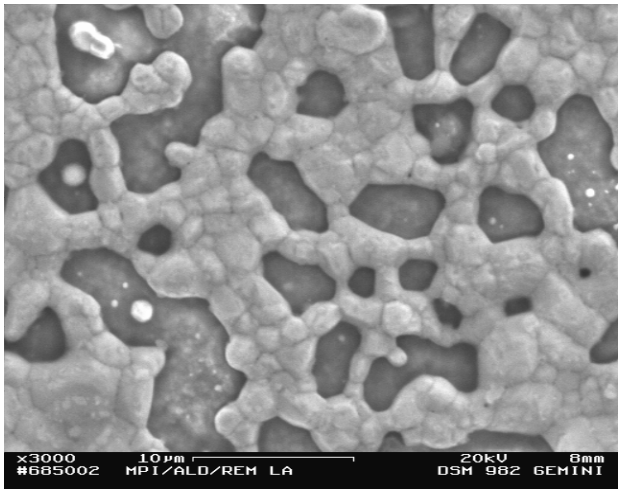

Fig. 8.21: SEM image of net-like part of structure of the $Pt_{0.8}Au_{0.2}$ sensing electrode

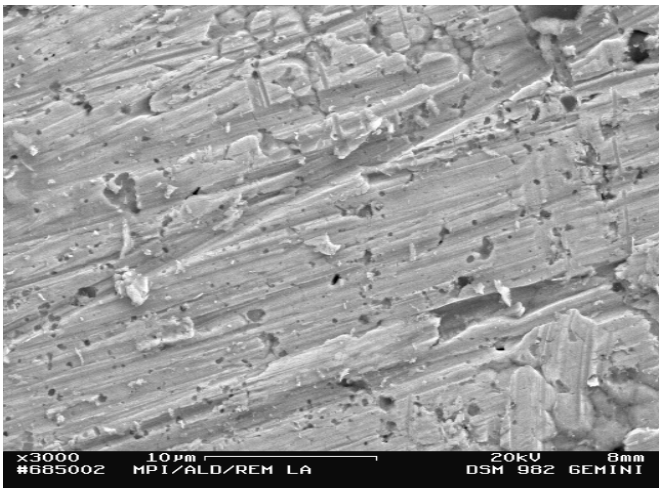

Fig. 8.22: SEM image of fully dense part of structure of the $Pt_{0.8}Au_{0.2}$ sensing electrode

The other possible reason of the reducing CO sensitivity for the $Pt_{1-x}Au_x$ sensing electrodes used in the two-compartment galvanic cells could be due to formation of oxides or chemisorbed oxygen (Pt-O bonds) on the surface of sensing electrode. In the literature [95] there is discussion about the formation of platinum oxide (PtO_2) on the surface of Pt electrode, which blocked the surface of the electrode. X-ray analysis of the present sensing electrodes after long-time maintaining in the galvanic cells did not show the presence of typical peaks for platinum or gold oxides. However, on one side X-ray analysis has the relatively high error of determination of low content and on the other even very small amounts of oxides could lead to changes of the voltage response of the

galvanic cell. Indeed, EDX analyses of these electrodes have shown the presence of small peaks of oxygen. The relative intensity of these oxygen peaks decrease with increasing the amount of Au (*x*) in the $Pt_{1-x}Au_x$ sensing electrodes.

According to this discussion, it has to be concluded that the estimation of the experimental obtained data of CO sensitivity has to be done very carefully. The experimental conditions (at least, temperature and time), as well as reference electrode potential, play a very important role at the determination of the response of the $Pt_{1-x}Au_x$ sensing electrodes in presence of CO in the gas stream.

Nevertheless, summing up all the obtained results about characterization of the CO sensitivity for the $Pt_{1-x}Au_x$ sensing electrodes by the two-compartment galvanic cell (I), one can make the following conclusions. The Pt-Au alloy sensing electrodes show much higher CO sensitivity than the pure metals, whose values are always close to the theoretical voltage. Among the alloy sensing electrodes, $Pt_{0.8}Au_{0.2}$ material exhibits the maximum sensitive properties in presence of CO in gas phase independent of the experimental conditions of characterization of the CO sensitivity, whereas the Au-rich alloy ($Pt_{0.2}Au_{0.8}$) behaves similar to pure Au.

In view of the maximum CO sensitivity the most preferable temperature range for using the $Pt_{1-x}Au_x$ sensing electrodes is 400-500 °C. At higher temperatures the CO sensitivity decreases essentially and approaches very low values independent of the type of reference electrode potential and the experimental conditions of exploitation of the two-compartment galvanic cells.

8.2. Characterization of the CO sensitivity for the $Pt_{1-x}Au_x$ sensing electrodes using bi-electrolyte galvanic cell configuration

In order to a better understanding of the CO sensitivity and especially the behaviour for the $Pt_{1-x}Au_x$ sensing electrode materials in presence of traces of CO in gas stream, a new approach for characterization of the CO sensitivity have been performed based on the bi-electrolyte galvanic cell. The construction and working principle of which are described in chapters (6.1.2) and (7.3.2).

The reason of the development of the bi-electrolyte cell for characterization of the CO sensitivity is that, according to the previous obtained results for the cell (I) with YSZ, with small CO concentrations voltages initially increase with increasing CO content much stronger in comparison with the theory, whereas at further increasing CO concentration (in the middle range between 1 000 and 30 000 ppm of CO) voltage remains almost constant. That makes the practical evaluation of the CO sensitivity of the $Pt_{1-x}Au_x$ electrodes very difficult. However, it is very well known, that galvanic cells with cation-conducting solid electrolytes, which are widely used, for example, as CO_2 sensors, have evident and clear dependence of voltage on gas concentration. Consequently, if one

combines these two principles, one has to get legible dependence of voltage for bi-electrolyte cells based on combination of YSZ and NBA solid electrolytes on CO concentration in the whole gas concentration range and possibly higher CO sensitivity.

Based on this assumption, initially, the planar bi-electrolyte galvanic cell

$$Au, O_2, CO, Na_2CO_3 \mid Na\text{-}(ß+ß'')\text{-}Al_2O_3 \mid YSZ \mid O_2,CO, Pt_{1-x}Au_x \ (x=0, 0.2) \qquad (8.2)$$

has been proposed, in which CO participates directly in the electrochemical electrode processes on the sensing and counter electrodes simultaneously. Here, Na-(ß+ß´´)-Al_2O_3 (NBA) and YSZ represent sodium and oxygen ion-conducting solid electrolytes, respectively; $Pt_{1-x}Au_x$ and Na_2CO_3 are sensing and counter electrodes, respectively. For the preparation of the bi-electrolyte galvanic cells the galvanic cell used as CO_2 sensor [179, 180] was modified.

According to this cell configuration, with participation of CO the thermodynamic equilibrium

$$Na_2CO_3 \leftrightarrow 2Na + CO + O_2 \qquad (8.3)$$

must establish on the counter electrode.

Unfortunately, in the CO concentration range between 100 and 900 ppm and at all the investigated temperatures (400-650 °C) steady-state values of voltage for this type of galvanic cell (see Eq. 8.2) were not achieved. The voltage decreases slowly on time and the absolute magnitudes of voltage were much lower than those expected from theoretical calculations in accordance with thermodynamic data [179, 181-183]. It could mean that the thermodynamic equilibrium on the counter electrode (see Eq. 8.3) establishes very slowly or even will not be reached at all.

Based on the first obtained results it was decided to modify further the bi-electrolyte galvanic cell configuration by means of adding thin catalyst layer on the counter electrode in order to oxidize CO to CO_2. This allows to achieve the thermodynamic equilibrium on the counter electrode and steady-state values of voltage in the bi-electrolyte galvanic cell.

8.2.1 Bi-electrolyte galvanic cell with thin catalyst layer

Four different constructions of the bi-electrolyte galvanic cell have been investigated using two absolutely polar kinds of the sensing electrodes, namely, Pt and $Pt_{0.8}Au_{0.2}$. The choice of the alloy composition of sensing electrode is based on the previous obtained results of characterization of the CO sensitivity for the $Pt_{1-x}Au_x$ sensing electrodes by means of the two-compartment galvanic cell (I), which are discussed above in chapter (8.1). According to these results, the galvanic cell with $Pt_{0.8}Au_{0.2}$ sensing electrode exhibits the maximum CO sensitivity in the investigated temperature range in comparison with the other alloy compositions of the sensing electrodes independent of the reference electrode potential. In opposite to that, Pt electrode has very low CO sensitivity, but this is the best material for the oxygen electrochemical electrode reaction.

8.2.1.1 Time dependence of voltage and reproducibility of the different bi-electrolyte cells

It is noteworthy to be emphasized again that the most important parameters at the theoretical investigation and practical application of solid electrolyte galvanic cells is the achievement of steady-state values of voltage while all experimental conditions are kept constant. The achievement of steady-state magnitudes means that solid electrolyte galvanic cell and all the processes in that are electrochemically and thermodynamically in equilibrium.

According to this, initially, special experiments have been carried out in order to understand the behavior of voltage for the bi-electrolyte galvanic cells with time. Figure 8.23 shows the time dependence of the voltage of the bi-electrolyte galvanic cell (II) with $Pt_{0.8}Au_{0.2}$ sensing electrode at constant temperature (550 °C) and at different CO concentrations in the gas phase. The real-time dependence of the experimentally obtained voltage at changing CO concentration for the bi-electrolyte cell (V) with Pt sensing electrode at the same temperature is shown in Fig. 8.24.

As it is seen from Figs 8.23 and 8.24, independent of the cell construction the voltage reaches steady-state values at each CO concentration and further response of the bi-electrolyte galvanic cells remains constant and independent of time, since at each CO concentration there are the plateaus on the experimental curves.

However, it should be also noted that time, which is necessary for achievement of the steady-state values, depends essentially on both the experimental temperature and the configuration of the cell. For example, at 550 °C, in accordance with Fig. 8.23, the steady-state values of voltage achieved after 14-20 hours. On the other hand, as it is visible from Fig. 8.24, at the same temperature the voltage response of the cell (V) is very fast and steady-state values are achieved after 10-15 min.

At other temperatures the time dependence has similar behaviour but there is general tendency that the time of achievement of the steady-state voltages increases with decreasing temperature.

The second and main important conclusion following from Figs. 8.23 and 8.24 is the demonstration that the values of voltage for the bi-electrolyte galvanic cells are reversible and reproducible. It follows from the fact that the difference between two experimental obtained magnitudes of the voltage does not exceed 2-3 mV at constant CO concentration. At repeated cycles of increasing or decreasing CO concentration the magnitudes of voltage have similar values.

Reproducibility of the experimental results is very important at practical application of the bi-electrolyte galvanic cells, in particular, for example, as sensors for characterization and determination of the CO traces in the gas phase.

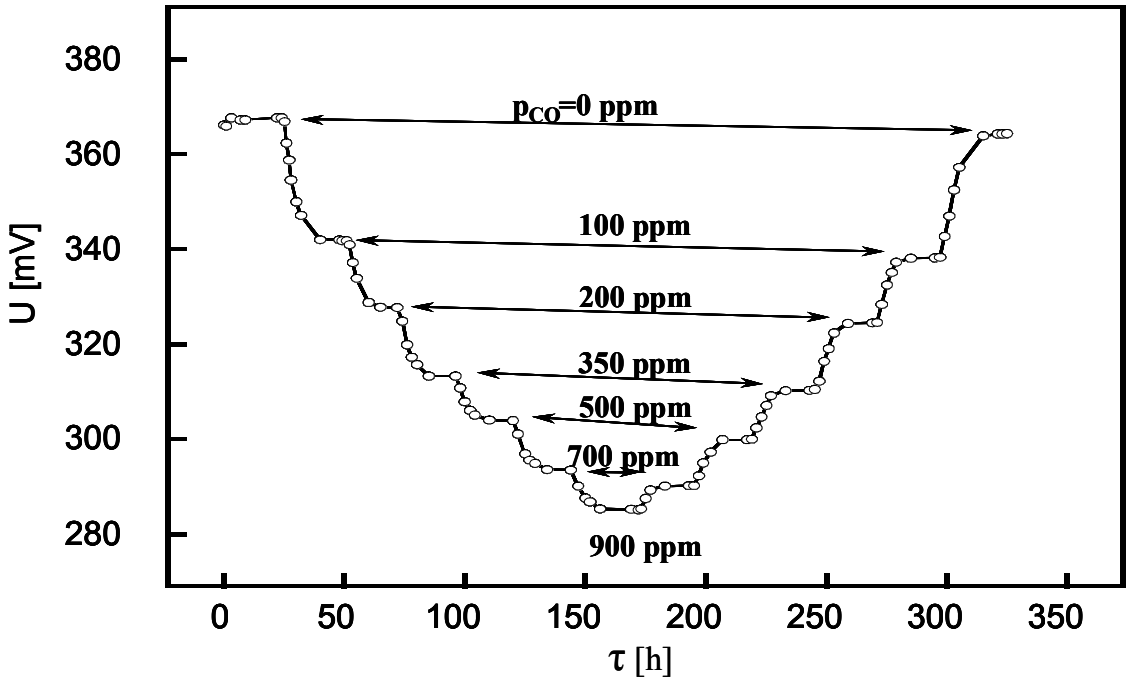

Fig. 8.23: Time dependence of the voltage for the bi-electrolyte galvanic cell (II) with $Pt_{0.8}Au_{0.2}$ sensing electrode at 550 °C and at different CO concentrations

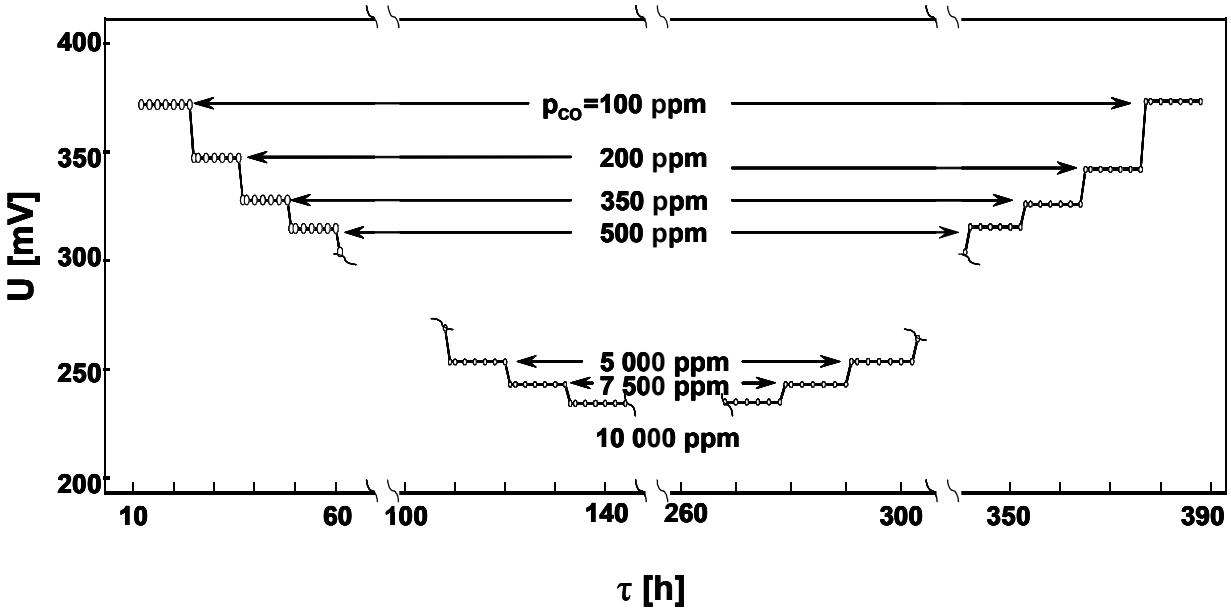

Fig. 8.24: Real-time dependence of the obtained voltage for the bi-electrolyte cell (V) with Pt sensing electrode

8.2.1.2 Voltage response to CO concentration for the one-compartment bi-electrolyte

Two one-compartment (planar) bi-electrolyte galvanic cells with non-short-circuited NBA solid electrolyte pellet (cell (II)) and short-cicuited one (cell (III)), and with different working electrodes (Pt and $Pt_{0.8}Au_{0.2}$) have been developed and investigated.

Figures 8.25 (a) and (b) show the voltage dependence on CO concentration for cell (II) using in that different working electrodes in whole investigated temperature range. It is well visible that voltage dependences have linear behaviour and the cells show very clearly a linear dependence on log(CO) concentration and on temperature. However, from the comparison of the Figs. 8.25 (a) and (b) it is possible to note that absolute values of voltage are different using various working electrodes. The second distinctive feature is that the slope of the experimental obtained curves, which characterizes the CO response of $Pt_{1-x}Au_x$ electrodes, is also different. Moreover, the slope of the linear dependences depends both on used working electrode material and on the temperature of experiment.

Temperature dependence of voltage for the bi-electrolyte cell (III) with $Pt_{0.8}Au_{0.2}$ working electrode is shown in Fig. 8.26 in whole CO concentration range.

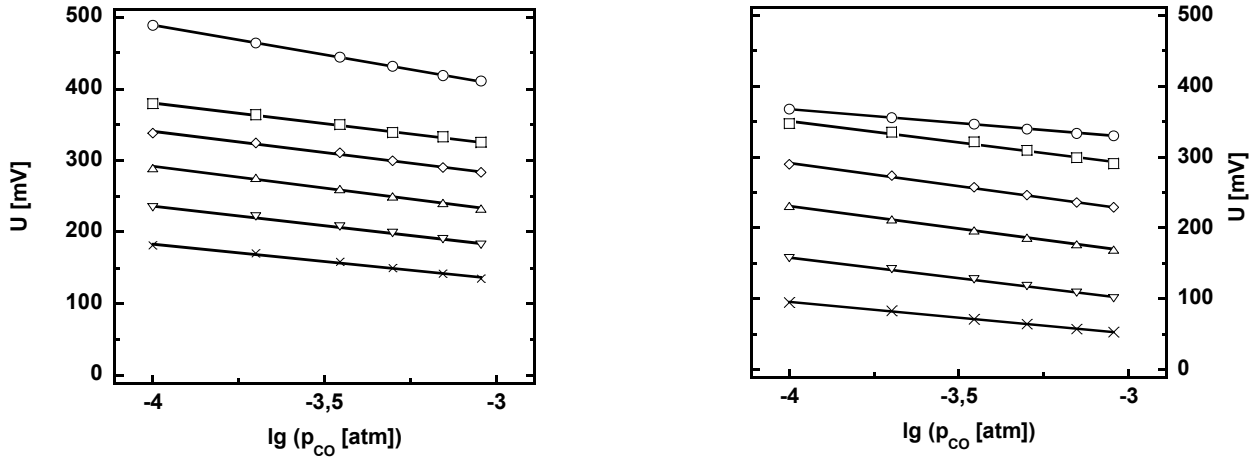

(a) *(b)*

Fig. 8.25: Voltage response with respect to CO concentration for the planar bi-electrolyte galvanic cells (II) with (a) $Pt_{0.8}Au_{0.2}$ and (b) Pt working electrodes. ○ - 650 °C; □ - 600 °C; ◊ - 550 °C; △ - 500 °C; ▽ - 450 °C; × - 400 °C

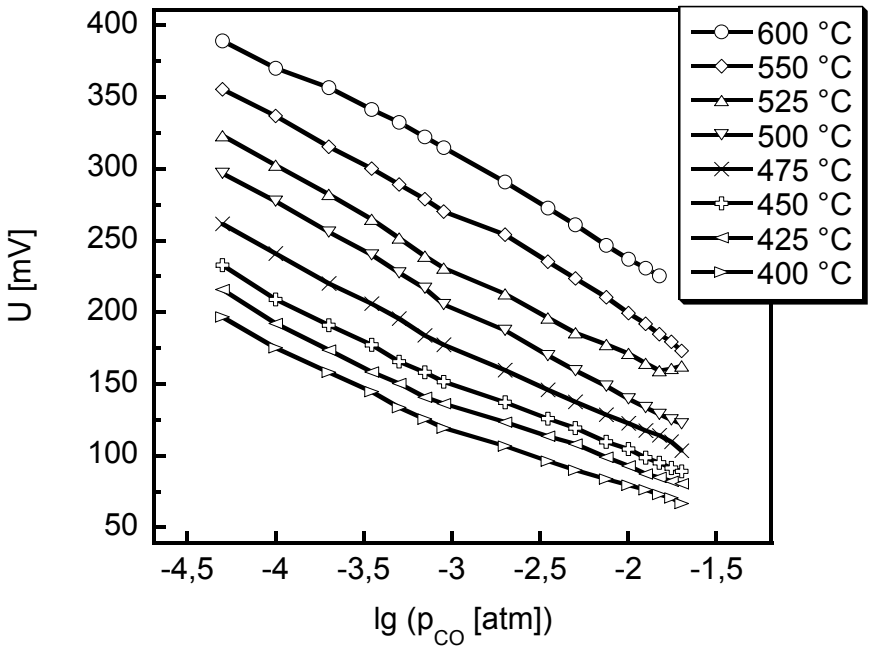

Fig. 8.26: Temperature dependence of voltage for the bi-electrolyte cell (III) with $Pt_{0.8}Au_{0.2}$ working electrode in whole CO concentration range

The cell (III) has also clear and legible voltage response on changing the CO content in the gas phase. Moreover, as it can be seen in Fig. 8.26, the shape of the experimental curves changes at decreasing the temperature. At higher temperatures the results have the almost linear dependence where as at lower ones the curves show the slight bending in the middle CO concentration range. This confirms the assumption that the planar cell (III) has to exhibit higher voltage response at low temperature and low CO concentrations due to best CO sensing properties of $Pt_{0.8}Au_{0.2}$ electrode in that temperature region. Two cycles of measurements at temperature of 550 °C are represented in Fig. 8.26, which are absolutely identical to each other, in order to display and to prove that all experimentally obtained results are reversible and reproducible at increasing/decreasing CO concentrations.

Lets consider the advantages and disadvantages of the planar bi-electrolyte geometry and the measuring principle. The first and main advantage is that this bi-electrolyte principle is working in presence of CO in the whole investigated temperature and CO concentration ranges. Moreover, the planar cell with alloy sensing electrode shows expected trend of behavior at low temperatures and at low CO concentrations. Consequently, these cells can be successfully used for characterization of CO traces in the gas phase. One-compartment bi-electrolyte cells with different working electrodes exhibit stable, reproducible and very well defined voltage response on CO concentration under all

experimental conditions. One more advantage is the easy preparation of such kinds of the cells, because it is not necessary to make a sealing of two gas compartments.

However, these bi-electrolyte cells have several disadvantages. Namely, since the influence of CO on processes at the working electrode is not known and that can not be taken into consideration, the theoretical dependence of voltage can not be calculated. Consequently, initially, each of the cell must be calibrated just before the theoretical investigation or practical application. One-compartment cells show relatively long time for achievement of the steady-state voltages (see Fig. 8.23). And last, the cells could react on presence of impurities, such as CO_2 and hydrocarbons, in the measured gas. CO_2 participates in thermodynamic equilibrium on the counter electrode, whereas sensing electrodes ($Pt_{1-x}Au_x$) are very sensitive to hydrocarbons. That could lead to distortion of the experimental results or even the results could be absolutely wrong.

If one compares the results obtained for the cells (II) and (III) with $Pt_{0.8}Au_{0.2}$ electrode (see Fig. 8.27), it is possible to note the following. At high temperatures (500-600 °C) voltages of both the cells are equal to each other. However, if temperature is decreasing, the difference between two magnitudes of voltage begins to increase. It might be caused due to ß/ß´´-equilibrium into NBA pellet. Two different modification of NBA solid electrolytes are used into cell (II) and (III): the non-short-circuited and short-circuited one. At low temperature the achievement of the ß/ß´´-equilibrium into NBA could play an important role at characterization of the voltage response of the cell.

The ß/ß´´-equilibrium achieves much faster using the short-circuited NBA solid electolyte. However, calculation of the sodium oxide activity into NBA from the obtained voltages shows that difference between two calculated values is not so high and these values lie in less than half order of magnitude.

The assumption about slight influence of the ß/ß´´-equilibrium on the cell response is well illustrated on Fig. 8.28, where the temperature dependence of the voltages for all the investigated one-compartment cells is shown at constant CO concentration (200 ppm). As it can be seen from Fig. 8.28, values of voltage for the cells (II) and (III) with $Pt_{0.8}Au_{0.2}$ working electrode are equal to each other in the temperature range of 500-600 °C.

It could be supposed that in this temperature region all processes into galvanic cell are facilitated and the rate of achievement of the ß/ß´´-equilibrium does not depend on which kind of solid electrolyte (short-circuited or not) is used. However, at decreasing temperature the divergence between two obtained magnitudes takes place that might be due to the low establishment of the ß/ß´´-equilibrium into NBA.

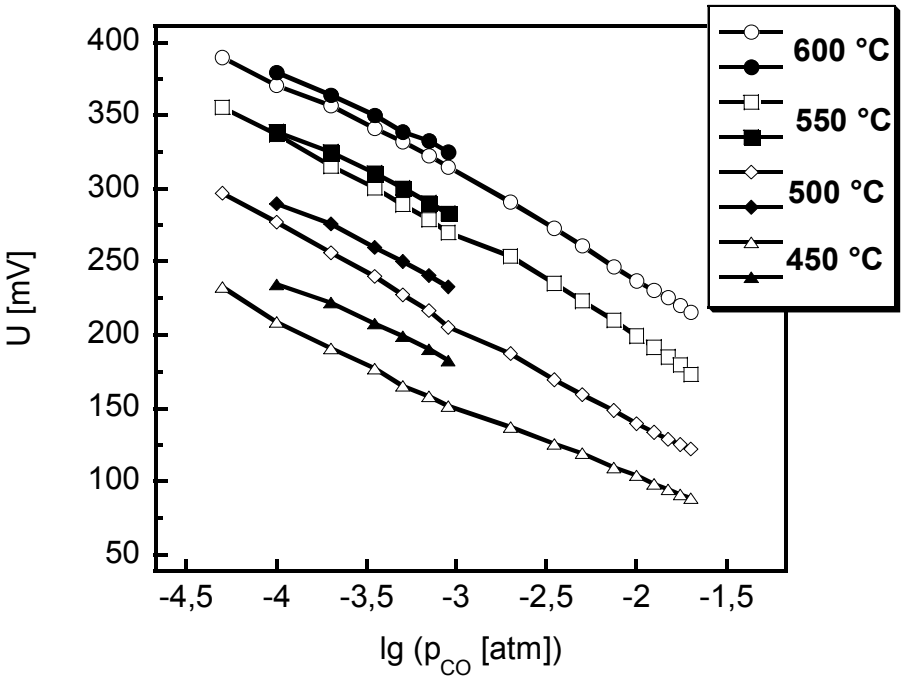

Fig. 8.27: Comparison of the obtained results for different one-compartment bi-electrolyte cells with $Pt_{0.8}Au_{0.2}$ working electrode. Closed symbols – cell (II), open symbols – cell (III)

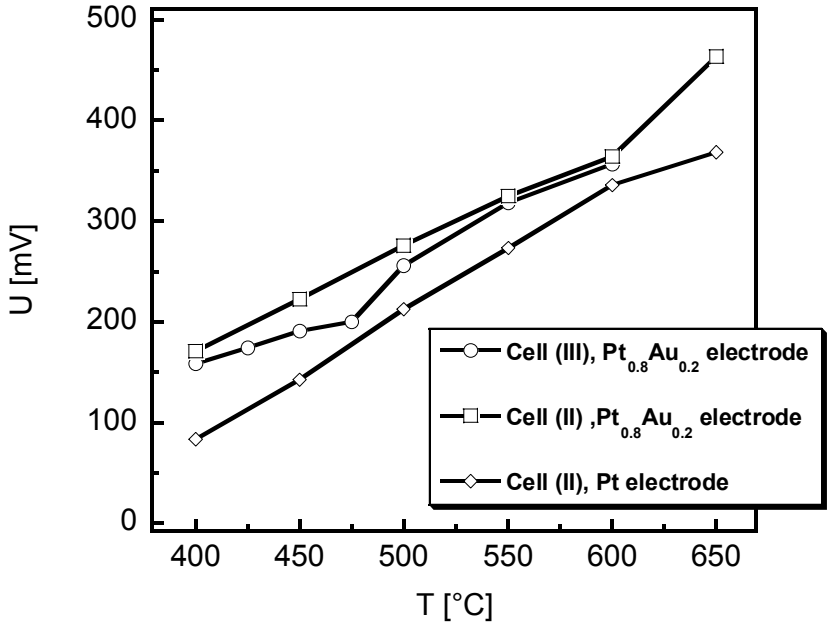

Fig. 8.28: Temperature dependence of the experimental obtained voltages for the cells (II) and (III) with different working electodes (lg (p_{CO} [atm])=-3.7)

In addition to that, in Fig. 8.28 two temperature dependences are shown for the cell (II) using various working electrodes. It is well visible that voltage response for the cell with $Pt_{0.8}Au_{0.2}$ electrode is higher than that for the Pt one in whole investigated temperature range. The same dependence is also observed at all another temperatures. It could be concluded that $Pt_{0.8}Au_{0.2}$ electrode used into bi-electrolyte cell reveals better sensor properties in presence of CO in the gas phase.

8.2.1.3 Voltage response to CO concentration for the two-compartment bi-electrolyte cells with Pt sensing electrode

In order to clarify and understand the influence of CO on the voltage response the planar geometry of the bi-electrolyte cell has been reconstructed to the two-compartment one (cell (IV), see Eq. 6.18 and chapter (7.3.2)). The sealing of the two gas compartments allows to avoid indefiniteness at determination of theoretical voltage, which now can be calculated by Eq.(6.20). In the cell (IV) there is certain CO concentration at the counter electrode side and only oxygen is at the sensing electrode side. The partial pressure of which is completely different and independent. Since there only is oxygen electrochemical reaction on the working electrode, Pt has been choosen as electrode material for further investigations.

Figure 8.29 shows the obtained results of voltage for the bi-electrolyte cell (IV) in the whole investigated range of CO concentration. Thin solid and dashed lines represent theoretically calculated voltages by Eq. (6.20) at different temperatures. The jump of the voltage up to infinity defines the stoichiometric ratio between CO and oxygen, according to the oxidation reaction (see Eq. 6.7) at the counter electrode by means of catalyst. At this stoichiometric ratio there is no free oxygen any more in the gas phase, so p''_{O_2} becomes equal to zero, that leads to increasing the voltage up to infinity in accordance with theoretical equation (6.20). From practical point of view, it means that characterization of the CO concentration by such bi-electrolyte cell construction is limited by stoichiometric ratio of the oxidation reaction (6.7). However, it should be stressed once again that the bi-electrolyte cells are working under excess of oxygen (i.e., $p''_{O_2} >> p_{CO}$). So, the limit of theoretical investigation and practical application of the bi-electrolyte cell can be shifted by simple increasing the initial oxygen partial pressure in the gas phase.

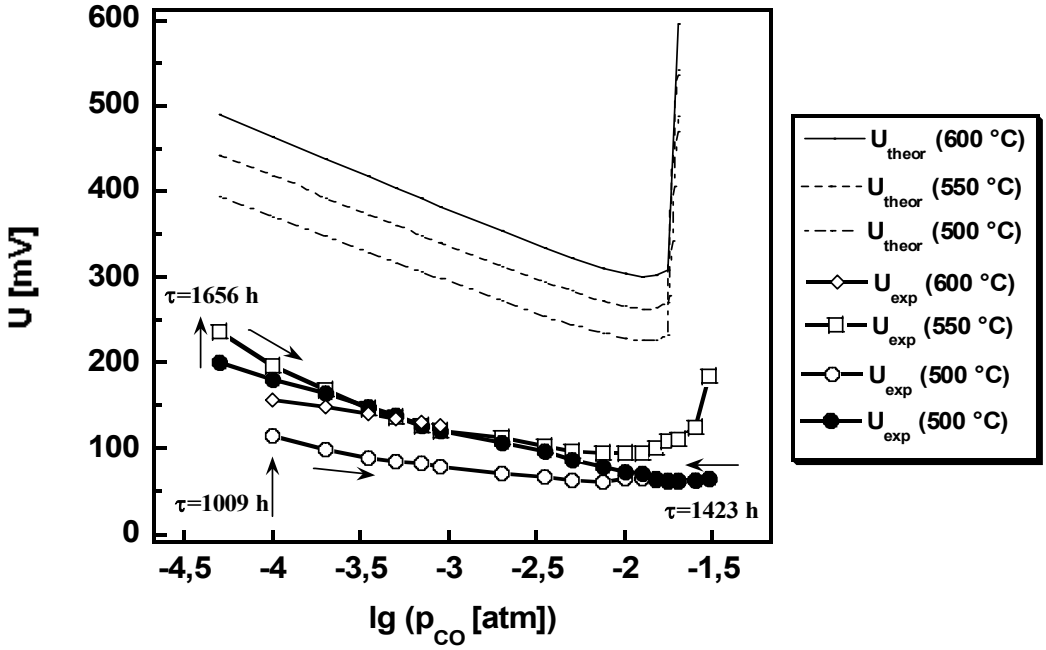

Fig. 8.29: Experimental obtained voltages for the cell (IV)

If one considers the experimental obtained results (thick lines with symbols in Fig. 8.29), it could be noted that the voltage has very low values in comparison with the theory and such very low voltages are achieved after extremely long time. For example, at 500 °C first steady-state values, which are still quite low, are achieved only after 1009 h. In addition, it is well visible, that experimental curves do not show clear temperature dependence. The voltages are almost the same at all the investigated temperatures.

Such behaviour might be explained by very long time of achievement of the ß/ß´´-equilibrium into non-short-circuited NBA what was mentioned in the previous chapter. For example, if one calculates the sodium oxide activities into NBA from the obtained results of voltage at 500 °C and adds these calculated results to the dependence of sodium oxide activity as a function of sodium activity obtained in [184] (see Fig. 8.30), it can be seen that calculated sodium oxide activities (a_{Na_2O}) are far enough from the plateau, which represents ß/ß´´-equilibrium into NBA. In Fig. 8.30 solid line denotes literature date [184].

However, as it could be seeen from Fig. 8.29, the experimental obtained results of the voltage exhibit the right trend. At 500 °C the voltages at the second run of the experiment are higher on ~60-70 mV than those at the first cycle. The experimental dependence will somewhen be achieved the theoretical one, however it will take extremely long time, which is quite impossible at practical use of the bi-electrolyte cells, for example, as CO sensors.

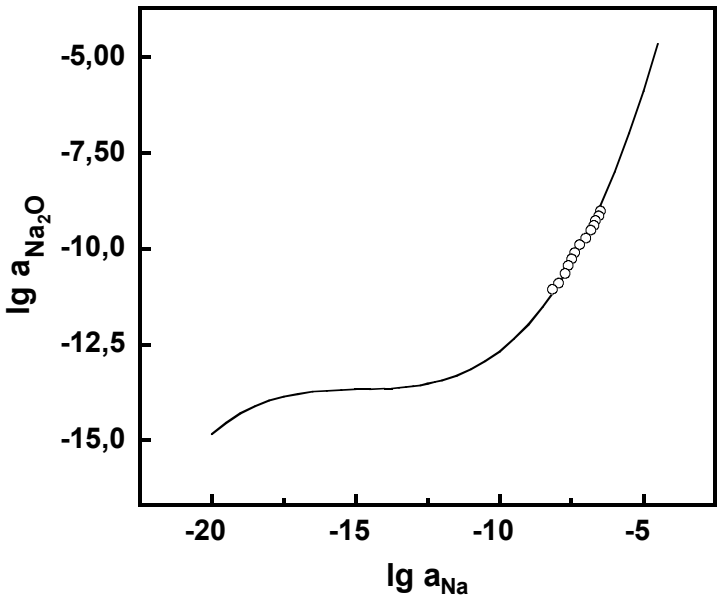

Fig. 8.30: Calculated a_{Na_2O} *from obtained voltages at 500 °C with comparison with the literature [184] as a function of* a_{Na}

Based on the obtained results for the bi-electrolyte cell (IV), the two-compartment cell construction have been modified to the cell (V) by using short-circuited NBA solid electolyte. It allows to achieve much faster the ß/ß´´-equilibrium into NBA and, finally, to improve the cell response in dependence of CO concentration. The theoretical values of voltage for the cell (V) are calculated by the same equation as for the cell (IV) (see Eq. 6.20).

The first obtained results of the voltage dependence on CO concentration for the bi-electrolyte cell configuration (V) seem to be most promising. Figure 8.31 shows several cycles of the voltage measurements at 550 °C in the whole CO concentration range.

It is visible that high enough voltages are already achieved after 148 hours. It confirms the assumption that in case of using short-circuited NBA the ß/ß´´-equilibrium into that is established much faster. After 562 h cell (V) exhibits already experimental values which repeat the theoretical ones. And, finally, after 795 h the experimental dependence coincides completely with the theoretical behaviour. Experimentally obtained results reproducible and are much close to theoretical ones. The reproducibility is also confirmed by additional cycles of the measurements at this temperature (see cycles 3 and 4 in Fig. 8.31). However, the results provide a bit smaller values than theory, but it can be explained by complication of the experimental cell. The same deviations of the experimental results are observed at all temperatures investigated.

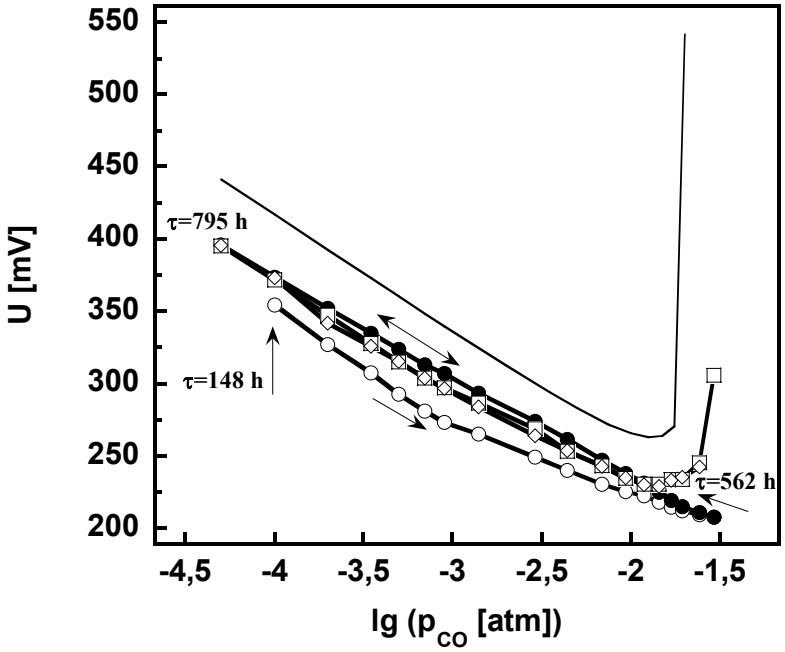

Fig. 8.31: Time behavior of the cell (V) with Pt sensing electrode at 550 °C: ○ - 1 cycle; ● - 2 cycle; □ - 3 cycle; ◊ - 4 cycle

Apart from the discussed results it would be necessary to discuss the behavior of the galvanic cell (V) beyond the stoichiometric point of the oxidation reaction (6.7) where theoretical voltages jump up to infinity, according to Eq. (6.20). As it is seen from Fig. 8.31, at the first run of the experiment the values of voltage continue to decrease weakly in the region where $2p_{CO} > p''_{O_2}$. This could be due to the behavior of catalysis at the oxidation of CO to CO_2. As mentioned above, under the investigations the commercially available catalyst powder "Hopkalit HTK15" was used, which consists of oxide materials (MnO_2 and CuO). Since manganese has several valent states, the CO can be oxidized by manganese (IV) oxide itself, reducing the oxidation state of manganese. In other words, the catalyst powder itself has buffer capacitance for CO oxidation. However, at further repetition of the measurements (see cycles 3 and 4 in Fig. 8.31) the behavior of experimental curves begins to repeat completely the theoretical one. The voltage increases slightly around the stoichiometric point in accordance with Eq. (6.20). After stoichiometry of the oxidation reaction the experimental obtained voltages are stable for 1 h, after that they continue to increase again

In opposite to the results of the bi-electrolyte cell (IV), the cell (V) shows a very well defined temperature dependence of the obtained voltages, which is shown in Fig. 8.32. As it is seen form Fig. 8.32, the experimental curves are absolutely the same and repeat fully the theoretical behaviour at all the investigated temperatures.

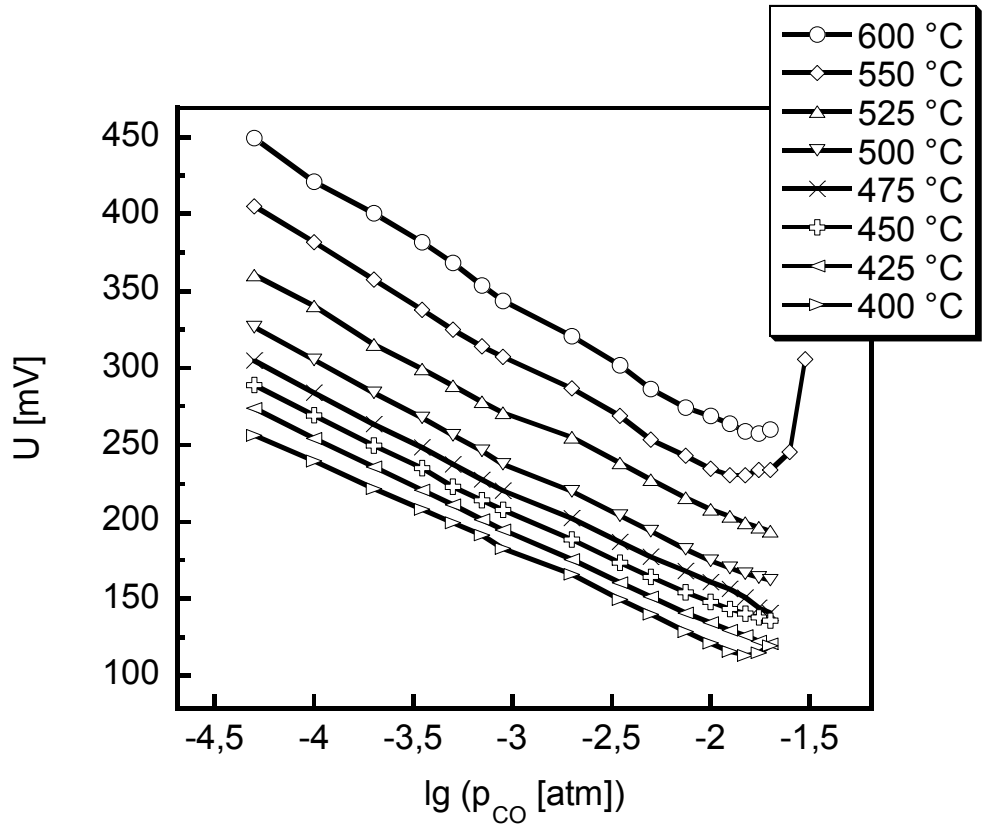

Fig. 8.32: Temperature dependence of the obtained voltages for the bi-electrolyte cell (V)

Figure 8.32 shows one additional, and most important, advantage of this principle of the investigation. All voltages have very clear and well defined dependence in the whole CO concentration range. This justifies that the bi-electrolyte cell (V) can be successfully used for the characterization and determination as very small amount (even traces) as large CO concentrations in the analyzed gas phase.

That conclusion can be once more illustrated by dependence of the voltage as a function of temperature at two constant CO concentrations, namely 200 and 15 000 ppm, which are shown in Fig. 8.33. At small CO concentrations the experimental voltages are slightly deviated from the theoretical line, whereas at large ones the response is more stable and experimental dependence exhibit clear linear behavior.

According to the thermodynamic equilibrium on the counter electrode (see Eq. 6.9), this phenomenon could be explained by that the sodium activity into sodium carbonate and NBA is decreasing at increasing CO concentration in gas phase. That leads to a faster achievement of the local equilibrium in the whole bi-electrolyte cell. The cell shows more stable results, whereas at decreasing the CO concentration the sodium activity is increasing, achieving finally extremely high values at traces of CO monoxide in the gas phase. However, as it is well visible from Fig. 8.33, in

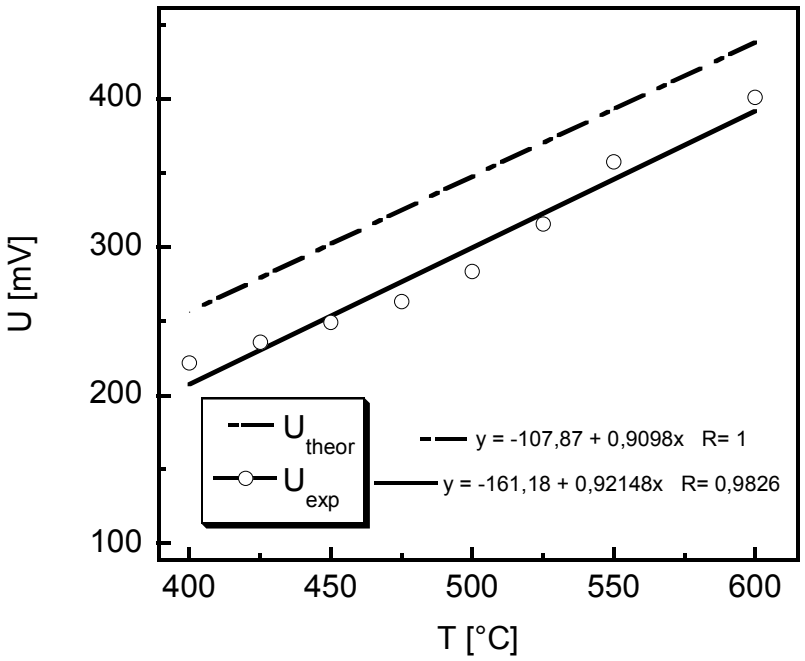

(a)

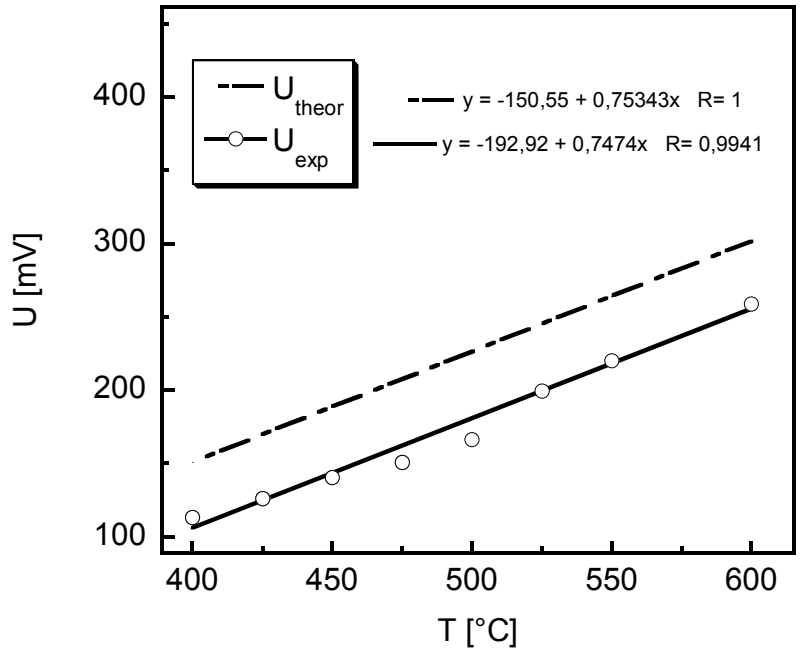

(b)

Fig. 8.33: Voltage dependence as a function of temperature for the bi-electrolyte cell (V) at (a) 200 and (b) 15 000 ppm of CO

both the cases the slope of experimental lines is very close to theory, confirming the assumption about the possibility of using the bi-electrolyte cell (V) in very wide range of CO concentrations.
Summing up all the obtained results it could be preliminary concluded that real progress is achieved in the development of the bi-electrolyte principle for the characterization and determination of CO concentration in the gas phase. The investigated bi-electrolyte cell (V) exhibits much stable and well reproducible voltage response which is very important. The steady-state voltages are achieved very fast and they have values which are very close to theoretical ones. The bi-electrolyte cell reveals well defined dependence in whole determined CO concentration interval and at all investigated temperatures in the interval from 400 to 600 °C.
Coming back to results of the planar bi-electrolyte cell (III) with $Pt_{0.8}Au_{0.2}$ working electrode (see Fig. 8.26), and comparing those with results for the two-compartment cell (V), it could be noted that these two dependences are identical to each other. Of course, the absolute voltages are different because the reference electrode is used in the cell (V), which does not exist in the planar cell configuration. Consequently, the two-compartment cell shows relatively higher experimental obtained values. Nevertheless, it is seen, that the behavior of the different bi-electrolyte cells with various working electrodes is absolutely similar.
An absolute voltage response of the bi-electrolyte cells (II)-(V) depends mostly on ß/ß´´-equilibrium established into NBA pellet, which is depending on purity, composition and pretreatment of the used pellet, surrounding atmosphere and configuration of the cell. It means, that there is necessity to make individual calibration curves fot each the bi-electrolyte cell. However, further the cells show absolutely reproducible and reversible behavior in the whole CO concentration range and at all temperatures investigated.
Based on all the obtained results it can be finally concluded that both the configuration of the bi-electrolyte galvanic cells (planar and two-compartment) are working and could be used for characterization of CO in gas phases in a wide range of CO concentrations.

8.3 Investigation of the working electrode resistance by impedance spectroscopy

8.3.1 The Nyquist plots for the two-compartment galvanic cells with the $Pt_{1-x}Au_x$ sensing electrode

Figures 8.34 (a) and (b) show the original obtained semicircles (Nyquist plots) of impedance for the two-compartment galvanic cell (I) with $Pt_{0.8}Au_{0.2}$ sensing electrode at temperature of 600 °C and at the different CO concentrations in gas stream under (a) high and (b) low reference electrode potentials, respectively. Z´ represents real part of impedance and Z´´ is the imaginary one.

Of course, the response of the galvanic cell must be different using various reference electrode potentials, but, nevertheless, in general case, the impedance of the cell (I) with the $Pt_{1-x}Au_x$ sensing electrodes characterizes by two semicircles, as it is usually observed for zirconia-based oxygen sensors. The equivalent circuit for the two semicircles, which could be used for fitting the experimentally obtained results, is shown in Fig. 6.1 (b) of chapter (6.2). In the present case, the first semicircle in high-frequency range is very small due to very dense YSZ tube used under this investigation.

According to the literature [185-187], the intersection of the high-frequency semicircle at the extremely left side of the abscissa is determined by the bulk resistance of the YSZ solid electrolyte, based on which it is possible to calculate total conductivity of YSZ. The calculated results have shown that the total conductivity in the whole investigated temperature range is very close to that, which is known in the literature [191]. The intersection of low-frequency semicircle at the extremely right side of the abscissa is determined by the resistance arising from reactions proceeding on the sensing electrode.

If one takes into consideration the theory of mixed potential or the theory of preferential CO adsorption, one can see that in the first theory CO participates directly in electrochemical process on the sensing electrode, but in the second one oxygen activity at the vicinity of the sensing electrode surface reduces sufficiently due to adsorption of CO. It could mean that resistance of electrode process could change at changing CO concentration in gas phases while oxygen partial pressure is kept constant. As it is very well seen from Fig. 8.34, the magnitudes of impedance for the galvanic cell (I) with $Pt_{0.8}Au_{0.2}$ sensing electrode are different under various reference electrode potentials. However, the second semicircle increases at increasing the CO concentration independent of the nature of reference electrode potential. It means that the resistance of electrode process, which is further represented by R_3, increases also with raising the CO concentration in the gas phase. It should be noted that for the residual sensing electrodes the experimentally obtained dependences have the same behavior.

It could be possible to assume that while all the other parameters are kept unchangeable the presence of CO in gas phase could influence directly on electrochemical processes proceeding on the sensing electrode in the two-compartment galvanic cell.

8.3.2 Dependence of sensing electrode resistance on CO concentration and temperature

The enhancement of resistance of electrode process (R_3) at increasing the CO concentration is well visible from the semilogarithmic dependences, which are shown in Figs. 8.35 (a) and (b) for all the

investigated sensing electrodes at 600 °C under (a) high and (b) low reference electrode potentials, respectively. According to these dependences, the general tendency of changing the resistance of electrode process is very well clear independent of the nature of reference electrode potential.

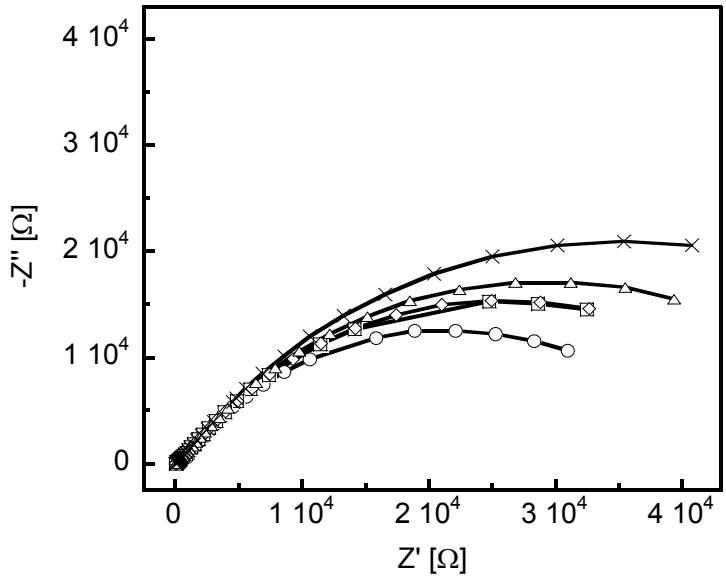

(a)

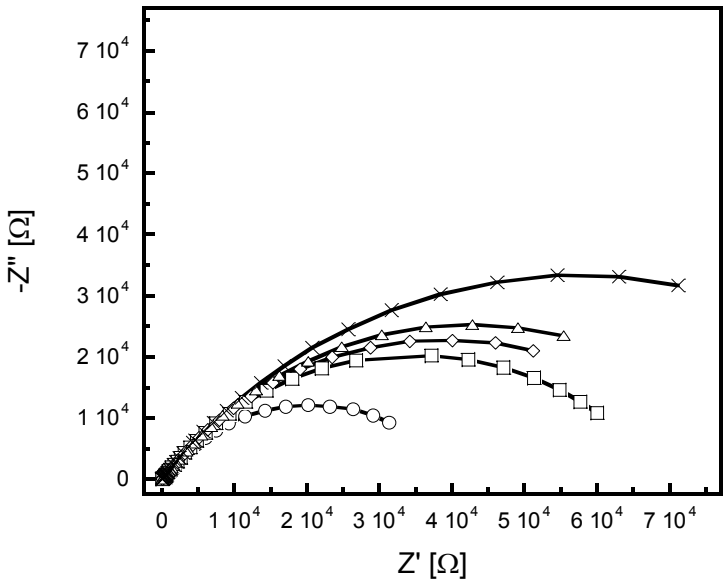

(b)

Fig. 8.34: Nyquist plots of the impedance (Z′ vs. Z′′) for the cell (I) with $Pt_{0.8}Au_{0.2}$ sensing electrode at 600 °C under (a) high and (b) low reference electrode potentials at (○) 0, (□) 200, (◊) 500, (△) 700, and (×) 900 ppm of CO

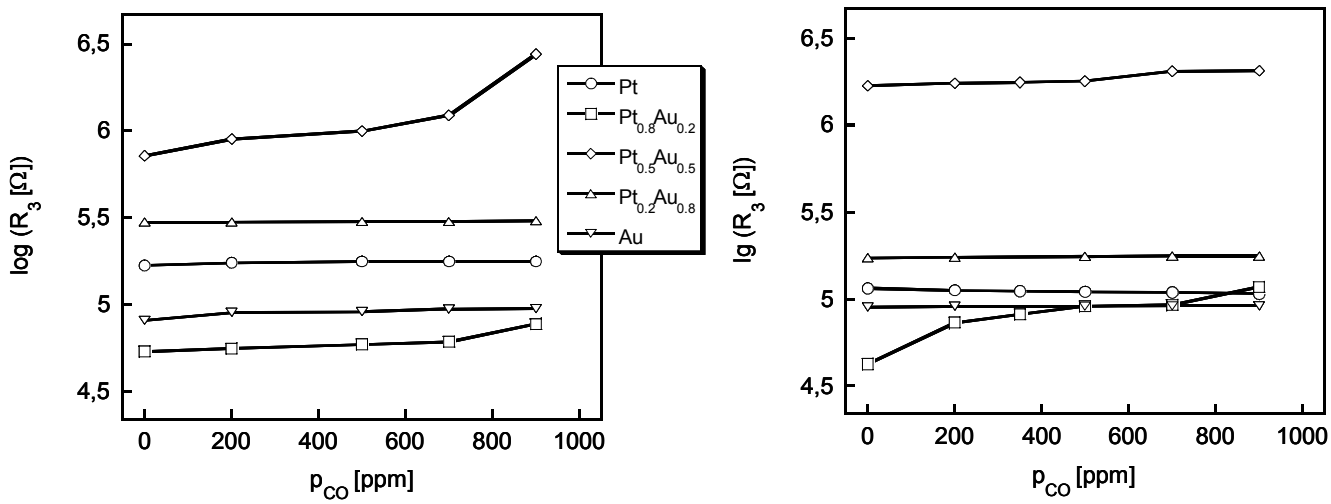

(a) *(b)*

Fig. 8.35: Dependences of the R_3 on CO concentration for the cell (I) with the $Pt_{1-x}Au_x$ sensing electrodes at 600 °C under (a) high and (b) low reference electrode potentials

At 600 °C the magnitudes of R_3 for pure metal sensing electrodes (Pt and Au) do not actually depend on changing the CO concentration in the gas phase. In the opposite to that, the values of R_3 for the residual $Pt_{1-x}Au_x$ sensing electrode (excepting the pure metals) exhibit legible enough dependences and they increase at increasing the CO concentration.

The behavior of these dependences does not change at the further enhancement of CO concentration in gas phase. The resistance of electrode process for the $Pt_{1-x}Au_x$ sensing electrodes continues to increase with respect to CO concentration, whereas the magnitudes of R_3 for the pure metals remain actually unchanged. The same dependences have been obtained at lower temperatures (400 and 500 °C).

On the basis of these results one can plot the temperature dependence of the resistance of the electrode process for each of the sensing electrode at constant CO concentration in the gas phase. Figures 8.36 (a) and (b) show the semilogarithmic dependences of R_3 on temperature at two boundary concentrations of CO (0 and 900 ppm) under (a) high and (b) low reference electrode potentials, respectively. Solid lines and open symbols represent zero CO concentration, whereas dashed lines and closed symbols are the results at 900 ppm of CO in the gas phase. The dependences of resistance for pure Au electrode are not shown on these graphs due to that Au sensing electrode exhibits the same behavior with that for pure Pt one.

According to the obtained temperature dependences, it is possible to note some distinctive features. Firstly, all the studied sensing electrodes show the same dependence of R_3 on temperature under high reference electrode potential (see Fig. 8.36, a).

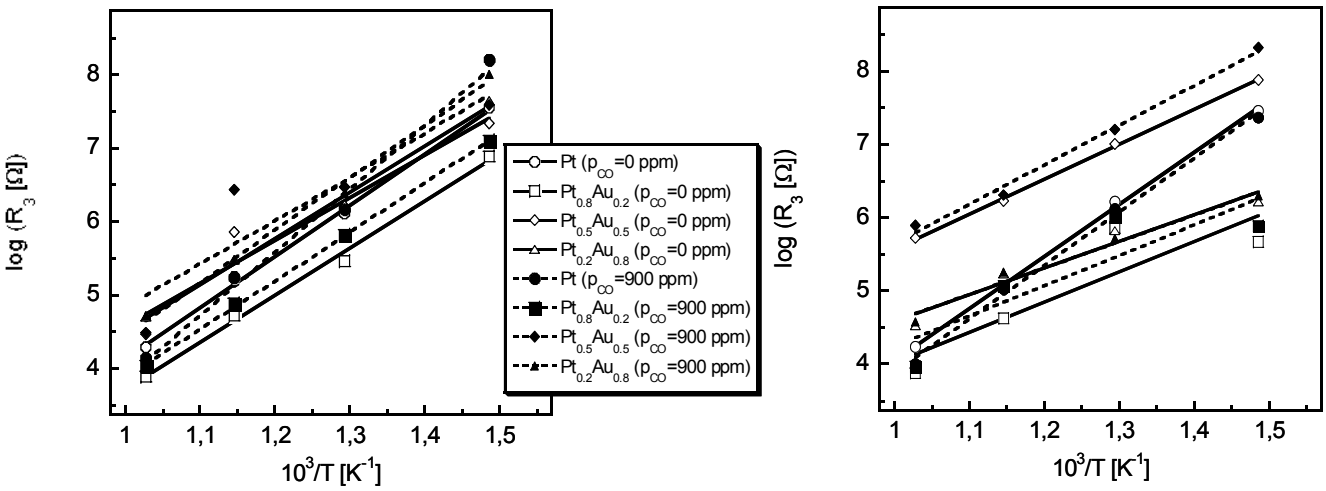

Fig. 8.36: Dependences of the R_3 on temperature for the cell (I) with four different $Pt_{1-x}Au_x$ sensing electrodes under (a) high and (b) low reference electrode potentials at two boundary conditions: (open symbols) 0 and (closed symbols) 900 ppm of CO

In other words, the slope of the experimental temperature dependences depends slightly on the composition (x) of the sensing electrodes and the absolute values of R_3 are close to each other.

A somewhat other situation takes place using the galvanic cell (I) with the $Pt_{1-x}Au_x$ sensing electrodes under low reference electrode potential (see Fig. 8.36, b). It is seen that in this case the absolute values of R_3 distinguish sharply for the various sensing electrode materials. Namely, for the pure metal sensing electrodes (Pt and Au) the values of R_3 and the slopes of the experimental temperature dependences do not essentially change. At the same time, the values of R_3 for the another $Pt_{1-x}Au_x$ compositions distinguish almost in two orders of magnitude.

Thus, the $Pt_{0.8}Au_{0.2}$ sensing electrode shows the lowest values of electrode resistance, whereas the $Pt_{0.5}Au_{0.5}$ sensing electrode has the highest ones. Simultaneously with changing the absolute values of electrode resistance, the slope of the experimental dependences for the $Pt_{1-x}Au_x$ sensing electrodes (excepting pure metals) changes as well, which becomes much lower under low reference electrode potential.

Moreover, it is very well seen from the dependences shown in Figs. 8.36 (a) and (b) that the resistance of electrode process does not change at two boundary CO concentrations in the gas phase using the galvanic cells with the pure metal sensing electrodes, whereas that increases essentially for the cells with the alloy-type of electrodes in the presence of CO.

Based on the obtained temperature dependences for the resistance of electrode process (R_3), one can determine activation energy (E_a) of electrode process for each of the $Pt_{1-x}Au_x$ sensing electrode used

in the two-compartment galvanic cell. The activation energy can be determined from the slope of the temperature dependences of R_3, which, in accordance with Arrhenius equation, must be equal to E_a divided by R, where R is universal gas constant.

Of course, it is very well known that the activation energy can be calculated for one electrode process or for one stage of that only. The influence of CO on processes proceeding on the surface of the sensing electrode is not known yet. However, if one assumes that there is one electrode electrochemical process only in which oxygen participates, which proceeds on (tpb) sites of the sensing electrode, it could be possible to estimate the influence of CO in the gas phase on the activation energy of the electrochemical process.

8.3.3 Estimation of the activation energy for electrochemical process on the sensing electrode in presence of CO in gas stream

Figure 8.37 shows the dependences of experimentally obtained activation energies for the electrochemical electrode process with participation of oxygen on the composition (x) of the sensing electrode at two boundary CO concentrations. Thin solid and dashed lines represent the dependence under high reference electrode potential used in the two-compartment galvanic cells whereas the thick same lines show those under the low one.

According to these dependences, it should be possible to note that the values of the activation energy of the electrode process for the cells under high reference electrode potential are much higher than those under the lower one. Of course, the activation energies of the electrochemical electrode process must be different using various reference electrode potentials. However, if one considers the dependence of the activation energy using different reference electrode potentials separately, we could note the following feature.

The presence of CO in the gas phase makes fully definite influence on the proceeding electrode process under high reference electrode potential and the activation energies increase essentially at finite CO concentration. At the same time, the similar dependences under low reference electrode potential show that in this case CO does not have such important influence and the values of activation energies are close to each other at finite CO concentration and without CO in the gas phase (see Fig. 8.37). All the obtained values of activation energies of the electrode process for the investigated sensing electrodes are summed up in Table 8.1 at two boundary conditions and under two different reference electrode potentials.

Based on the obtained results, it could be preliminary concluded that the presence of CO in the gas phase makes definite influence on reactions proceeding on the sensing electrodes. However, this

influence is different and that depends on the experimental conditions used for characterization of the CO sensitivity of the $Pt_{1-x}Au_x$ electrodes by the two-compartment galvanic cells.

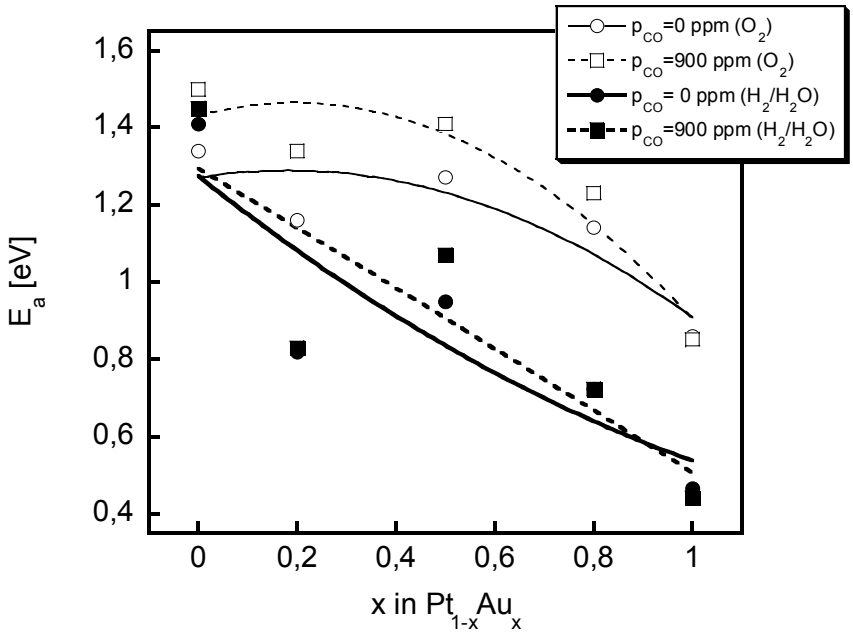

Fig. 8.37: Dependence of the experimentally obtained activation energies (E_a) on the composition (x) of the $Pt_{1-x}Au_x$ sensing electrode under high (open symbols) and low (solid symbols) reference electrode potentials at (○) 0 and (□) 900 ppm of CO

Sensing electrode composition	Reference electrode potential	E_a [eV]	
		p_{CO}=0 ppm	p_{CO}=900 ppm
Pt	High (O_2)	1.34	1.50
	Low (H_2/H_2O)	1.41	1.45
$Pt_{0.8}Au_{0.2}$	High (O_2)	1.16	1.34
	Low (H_2/H_2O)	0.82	0.83
$Pt_{0.5}Au_{0.5}$	High (O_2)	1.27	1.41
	Low (H_2/H_2O)	0.95	1.07
$Pt_{0.2}Au_{0.8}$	High (O_2)	1.14	1.23
	Low (H_2/H_2O)	0.72	0.72
Au	High (O_2)	0.86	0.85
	Low (H_2/H_2O)	0.47	0.44

Table 8.1: The obtained values of activation energies (E_a) for the various $Pt_{1-x}Au_x$ sensing electrodes under different reference electrode potentials at two limitary conditions

The resistance of the $Pt_{1-x}Au_x$ sensing electrodes increases essentially at increasing the CO concentration in gas phase excepting for the pure metals (Pt and Au), the values of electrode resistance remain actually unchanged. Taking into consideration that the $Pt_{1-x}Au_x$ sensing electrodes (x=0.2, 0.5) exhibit the high CO sensitivity in the presence of CO in the gas phase and the CO sensitivity for the pure metals (Pt and Au) is close to zero, it is possible to assume that CO participates directly in the electrochemical electrode process in case of using the $Pt_{1-x}Au_x$ alloys as sensing electrodes in the two-compartment galvanic cells. That could lead to appearing the Non-Nernstian Electrode Potential for the $Pt_{1-x}Au_x$ sensing electrode materials.

9 Conclusions

- Two-compartment cell (I) with all the used sensing electrodes exhibits stable and unchangeable voltage response on time at all the temperatures and CO concentrations. The galvanic cell with $Pt_{0.8}Au_{0.2}$ sensing electrode shows fast voltage response on time (about few seconds) at changing the CO concentration independent of the experimental conditions.
- The alloy sensing electrodes show much higher CO sensitivity than the pure metals, whose values are always close to the theoretical voltage. Among the $Pt_{1-x}Au_x$ sensing electrodes, $Pt_{0.8}Au_{0.2}$ material exhibits the highest sensitive properties in presence of CO independent of the experimental conditions. In the view of a maximum CO sensitivity the most preferable temperature range for the $Pt_{1-x}Au_x$ sensing electrodes is 400-500 °C.
- The values of CO sensitivity for the $Pt_{1-x}Au_x$ sensing electrodes distinguish between each others using different reference electrode potential. The CO sensitivity obtained under high reference electrode potential is always higher than that under the low one.
- The values of CO sensitivity for the $Pt_{1-x}Au_x$ sensing electrodes after the first and second run of experiment are not reproducible, however, those are reproducible at the further cycles of measurements. It can be concluded that one should be very careful at the estimation of the experimental obtained CO sensitivities. The experimental conditions (at least, temperature and time), as well as reference electrode potential, can play a very important role at characterization of the CO sensitivity of $Pt_{1-x}Au_x$ sensing electrodes in presence of CO in the gas stream.
- The resistance of electrode process for the alloy sensing electrodes in the cell (I) obtained by impedance spectroscopy increases essentially with respect to CO concentration, whereas the magnitudes of that for the pure metals does not actually depend on presence of CO at all the investigated temperatures. The presence of carbon monoxide in gas phase makes definite influence on the electrode resistance under high reference electrode potential and the activation energies increase at finite CO concentration. The similar dependencies under low reference electrode potential show that the values of activation energies are close to each other at finite CO concentration and without CO.
- A new approach for characterization of the CO sensitivity have been performed based on the bi-electrolyte principle. The planar and two-compartment bi-electrolyte cells with the $Pt_{1-x}Au_x$ (x=0, 0.2) sensing electrodes have been developed. Both the bi-electrolyte cell configurations show stable, reversible, and reproducible voltage response to changing the CO concentration in the gas phase at all the investigated temperatures revealing clear and legible voltage dependence, and exhibiting very good sensitive properties.

- The planar bi-electrolyte cell with $Pt_{0.8}Au_{0.2}$ sensing electrode exhibits higher voltage response at low temperatures and at low CO concentrations due to best CO sensing properties of $Pt_{0.8}Au_{0.2}$ electrode in that temperature region. Voltage dependence for the two-compartment bi-electrolyte cell coincides completely with the theoretical behaviour and experimentally obtained results are much close to theoretical ones.
- An absolute voltage response of the bi-electrolyte cells (II)-(V) depends mostly on ß/ß´´-equilibrium established into NBA pellet, which in turn depends on purity, composition and pretreatment of the used pellet, surrounding atmosphere and configuration of the cell. It means, that there is necessity to make individual calibration curves for each the bi-electrolyte cell. However, further the cells show absolutely reproducible and reversible behavior in the whole CO concentration range and at all temperatures investigated.
- Based on all the obtained results it can be finally concluded that both the configurations of the bi-electrolyte galvanic cells (planar and two-compartment) are working and can be used for characterization of CO in gas phases in a wide range of CO concentrations.

10 Appendixes

Appendix A

X-ray diffraction patterns for the pure Pt and Au sensing electrode materials.

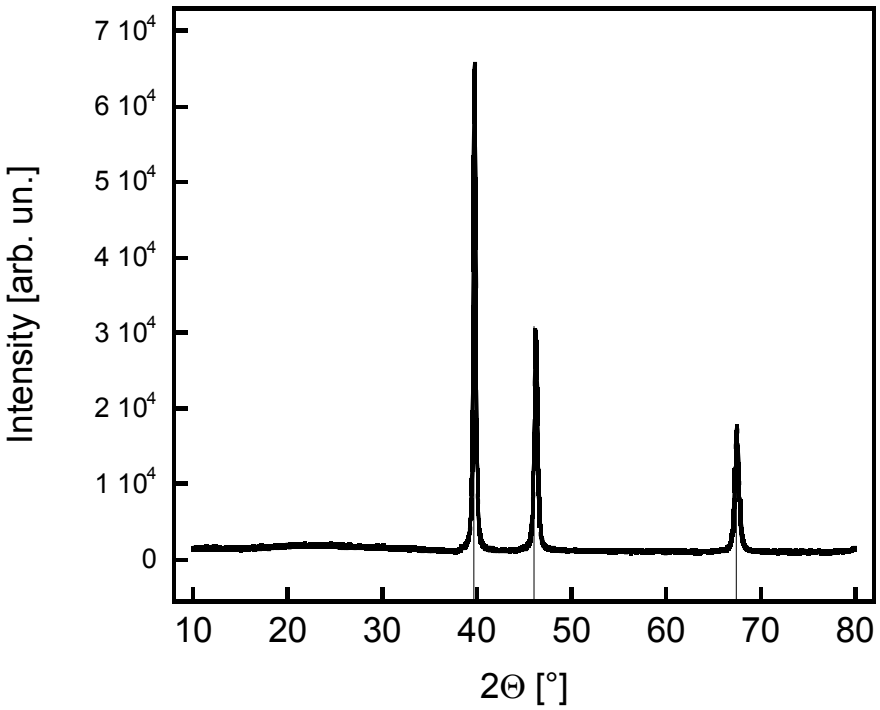

Fig. 10.1: X-ray diffraction pattern for pure Pt sensing electrode after annealing at 950 °C for 15 min (solid lines represent Pt)

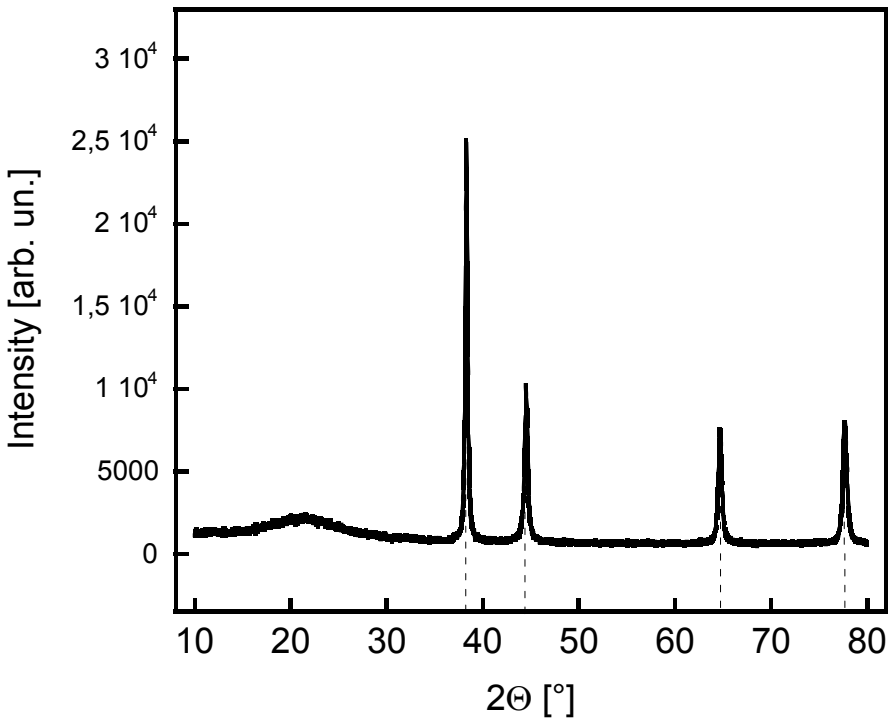

Fig. 10.2: X-ray diffraction pattern for pure Au sensing electrode after annealing at 950 °C for 15 min (dash lines represent Au)

Appendix B

The CO sensitivity of the investigated galvanic cells with the $Pt_{1-x}Au_x$ sensing electrodes under high and low reference electrode potentials.

High reference electrode potential *Low reference electrode potential*

400 °C

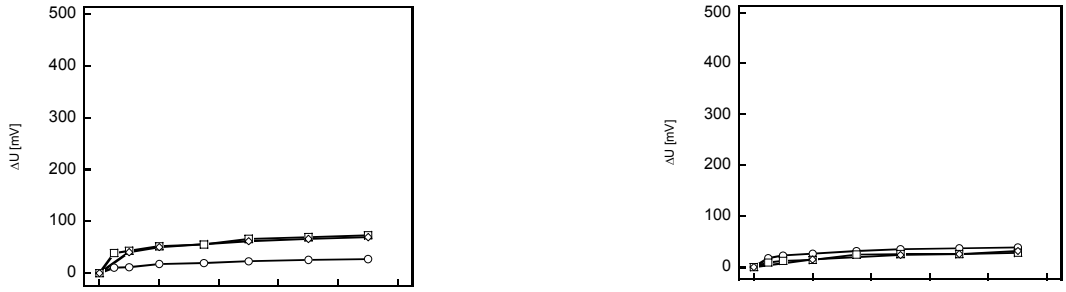

500 °C

600 °C

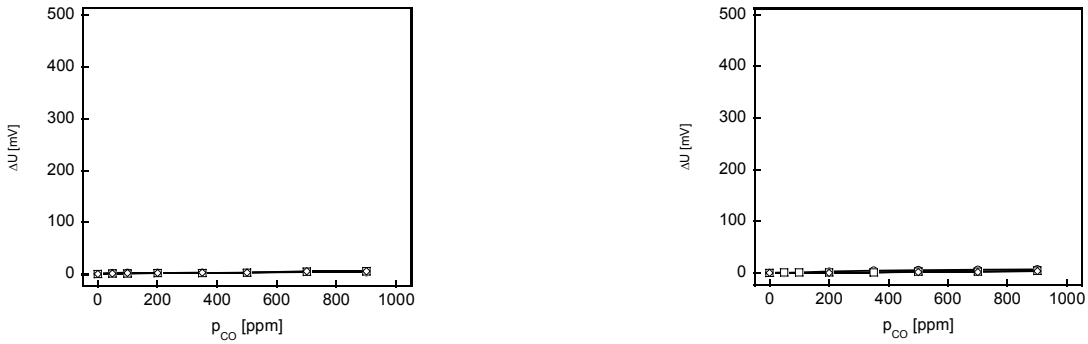

Fig. 10.3: The CO sensitivity of the cell with Pt sensing electrode in whole investigated temperature range after (○) first, (□) second, and (◊) third runs of the measurements

High reference electrode potential *Low reference electrode potential*

400 °C

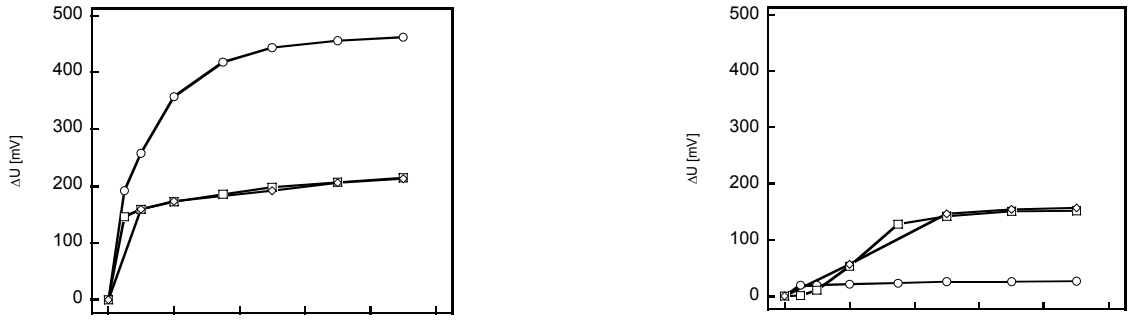

500 °C

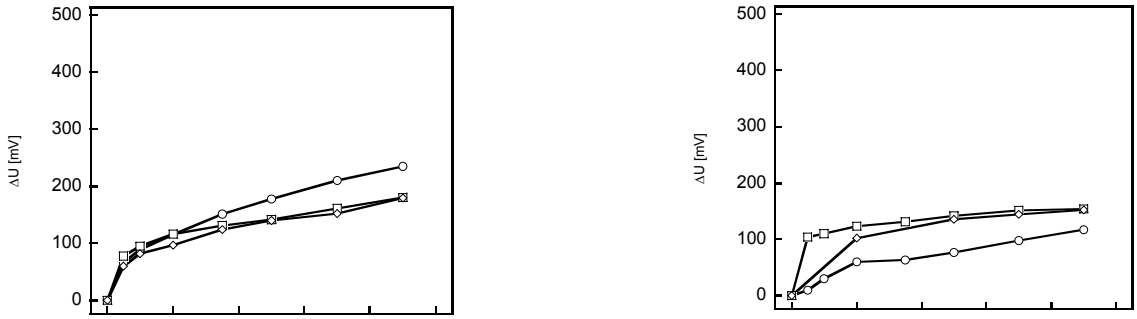

600 °C

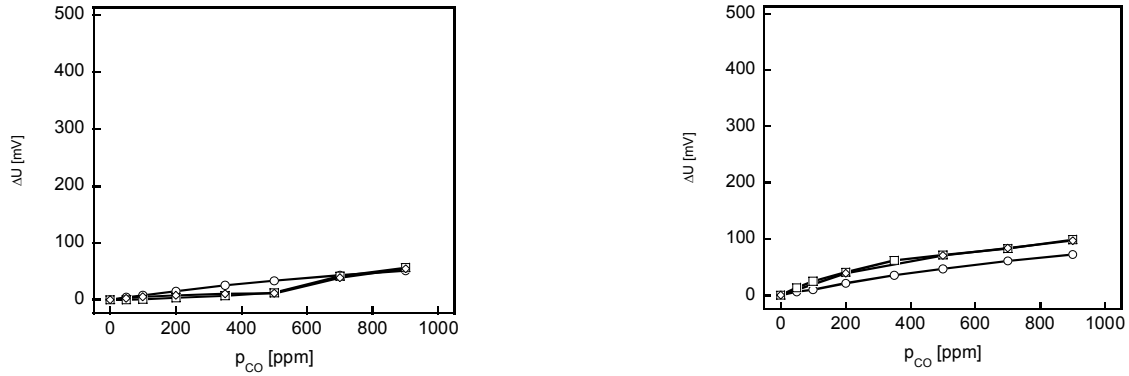

Fig. 10.4: The CO sensitivity of the cell with $Pt_{0.8}Au_{0.2}$ sensing electrode in whole investigated temperature range after (○) first, (□) second, and (◊) third runs of the measurements

High reference electrode potential *Low reference electrode potential*

400 °C

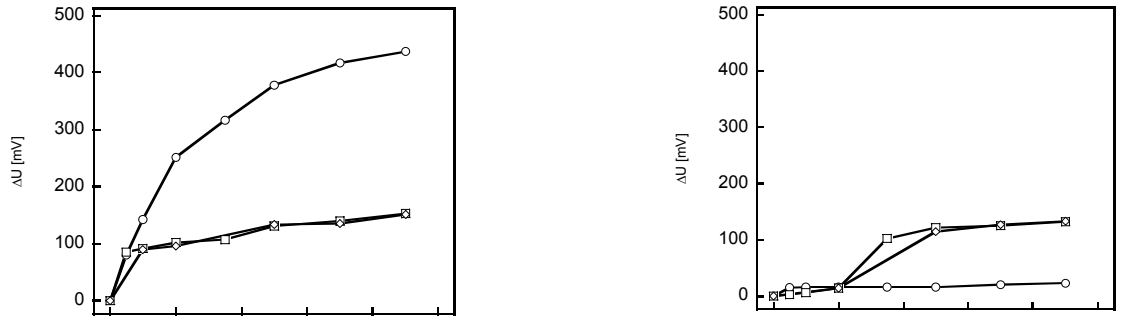

500 °C

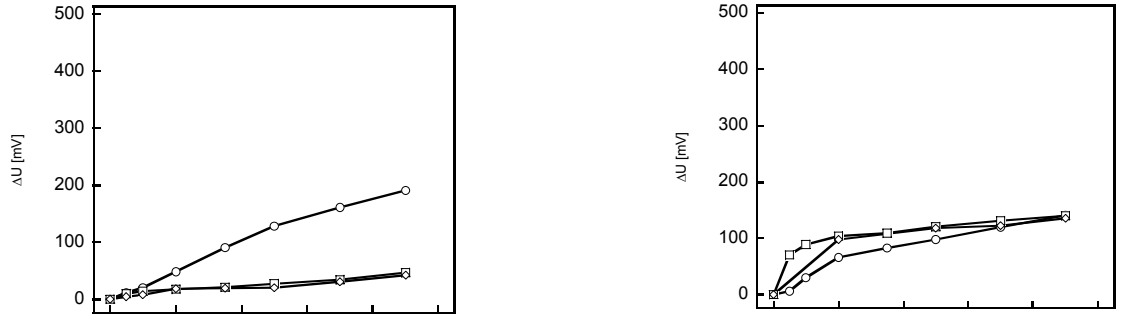

600 °C

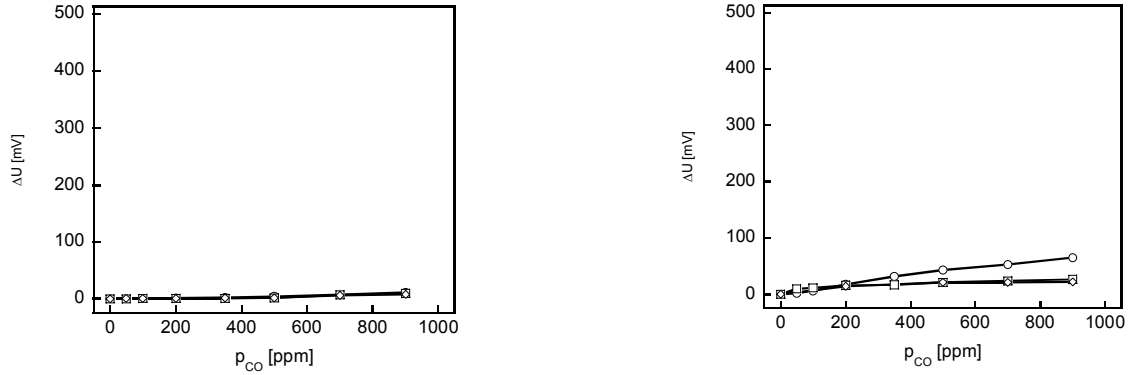

Fig. 10.5: The CO sensitivity of the cell with $Pt_{0.5}Au_{0.5}$ sensing electrode in whole investigated temperature range after (○) first, (□) second, and (◊) third runs of the measurements

High reference electrode potential *Low reference electrode potential*

400 °C

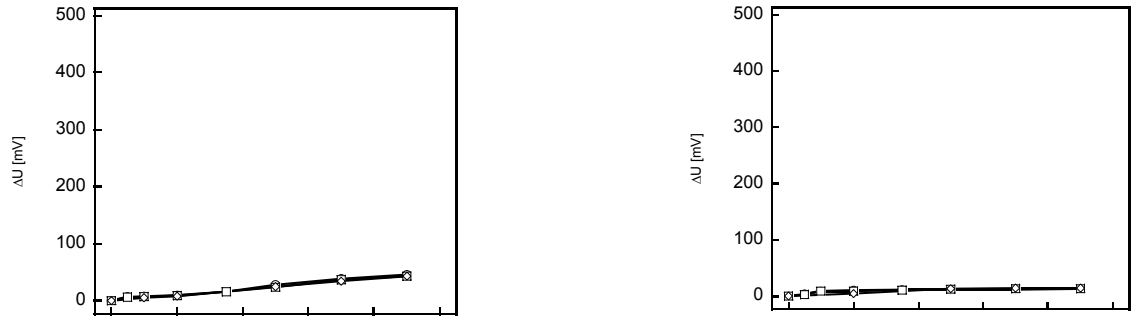

500 °C

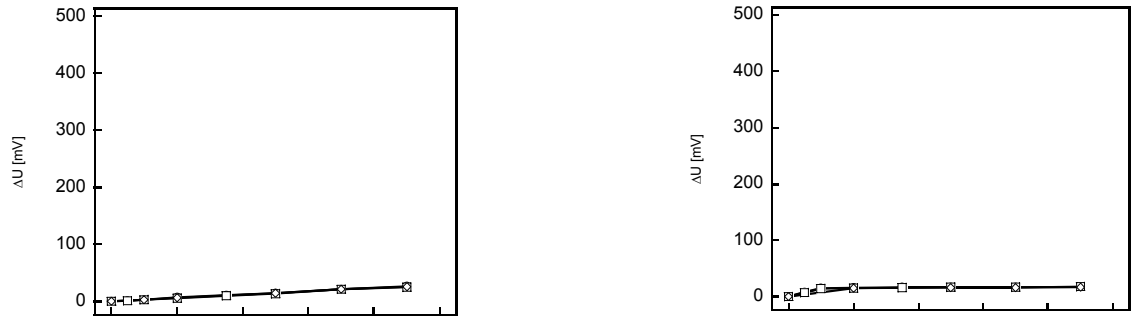

600 °C

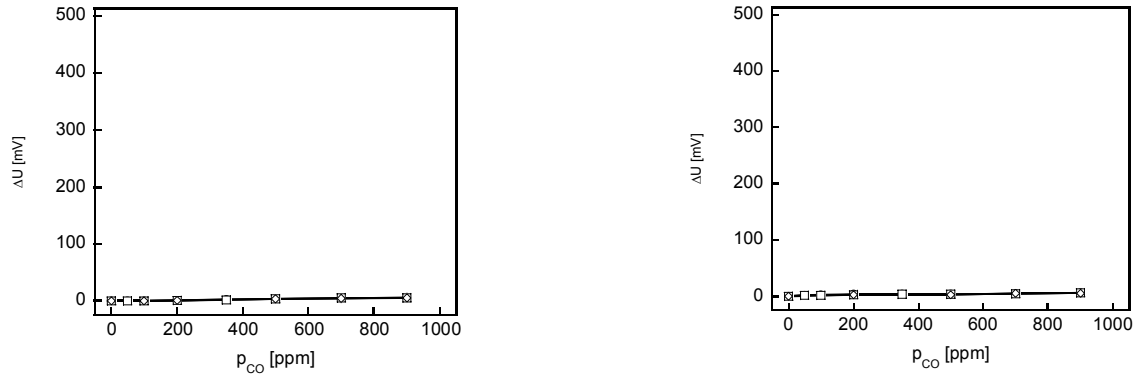

Fig. 10.6: The CO sensitivity of the cell with $Pt_{0.2}Au_{0.8}$ sensing electrode in whole investigated temperature range after (○) first, (□) second, and (◊) third runs of the measurements

High reference electrode potential *Low reference electrode potential*

400 °C

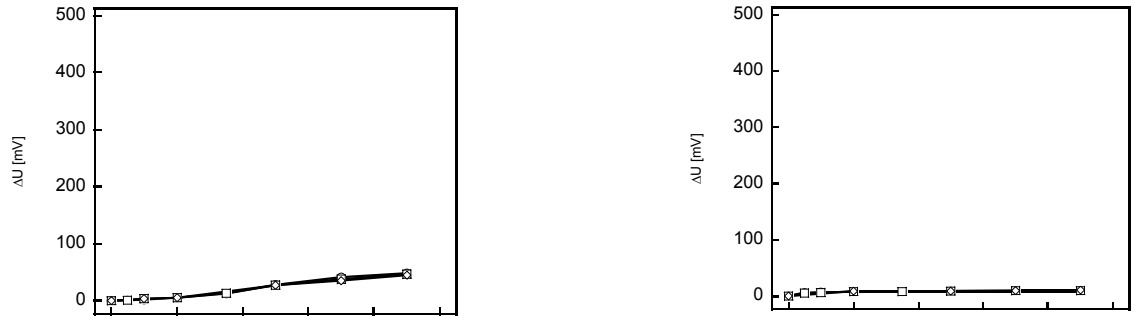

500 °C

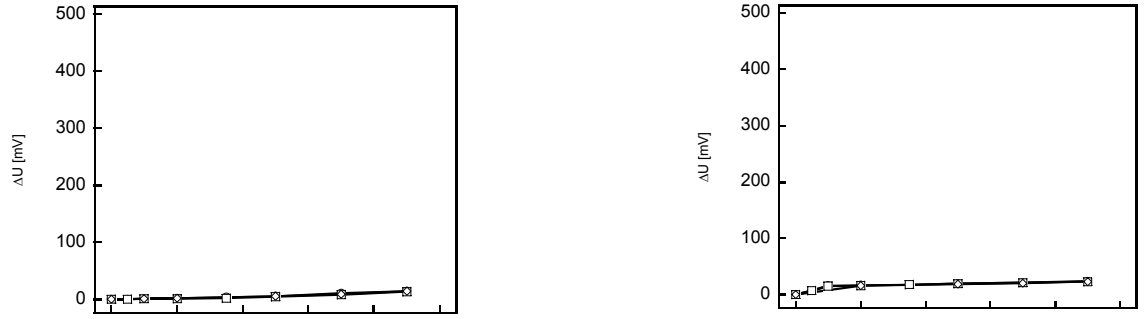

600 °C

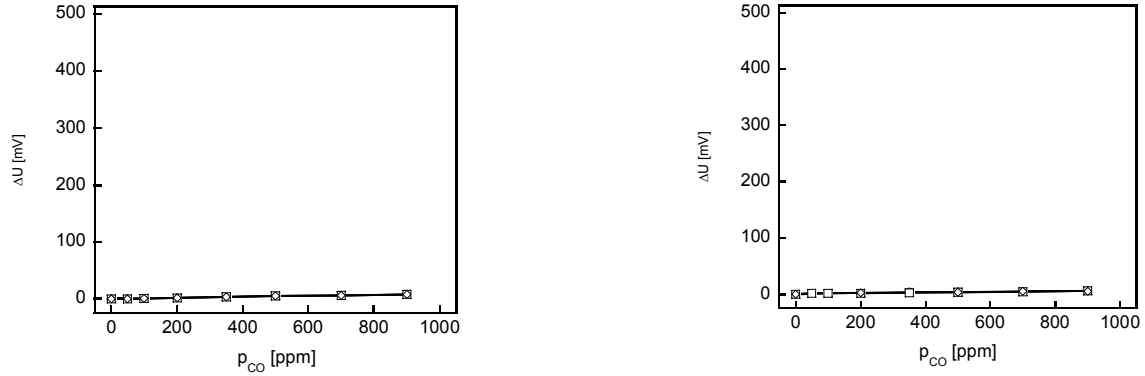

Fig. 10.7: The CO sensitivity of the cell with Au sensing electrode in whole investigated temperature range after (○) first, (□) second, and (◊) third runs of the measurements

11 References

[1] “Electrical Transducer Nomenclature and Terminology”, *ANSI Standard MC6.1-1975 (ISA S37.1)* Research Triangle Park, NC: Instrument Society of America (1975)

[2] *Terms and Definitions in Industrial-Process Measurement and Control*, (IEC draft 65/84), International Electrochemical Committee (1982)

[3] W.G. Wolder, K.D. Wise, in: “Sensors Development in the Microcomputer Age”, *IEEE Transactions* **ED-26** (1979) 1864

[4] S. Middel, D.J.W. Noorlag, Sensors and Actuators **2** (1981/82) 29

[5] T. G. Nemov, S.P. Yordanov, in: “Ceramic Sensors. Technology and Applications”, Technomic Publishing Co., Lancaster-Basel (1996)

[6] T. Grandke, J. Hesse, in: „Sensors: A Comprehensive Survey“, ed.: W. Göpel, J. Hesse, and J.N. Zemel, VCH Weinheim **1** (1989) 2

[7] M. Ando, T. Kobayashi, and M. Haruta, Sensors and Actuators B **24-25** (1995) 851

[8] W.C. Maskell, J. Phys. E: Sci. Instrum **20** (1987) 1156

[9] H. Dietz, Solid State Ionics **6** (1982) 175

[10] L. Heyne, in: “Measurement of Oxygen”, ed.: H. Degn, et. al., Elsevier, Amsterdam (1976) 65

[11] D.M. Haaland, Anal. Chem. **49** (1977) 1813

[12] R.E. Hetrick, W.A. Fate, and W.C. Vassell, Appl. Phys. Lett. **38** (1981) 390

[13] W.C. Maskell, H. Kaneko, and B.C.H. Steele, Proc. 2nd Int. Meeting on Chemical Sensors, ed.: J.L. Aucouturier et. al. (1986) 302

[14] N. Savage, B. Chwieroth, A. Ginwalla, B.R. Patton, S.A. Akbar, and P.K. Dutta, Sensors and Actuators B **79** (2001) 17

[15] J. Fouletier, Sensors and Actuators B **3** (1982) 295

[16] J. Wiessbert, and R. Ruka, Rev. Sci. Instru. **32** (1961) 593

[17] J. E. Anderson, and Y. B. Graves, J. Electrochem. Soc. **128** (1981) 294

[18] N. Miura, G. Lu, and N. Yamazoe, Solid State Ionics **136-137** (2000) 533

[19] F. Shimizu, N. Yamazoe, and T. Seiyama, Chem. Lett. (1978) 299

[20] H. Okamoto, H. Obayashi, and T. Kudo, Solid State Ionics **1** (1980) 319

[21] M. Katsumoto, H. Okamoto, and M. Kobayashi, Denki Kagaku **53** (1985) 577

[22] N. Miura, K. Kanamaru, Y. Shimizu, and N. Yamazoe, Solid State Ionics **40-41** (1990) 452

[23] N. Li, T. C. Tan, and H. C. Zeng, J. Electrochem. Soc. **140** (1993) 1068

[24] R. Lalauze, E. Visconte, L. Montanaro, and C. Pijolat, Sensors and Actuators B **13-14** (1993) 241

[25] Z. Y. Zhang, H. Narita, J. Mizusaki, and H. Tagawa, Solid State Ionics **79** (1995) 344

[26] R. Sorita, and T. Kawano, Sensors and Actuators B **40** (1997) 29

[27] N. Miura, T. Raisen, G. Lu, and N. Yamazoe, J. Electrochem. Soc. **144** (1997) L198

[28] E. Haefele, K. Kaltenmaier, and U. Schoenauer, Sensors and Actuators B **4** (1991) 525

[29] Y. Shimizu, and K. Maeda, Chem. Lett. (1996) 117

[30] N. Miura, H. Kurosawa, M. Hasei, G. Lu, and N. Yamazoe, Solid State Ionics **86-88** (1996) 1069

[31] G. Lu, N. Miura, and N. Yamazoe, J. Mater. Chem. **7** (1997) 1445

[32] G. Lu, N. Miura, and N. Yamazoe, Ionics **4** (1998) 16

[33] E. Haefele, K. Kaltenmaier, and U. Schoenauer, Sensors and Actuators B **4** (1991) 529

[34] T. Hibino, and H. Iwahara, J. Appl. Electrochem. **24** (1994) 102

[35] T. Hibino, Y. Kuwahara, S. Wang, S. Kakimoto, and M. Sano, Electrochem. Solid State Lett. **1** (1998) 197

[36] W. J. Fleming, J. Electrochem. Soc. **124** (1977) 21

[37] K. Kiukkola, and C. Wagner, J. Electrochem. Soc. **104** (1957) 379

[38] C. Wagner, Adv. Catal., **21** (1970) 323

[39] J. Weissbart, and R. Ruka, Rev. Sci. Instr. **32** (1961) 593

[40] Y. Tan, and T. C. Tan, Bull. Singapore Nat. Inst. Chem. **20** (1992) 101

[41] H.-H. Moebius, in: “Sensors: A Comprehensive Survey”, VCH Weinheim **3** (1991) 1105

[42] E. M. Logothesis, in: “Chemical Sensor Technology”, Elsevier, Tokyo **3** (1991) 89

[43] T. Takeuchi, and I. Igarashi, in: “Chemical Sensor Technology”, Elsevier, Tokyo **1** (1988) 109

[44] W. C. Maskell, and B. C. H. Steele, J. Appl. Electrochem. **16** (1986) 475

[45] S. Kimura, S. Ishitani, and H. Takao, in: “Fundamentals and Applications of Chemical Sensors”, ACS Symposium Series **309** (1986) 101

[46] E. M. Logothesis, and R. E. Hetrick, in: “Fundamentals and Applications of Chemical Sensors”, ACS Symposium Series **309** (1986) 137

[47] T. Takeuchi, and I. Igarashi, in: “Chemical Sensor Technology”, Elsevier, Tokyo **1** (1988) 79

[48] B. Y. Liaw, and W. Weppner, Solid State Ionics **40-41** (1990) 428

[49] K. Saji, J. Electrochem. Soc. **134** (1987) 2430

[50] E. M. Logothesis, J. H. Visser, R. E. Soltis, and L. Rimai, Sensors and Actuators B **9** (1992) 183

[51] T. Usui, A. Asada, M. Nakazawa, and H. Osanai, J. Electrochem. Soc. **136** (1989) 534

[52] A. S. Ioannou, and W. C. Maskell, Solid State Ionics **53-56** (1992) 85

[53] Y. Tan, and T. C. Tan, Sensors and Actuators B **28** (1995) 113

[54] N. Yamazoe, and N. Miura, Sensors and Actuators B **20** (1994) 95

[55] T. Kudo, in: Gas sensors, Catalysis Today (1990) 263

[56] G. Baier, V. Schuele, and A. Vogel, Appl. Phys. A **57** (1993) 51

[57] A. Vogel, G. Baier, and V. Schuele, Sensors and Actuators B **15-16** (1993) 147

[58] H. Okamoto, H. Obayashi, and T. Kudo, Solid State Ionics **3/4** (1981) 453

[59] H. Okamoto, G. Kawamura, and T. Kudo, J. Catal. **82** (1983) 322

[60] H. Okamoto, G. Kawamura, and T. Kudo, J. Catal. **82** (1983) 332

[61] H. Okamoto, G. Kawamura, and T. Kudo, J. Catal. **86** (1984) 437

[62] D. M. Haaland, J. Electrochem. Soc. **127** (1980) 796

[63] O. A. Mar’ina, and V. A. Sobyanin, Catal. Lett. **15** (1992) 61

[64] J. Mizusaki, H. Tagawa, Y. Miyaki, S. Yamauchi, K. Fueki, I. Koshiro, and K. Hirano, Solid State Ionics **53-56** (1992) 126

[65] S. Setric, L. Rabco, and A. Diaconu, Proc. Int. Semicond. Conf. (1997) 153

[66] Z. Y. Can, H. Narita, J. Mizusaki, and H. Tagawa, Solid State Ionics **75** (1995) 344

[67] T. Hibino, S. Wang, S. Kakimoto, and M. Sano, Sensors and Actuators B **50** (1998) 149

[68] T. Hibino, S. Tanimoto, S. Kakimoto, and M. Sano, Electrochem. Solid State Lett. **2** (1999) 651

[69] T. Hibino, S. Kakimoto, and M. Sano, J. Electrochem. Soc. **146** (1999) 3361

[70] R. E. Hetrick, and E. M. Logothesis, Appl. Phys. Lett. **34** (1979) 117

[71] N. Miura, T. Raisen, G. Lu, and N. Yamazoe, Sensors and Actuators B **47** (1998) 84

[72] K. Saji, H. Kondo, T. Takeuchi, and I. Igarashi, J. Electrochem. Soc. **135** (1988) 1686

[73] Z. Lukacs, M. Sinz, G. Staikov, W. J. Lorenz, G. Baier, and A. Vogel. Solid State Ionics **68** (1994) 93

[74] R. Mukundan, E. L. Brosha, D. R. Brown, and F. H. Garzon, Electrochem. Solid State Lett. **2** (1999) 412

[75] R. Mukundan, E. L. Brosha, D. R. Brown, and F. H. Garzon, J. Electrochem. Soc. **147** (2000) 1583

[76] R. Sorita, and T. Kawano, Sensors and Actuators B **35-36** (1996) 274

[77] E. L. Brosha, R. Mukundan, D. R. Brown, F. H. Garzon, J. H. Visser, M. Zanini, Z. Thou, and E. M. Logothesis, Sensors and Actuators B **69** (2000) 171

[78] Y. Tan, and T. C. Tan, J. Electrochem. Soc. **141** (1994) 461

[79] L. Lloyd, D. E. Ridler, and M. V. Twigg, in: “Catalyst Handbook”, Wolfe, UK (1989) 283

[80] G. W. Bridger, and M. S. Spencer, in: “Catalyst Handbook”, Wolfe, UK (1989) 441

[81] G. I. Golodets, in: “Heterogeneous Catalytic Reactions Involving Molecular Oxygen”, Elsevier, New York (1983) 284

[82] M. S. Spencer, in: “Catalyst Handbook”, Wolfe, UK (1989) 32

[83] W. F. Libby, Science **171** (1971) 499

[84] J. M. D. Tascon, and L. G. Tejuca, React. Kinet. Catal. Lett. **15** (1980) 185

[85] Y. Y. Yao, J. Catal. **36** (1975) 266

[86] R. J. H. Voorhoeve, J. P. Remeika, and L. E. Trimble, Ann. N.Y. Acad. Sci. **272** (1976) 3

[87] D. J. Kuchynka, R. L. Cookand, and A. F. Sammells, J. Electrochem. Soc. **138** (1991) 1284

[88] A. Hammouche, E. Siebert, A. Hammou, M. Kleitz, and A. Caneiro, J. Electrochem. Soc. **138** (1991) 1212

[89] T. Miruyama, X.-Y. Ye, and Y. Saito, Solid State Ionics **23** (1987) 113

[90] T. Maruyama, X.-Y. Ye, and Y. Saito, Solid State Ionics **24** (1987) 281

[91] P. D. Petrolekas, S. Brosda, and C. G. Vayenas, J. Electrochem. Soc. **145** (1998) 1469

[92] T. Otagawa, M. Madou, S. Wing, J. R. Alexander, S. Kusanagi, T. Fujioka, and A. Yasuda, Sensors and Actuators B **1** (1990) 319

[93] A. Yasuda, N. Yamaga, K. Doi, T. Fujioka, and S. Kusanagi, J. Electrochem. Soc. **139** (1992) 1091

[94] M. Sato, in: "Research Techniques for High Pressure and High Temperature", Springer Verlag, Berlin, New York (1971) chap. 3

[95] I. V. Yentekakis, S. Neophytides, and C. G. Vayenas, J. Catal. **111** (1988) 152

[96] G. Wedler, and D. F. Klemperer, in: "Chemisorption: An Experimental Approach", London (1976) 199

[97] J. O'M. Bockris, and A. K. N. Reddy, in: "Modern Electrochemistry", Plenum Press New York **2** (1973) 1161

[98] N. V.Cant, and P. W. Frederickson, J. Catal. **37** (1975) 531

[99] A. G. Daglish, and D. D. Eley, Proc. 2nd Int. Congr. Catal. **2** (1960, 1961) 1615

[100] M. Haruta, N. Yamada, T. Kobayashi, and S. Iijima, J. Catal. **115** (1986) 301

[101] B. C. Nguyen, T. A. Lin, and D. M. Mason, J. Electrochem. Soc. **133** (1986) 1807

[102] B. C. Nguyen, L. M. Rincon-Rubio, and D. M. Mason, J. Electrochem. Soc. **133** (1986) 1860

[103] R. Hartung, R. Schroeder, and H.-H. Moebius, Z. Phys. Chem. **262** (1981) 961

[104] M. Maeda, M. Masato, and T. Kunitachi, German Patent Application, DE 3807752 A1 (1988)

[105] E. Haefele, and M. Kottler, Eur. Patent, EP 0241751 A2 (1987)

[106] M. Stoukides, Ind. Eng. Chem. Res. **27** (1988) 1745

[107] I. V. Yentekakis, and C. G. Vayenas, J. Catal. **111** (1988) 170

[108] M. E. Schrader, J. Colloid Interface Sci. **59** (1977) 456

[109] M. A. Chesters, and G. A. Somorjai, Surf. Sci. **52** (1975) 21

[110] N. B. Bazhutin, G. K. Boreskov, and V. I. Savchenko, React. Kinet. Catal. Lett. **10** (1979) 337

[111] P. Legare, L. Hilaire, M. Sotto, and G. Maire, Surf. Sci. **91** (1980) 175

[112] N. D. S. Canning, D. Outka, and R. J. Madix, Surf. Sci. **141** (1984) 245

[113] M. E. Schrader, Surf. Sci. **78** (1978) L227

[114] C. G. Vayenas, S. Bebelis, I. V. Yentekakis, P. Tsiakaras, and H. Karasali, Platinum Metals Rev. **34** (1990) 122

[115] G. Baier, A. Vogel, and V. Schuele, VDI Berichte **939** (1992) 439

[116] T. Hibino, S. Wang, and Y. Kuwahara, J. Electrochem. Soc. **146** (1999) 382

[117] A. M. Azad, S. G. Mhaisalkar, L. D. Birkefeld, S. A. Akbar, and K. S. Goto, J. Electrochem. Soc. **139** (1992) 2913

[118] D. Kohl, Sensors and Actuators B **1** (1990) 158

[119] M. J. Madou, and S. R. Morrison, in: "Chemical Sensing with Solid State Devices", Academic Press New York (1989)

[120] G. C. Bond, in: "Heterogeneous Catalysis: Principles and Applications", Clarendon Press Oxford (1987)

[121] N. Miura, G. Lu, N. Yamazoe, H. Kurosawa, and M. Hasei, J. Electrochem. Soc. **143** (1996) L33

[122] Y. Yan, N. Miura, and N. Yamazoe, Chem. Lett. (1994) 1733

[123] G. Lu, N. Miura, and N. Yamazoe, Sensors and Actuators B **35-36** (1996) 130

[124] N. Miura, Y. Yan, G. Lu, and N. Yamazoe, Sensors and Actuators B **34** (1996) 367

[125] G. Lu, N. Miura, and N. Yamazoe, J. Electochem Soc. **143** (1996) L154

[126] Z. Can, H. Narita, J. Mizusaki, and H. Tagawa, Solid State Ionics **79** (1995) 344

[127] N. L. Robertson, and J. N. Michaels, J. Electrochem. Soc. **137** (1990) 129

[128] A. D. Colvin, J. W. Butler, and J. E. Anderson, J. Electroanal. Chem. **136** (1982) 179

[129] J. E. Anderson, and Y. B. Graves, J. Appl. Electrochem. **13** (1983) 395

[130] M. Stoukides, and C. G. Vayenas, J. Electrochem. Soc. **131** (1984) 839

[131] J. N. Michaels, and C. G. Vayenas, J. Electrochem. Soc. **131** (1984) 2544

[132] W.L. Worrell, in: „Solid electrolytes“, ed.: S. Geller, Springer-Verlag, Berlin-Heidelberg-New York (1977) 142

[133] C.B. Choudhary, H.S. Maiti, E.C. Subbarao, in: “Solid electrolytes and Their Applications”, ed.: E.C. Subbarao, Plenum Press, New York-Lndon (1980) 1

[134] R.C. Garvie, in: „High temperature oxides“, part II, ed.: A.M. Alper, Academic Press, New York (1970) 117

[135] J. Arndt, in: “Sensors: A Comprehensive Survey”, ed.: W. Göpel, J. Hesse, and J.N. Zemel, VCH Weinheim **1** (1989) 248

[136] J.F. Baumand, P. Abelard, in: „Science and technology of zirconia II“, ed.: N. Claussen and M. Rühle, The Amer. Cer. Soc., Columbus (1984) 555

[137] W. Nernst, Z. Elektrochem. **6** (1899) 41

[138] H. Bauer, H. Preis, Z. Elektrochem. **43** (1937) 727

[139] C. J. Mogab, J. Vacuum Sci. Technol. **10** (1973) 852

[140] D. Yuan, and F. A. Kroeger, J. Electrochem. Soc. **116** (1969) 594

[141] J. Weissbart, and R. Ruka, J. Electrochem. Soc. **109** (1962) 723

[142] G.A. Rankin, H.E. Merwin, , J. Amer. Chem. Soc. **38** (1916) 568

[143] G. Yamaguchi, J. Japan Electrochem. Soc. **11** (1943) 260

[144] C.A. Beevers, M.A.S. Ross, Z. Kristallographie **97** (1937) 59

[145] J.D. Hodge, J. Am. Ceram. Soc. **66** (1983) 166

[146] J.P. Boilot, G. Collin, P. Colomban, R. Comes, Phys. Rev. B **22** (1980) 5912

[147] F.A. Kröger, and H.J. Vink, in: "Solid State Ionics" Vol. 3, ed.: F. Seitz, and D. Turnbull, Academic Press, New York (1956) 307

[148] F.A. Kröger, and H.J. Vink, J. Phys. Chem. Solids **5** (1958) 208

[149] H. Näfe, Sensors and Actuators B **21** (1994) 79

[150] H. Näfe, and M. Steinbrück, J. Electrochem. Soc. **141** (1994) 2779

[151] K.S. Goto, in: „Solid State Electrochemistry and Ist Application to Sensors and Electronic Devices", Material Science Monograph 45, Elsevier, Amsterdam-Oxford-New York-Tokyo (1988) 12

[152] H. Sato, in: "Topics in Applied Physics", Vol. 21: Solid Electrolytes, ed.: S. Geller, Springer-Verlag, Berlin-heidelberg-New York (1977) 3

[153] S. Pizzini, in: "Fast Ion Transport in Solids", ed.: W. van Gool, North Holland Publ., Amsterdam (1973) 461

[154] D. A. Emery, R. J. Luke, P. H. Middleton, and I. S. Metcalfe, J. Electrochem. Soc. **146** (1999) 2188

[155] D. E. Williams, P. McGeehin, and B. C. Tofield, Proc. 2nd Europ. Conf. Solid State Chem. (1982) 275

[156] H. G. Lintz, and C. G. Vayenas, Angew. Chem. **28** (1989) 708

[157] D. O. Hayward, and B. M. W. Trapnell, in: Chemisorption, London (1964) 159

[158] H. Okamoto, G. Kawamura, and T. Kudo, J. Catal. **87** (1984) 1

[159] R. A. Shigeishi, and D. A. King, Surf. Sci. **75** (1978) L397

[160] P. R. Norton, Surf. Sci. **44** (1974) 624

[161] E. McCarthy, J. Zahradnik, G. C. Kuczynski, and J. J. Carberry, J. Catal. **39** (1975) 29

[162] J. Wei, in: "Advances in Catalysis", Academic Press New York (1975) 57

[163] F. G. Dwyer, in: “Catalysis Reviews”, New York (1972) 261

[164] H. P. Bonzel, and R. Ku R, Surf. Sci. **33** (1972) 91

[165] H. P. Bonzel, and J. J. Burton, Surf. Sci. **52** (1975) 223

[166] H. Heyne, and F. C. Tompkins, Proc. Roy. Soc. London **292** (1966) 460

[167] A. Golchet, and J. M. White, J. Catal. **53** (1978) 266

[168] T. Engel, and G. Ertl, Adv. Catal. **28** (1979) 1

[169] J. L. Gland, Surf. Sci. **93** (1980) 487

[170] J. L. Gland, B. A. Sexton, and G. B. Fisher, Surf. Sci. **95** (1980) 587

[171] J. Mizusaki, M. Aoki, Y. Miyaki, S. Yamauchi, and K. Fueki, Denki Kagaku **58** (1990) 1169

[172] N. Miura, H. Kato, N. Yamazoe, and T. Seiyama, Proc. Inter. Meet. Chem. Sensors, Elsevier, Tokyo (1983) 233

[173] C. Vayenas, and H. Saltsburg, J. Catal. **57** (1979) 296

[174] C. G. Vayenas, B. Lee, and J. Michaels, J. Catal. **66** (1980) 36

[175] D. R. Baker, and M. W. Verbrugge, AIChE Journal **40** (1994) 1498

[176] Handbook of Chemistry and Physics, 70th Ed, USA (1989-1990) D-191

[177] NIST-JANAF Thermodynamic Tables, J. Phys.Chem. Ref. Data, Monograph 9 (1998) 1323

[178] T. Maruyama, S. Sasaki, Y. Saito, Solid State Ionics **23** (1987) 107

[179] H. Näfe, Solid State Ionics **93** (1997) 117

[180] H. Näfe, F. Aldinger, Sensors and Actuators B **69** (2000) 46

[181] JANAF Thermodynamic Tables, J. Phys.Chem. Ref. Data **14** (1985) 623

[182] JANAF Thermodynamic Tables, J. Phys.Chem. Ref. Data **14** (1985) 628

[183] JANAF Thermodynamic Tables, J. Phys.Chem. Ref. Data **14** (1985) 1576

[184] H. Näfe, F. Meyer, and F. Aldinger, Electrochim. Acta **45** (1999) 1631

[185] J. R. Macdonald, in: “Impedance Spectroscopy. Emphasizing Solid Materials and Systems”, A Wiley-Interscience Publication, New York (1987)

[186] J. E. Bauerle, J. Phys. Chem. Solids **30** (1969) 2657

[187] N. Matsui, Solid State Ionics **3-4** (1981) 525

[188] JCPDS, Powder Diffraction Files, Int. Centre for Diffraction Data Newtown Square, USA (1998)

[189] F. Harbach, H. Nienburg, J. Eur. Ceram. Soc. **18** (1998) 685

[190] K. Tekaia-Elhsissen, F. Bonet, P.-Y. Sivert, and R. Herrera-Urbina, J. Alloys Compd. **292** (1999) 96

[191] H. Näfe, Solid State Ionics **13** (1984) 255

CURRICULUM VITAE (LEBENSLAUF)

Family name:	PLASHNITSA
Given name:	Vladimir
Date of birth:	February 17, 1975
Place of birth:	Kirov, Russia
Nationality:	Russian
Family status:	Married

Education and Working Experiences:

9. 1982 – 6. 1992	Scholl of physics and mathematics, Kirov, Russia.
July 1992	National Examinations for University
9. 1992 – 7. 1997	Studying at Chemical Department of Vyatka State University, Kirov, Russia. Diploma work in Chair "Technology of Electrochemical Production", Chemical Department, Vyatka State University, Kirov, Russia. **Diploma thesis: "The synthesis and investigations of some Bi_2O_3-based solid electrolyte"** **Degree: Chemist – Engineer**
8. 1997 – 9. 2000	Working at Materials Science Department, Moscow State University, Moscow, Russia as a junior researcher. **Scientific work: "Synthesis, investigation and application of BIMEVOX-family solid electrolytes"**
10. 2000 – 7. 2004	Studying for a doctoral degree at Max-Planck-Institute für Metallforschung and Universität Stuttgart, Stuttgart, Germany, supported by a scholarship of the Max-Planck-Gesellschaft. **Ph.D. thesis: "Characterization of the CO sensitivity of electrode materials by solid electrolyte galvanic cells"**